Ocean circulation changes off southern Greenland during the abrupt climate events of mid-to-late MIS3

Lisa Griem

Thesis for the degree of Philosophiae Doctor (PhD)
University of Bergen, Norway
2021

UNIVERSITY OF BERGEN

Ocean circulation changes off southern Greenland during the abrupt climate events of mid-to-late MIS3

Lisa Griem

Thesis for the degree of Philosophiae Doctor (PhD)
at the University of Bergen

Date of defense: 18.03.2021

Year: 2021

Title: Ocean circulation changes off southern Greenland during the abrupt climate events of mid-to-late MIS3

Name: Lisa Griem

Print: Skipnes Kommunikasjon / University of Bergen

Scientific environment

The research leading to this thesis was performed at the Department of Earth Science, University of Bergen and the Bjerknes Centre for Climate Research, Bergen, Norway. The PhD project greatly benefitted from the collaboration with NORCE Climate, Norwegian Research Centre in Bergen, the section for Ice, Climate and Earth (PICE), Niels Bohr Institute, University of Copenhagen, Denmark and Dr. Antje Voelker at Divisão de Geologia e Georecursos Marinhos, Instituto Português do Mar e da Atmosfera (IPMA), Lisbon, Portugal and Centre of Marine Sciences (CCMAR), Universidade do Algarve, Faro, Portugal. Parts of the laboratory work leading to the research results presented in this thesis were conducted at the University of Portsmouth, United Kingdom in collaboration with Prof. Craig Storey.

The funding for this research was granted by the European Research Council under the European Community´s Seventh Framework Programme (FP7/2007-2013) ERC grant agreement no° 610055 as part of the *Arctic Sea Ice and Greenland Ice Sheet Sensitivity* project Ice2Ice. This PhD project has been supervised by Prof. Eystein Jansen (University of Bergen), Dr. Trond M. Dokken (NORCE Norwegian Research Centre) and Dr. Sarah M. P. Berben (University of Bergen).

"Any understanding of the natural world and what´s in it is a source of not only a great curiosity but great fulfilment."

Sir David Attenborough

Acknowledgements

First and foremost, I would like to thank the PIs of Ice2Ice for putting together the best project of all time! Being surrounded by so many great people with great spirit made my time in Bergen extra special. The annual meetings certainly felt like big family get-togethers that inspired my research. I want to thank my main supervisors Eystein Jansen and Trond M. Dokken for dealing with my impatience, supporting my research ideas, for the freedom that came with this support and the endless opportunities within Ice2Ice. Trond, your humor and the way you treat all your PhDs (and PostDocs) like a father helped me a lot to get along with all the INTERESTING data I generated! However, without my third supervisor, Sarah M. P. Berben, this thesis would have taken another four years. Thank you so much for your friendship, for giving me comfort when I needed it, for looking after me and sometimes stopping me, for great advice, and your strictness when it came to improving my writing skills, in particular.

Furthermore, I want to thank all my co-authors for all the feedback along the way. I want to highlight the special effort of Antje H. L. Voelker, Anne-Katrine Faber and Bjørg Risebrobakken. You are the quickest and most reliable co-authors one can ask for! I thank Craig Storey for giving me the opportunity to come to Portsmouth and work with his kind and very helpful research group, that resulted in high quality data. I´m also thankful for the scientific advice I got from Kerstin Perner, Hans Christian Steen-Larsen, Stijn De Schepper, Eirik V. Galaasen, Eivind W. Nagel Støren, Mary Elliot, Francesco Muschitiello, Ulysses S. Ninnemann and so many other colleagues. I thank Dag Inge Blindheim and my DAAD intern Nontje Rücker for all your help in the lab, and of course for initiating and participating in the Donkey rounds! For logistical and administrative support, I want to thank Mareile Andersson, Åse Kvinnsland Kodal, Charla K. Melander Olsen, Anja Bere, Maria Svåsand, Victoria Chimhutu, Linda Emdal and Jørund Raukleiv Strømsøe. I thank Margit, Sonja, Lukas, Amandine and Niklas for their feedback on parts of this thesis. I´m especially thankful to Eva for proofreading!

During my PhD I was lucky enough to participate in several conferences, summer schools, bootcamps and very special field trips. My PhD started with the cruise from Iceland to Greenland which was just breathtaking and all participants were the tip of the icebergs. I knew from previous cruises that, although I´m a marine geologist, the open ocean is not my element. I´m thankful to Marilena and Eliza for joining me on the couch and getting through the sea sickness together. Luckily, I also experienced a less nauseating second field trip to the Greenland Ice Sheet, fulfilling one of my biggest dreams. I never thought it would become true but it did. I´m over the moon that Kerim (with a little hint from Eliza and approval of my supervisors) made this dream a reality! Furthermore, I´m thankful that great people like Mari, Lasse, Sonja, Julien, Abby, Will, Helle, Bo, Jens, Nico, Chris, Iben and all the other participants made it an extra special experience. It was so nice to get to know you better during that time, Mari. Thanks to HC, Sonja and I got the chance to spend a lot more time together after EGRIP. I would like to thank Eva, Silje and Ida who made organizing and realizing the Ice2Ice bootcamp so easy and fun. On Svalbard I met many kind international researchers, but it is Thomas who immediately became a good friend.

I cannot stress enough that without all the nice colleagues and friends that were in Bergen, throughout or just part of the way, the time at UiB wouldn´t have been such a great experience. Without the help of Nele and Margit it would have been a lot harder for Niklas and me to get started in Bergen. Thank you, Margit, for being such a good friend since 2011, I will never forget our hearts skipping a beat ;). Henrik, Eva and family, Jordan and Niall, Björn, Alison, Carl: you left Bergen way too early and Carl left Bergen way too often! You are not only fun and helpful colleagues but also awesome friends. Continuing with awesome friends, a huge thanks goes to Lukas and Julie, Willem and Desiree, Davide and Siri, Sonja, Kerstin, HC, Sunniva, Mari, Morven, Thomas, Sevi, Karita, Fanny, Alvaro, Hanna and Robert and our great Dorfjugend companions Anna and Eoghan for the lunches, bar nights, the dinners, the BBQs, the day trips and all other adventures we enjoyed together! I thank Dusty Boots for making office days and our life in the country side even more joyful and for cheering me up during periods I was upset and desperate.

Last but not least I thank all of Niklas´ and my friends at home and our families who stayed with us and supported us the whole time. You make leaving our life in Bergen behind a little less hard! With all our belongings in a shipping container, I´m especially grateful that the three of us could live with my mom and Thorsten. Without your help and the space in Thorsten´s medical office it wouldn´t have been possible to finish my thesis. It´s great to have you close by again. I wouldn´t be the same person I am today and I clearly wouldn´t have come so far in my life without Niklas! I am the luckiest person to have you on my side, trusting me, supporting me and always believing in me especially during tough times. Thank you for being the best colleague, best partner and best father to our daughter. You and Karlotta are most certainly the ones who helped me keeping it together and finding new motivation, although it meant spending less time with you. Karlotta, you are such a strong and funny little girl. Your smile makes me forget all my troubles. I love you both soo much!

Abstract

Marine sediment cores from the North Atlantic and ice cores from the Greenland Ice Sheet serve as natural archives of past climate variability. Ice cores have revealed that during the last glacial period the climate comprises both relatively stable intervals such as the Last Glacial Maximum (LGM, ca. 26-19 ka) and unstable climate intervals such as Marine Isotope Stage 3 (MIS3, ca. 59-29 ka). The climate of MIS3 is characterized by abrupt changes from colder stadial to warmer interstadial conditions, well-known as Dansgaard-Oeschger events (DO). Although DO events had repercussions over the climate system outside of the high latitude Northern Hemisphere, they are especially pronounced in records from the North Atlantic region. North Atlantic marine sediments record changes in sea ice cover, surface productivity and iceberg discharge, which are all associated with DO events. Iceberg discharge from the Northern Hemisphere ice sheets, and hence release of fresh water into the North Atlantic was especially pronounced during so-called Heinrich (H) Stadials. H-Stadials occurred approximately every 7 to 10 kyrs and are particularly cold and long stadials within the DO event oscillations. The freshwater discharge further contributed to sea ice formation in the North Atlantic and Nordic Seas. This near-perennial sea ice cover during stadials prevented ocean-atmosphere interaction while during interstadials the Nordic Seas were seasonally ice-free. These interstadial periods allowed moisture to evaporate from the ocean´s surface where after it was transported towards the Northern Hemisphere Ice Sheets, and thereby sustain their growth during MIS3 and the LGM.

This thesis aims to give insights into the complex interactions between ice sheets, sea ice and ocean circulation during MIS3 and the LGM. Herein, the main focus lies on changes along the South-East Greenland margin, complemented by thoroughly studied sediment core sites from the Nordic Seas and Greenland ice core records.

Paper I investigates environmental conditions between 65 and 25 ka recorded by a deep-sea sediment core from the northeastern Labrador Sea. Stable isotope data, ice-rafted debris (IRD) and planktic foraminifer fluxes and assemblage counts are compared to sediment cores from the Irminger Basin and the Greenland Sea. The results are used to draw conclusions about the sensitivity of the northwest North Atlantic to changes in sea ice extent, surface hydrography and iceberg discharge during the DO events of MIS3. We find, that an expanded sea ice cover seems to be

characteristic for most stadials in the Labrador Sea while climate conditions during most interstadials allowed for open waters with a productive sea surface. Major iceberg calving events associated with H-Stadials 4 and 3 are documented. The influence of Atlantic Water is enhanced during Greenland Interstadials 14, 12 and 8.

Paper II takes a detailed look at the source areas that may have contributed to each IRD event observed in Paper I. X-ray spectroscopy and single grain Lead-isotope measurements are performed. Additionally, several petrologic tracers and X-ray fluorescence Calcium-to-Strontium ratios are analyzed. The main results indicate that there are no specific trends of IRD sources throughout MIS3 or during interstadials, stadials and H-Stadials. Greenland is the main contributor of the IRD deposits observed at the Eirik Drift, although icebergs from the Laurentide Ice Sheet melted at the core site during the ice sheet collapse associated with H-Stadial 4.

In Paper III, the knowledge gained within the scope of Papers I and II is combined with previously published and new datasets from three regions in the Nordic Seas and the subtropical North Atlantic. The datasets comprise biomarker, IRD and planktic foraminifer concentration as well as sea surface temperature records to evaluate changes in the North Atlantic sea ice extent during late MIS3 DO events and the LGM. The results from these proxy-data are then compared to stable oxygen isotope ($\delta^{18}O$) and deuterium excess (d-excess) records from the GRIP ice core. We find a strong link between the variability of d-excess data and the location of the sea ice edge in the North Atlantic. During interstadials and the LGM, sea surface conditions were similar and allowed for a northern moisture source of precipitation as sea ice retreated to the northwestern Nordic Seas. Additionally, the investigated regions were characterized by high plankton productivity during the LGM. The surface of the subtropical North Atlantic was as warm or warmer during the LGM than during MIS3 interstadials.

The results of this thesis reveal that the northeastern Labrador was a highly dynamic region during the DO events of MIS3. The high-resolution MIS3 data close the gap between the well-studied LGM and MIS5e and connect this part of the North Atlantic to the well-constrained sea surface conditions of the Nordic Seas and the mid-latitude North Atlantic. Furthermore, by mapping the North Atlantic sea surface conditions during MIS3 DO events and the LGM, a link between ice core d-excess and the Nordic Seas sea ice cover is demonstrated.

List of publications

Paper I

Griem, L.; Voelker, A. H. L.; Berben, S. M. P.; Dokken, T. M. and Jansen, E.: **Insolation and glacial meltwater influence on sea-ice and circulation variability in the northeastern Labrador Sea during the last glacial period.** *2019. Paleoceanography and Paleoclimatology.*

Paper II

Griem, L.; Storey, C.; Berben, S. M. P.; Dokken, T. M. and Jansen, E.: **Climate and ice sheet responses in northern latitudes during Marine Isotope Stage 3: A provenance study of ice-rafted debris from the Eirik Drift.**

Manuscript in preparation for Journal of Quaternary Science.

Paper III

Griem, L.; Dokken, T. M.; Risebrobakken, B.; Faber, A.-K.; Berben, S. M. P.; Vinther, B. M.; Sadatzki, H.; Gkinis, V. and Jansen, E.: **Similar conditions in the North Atlantic region during the Last Glacial Maximum and interstadials: Evidence from ice core and sediment core records.**

Manuscript in preparation for Quaternary Science Reviews.

Contents

1 Introduction

1.1 Motivation

During the last glacial period (see 1.2), the Earth´s climate was punctuated by at least 20 abrupt climate oscillations that occurred on centennial to decadal time-scales that are known as Dansgaard-Oeschger (DO) events (Dansgaard et al., 1993b; Kuhlbrodt et al., 2007; Maslin, 2013). The abrupt shift from cold stadial to warm interstadial conditions is characteristic for each DO event observed in Greenland ice cores, particularly during Marine Isotope Stage 3 (MIS3, 59-29 ka) (Huber et al., 2006; Kindler et al., 2014). The stadial-interstadial transitions are closely linked to sea ice cover retreat in the North Atlantic and Nordic Seas (Jansen et al., 2020). As Arctic sea ice-loss is a key driver of current Greenland warming (Pedersen & Christensen, 2019), we need to improve our knowledge about feedback mechanisms between the ocean, the ice and the atmosphere (Li & Born, 2019). This knowledge can be gained from reconstructions of past sea surface conditions using marine sediment cores from the North Atlantic and the Nordic Seas.

The North Atlantic and the Nordic Seas are both key areas to study ocean-ice-atmosphere interactions because these regions are locations of deep water-formation (Dickson & Brown, 1994; Rahmstorf, 2002) and A) are highly affected by sea ice retreat and rising ocean temperatures (IPCC, 2013), and B) are directly impacted by the increasing freshwater influx from the melting Greenland Ice Sheet and melting Arctic sea ice (Dickson et al., 2002; Rahmstorf et al., 2015). The atmosphere warms the most in the region where the sea ice diminishes (Jansen et al., 2020). In these key regions, the variability of sea surface processes, such as iceberg discharge, sea ice cover and surface current strength, are directly linked to atmospheric as well as Atlantic Meridional Overturning Circulation (AMOC) by feedback mechanisms (Jensen et al., 2016; Kuhlbrodt et al., 2007). Hence, studying the dynamic nature of continental and marine ice masses during past abrupt climate changes is vital for our understanding of larger scale climate processes today. Under present-day conditions, climate processes such as the weakening of local deep-water convection in the Labrador Sea are caused by the enhanced freshwater input of the melting Greenland Ice Sheet (Rahmstorf et al., 2015; Thornalley et al., 2018). The weakening, along with dense water supply in the

Irminger Sea and the Nordic Seas, controls the strength of the AMOC (Kuhlbrodt et al., 2007) and subsequently heat transport to high-latitudes (Rahmstorf, 2002).

Besides freshwater influx, sea ice dynamics have been identified as a key controlling mechanisms for explaining DO events. In particular, Sadatzki et al. (2019) argue that the northward heat transport into the Nordic Seas was possible during the interstadials of a DO event, but that it was reduced during stadials due to sea ice that covered the Nordic Seas. During especially long stadials, the so-called Heinrich Stadials the sea ice possibly extended into the subpolar North Atlantic (Dokken et al., 2013; Vettoretti & Peltier, 2016). This sea ice variablility not only had a profound effect on AMOC, but also on the continental ice sheets that surrounded the North Atlantic and the Nordic Seas during MIS3 and the Last Glacial Maximum (LGM, ca. 26-19 ka). In order to grow to their maximum extent which was reached during the LGM, the Northern Hemisphere Ice Sheets needed to receive moisture from an ice-free ocean during interstadials in the Nordic Seas. Hence, during stadials the moisture source was located somewhere south of the extensive sea ice cover.

The Labrador Sea is located between the well-studied Nordic Seas and the most southern limit of stadial sea ice cover in the subpolar North Atlantic. Yet, information from this regional about sea surface conditions during the DO events of MIS3 are missing. This thesis aims to close this gap by using a high-resolution multi-proxy approach for a deep-sea sediment core from the northeastern Labrador Sea and the Irminger Sea. The research conducted during this PhD project aims to provide insights into sea ice cover variability, calving events and surface hydrography in the northeastern Labrador Sea during MIS3 (Paper I). The observed calving events are further analyzed for their source areas in order to reconstruct iceberg trajectories and ice sheet sensitivity during DO events (Paper II). The findings from the Labrador Sea (Paper I and II) are combined with new and previously published multi proxy studies from the Irminger Sea and the Nordic Seas to map sea surface conditions during stadials, interstadials and the LGM (Paper III). The overall aim is to investigate the link between sea surface conditions in the North Atlantic and Nordic Seas, and proxy records from the Greenland Ice Sheet.

1.2 Quaternary Climate

Glacial-interglacial cycles

The Quaternary period is characterized by glacial-interglacial cycles (i.e. climate intervals with a large or small continental ice volume). Those cycles are forced by changes in the Earth´s orbit (Maslin, 2013) such as the roundness of the Earth´s orbit (eccentricity, ~100 ka-cycle), the tilt (obliquity, ~41 ka-cycle) and the wobbling (precession, ~21/19 ka-cycle) of the Earth´s rotation axis. Changes in eccentricity, obliquity and precession are known as Milankovitch cycles (e.g. Berger, 1988; Berger & Loutre, 1999; Milankovitch, 1930). During the last 800 ka, glacial-interglacial cycles occurred on the frequency of the eccentricity cycle and were increased in intensity compared to older time intervals (Berger & Loutre, 1999; Imbrie et al., 1993; Maslin, 2013). Combined, Milankovitch cycles control the amount of solar radiation (i.e. insolation) that reaches the Earth´s top atmosphere at different latitudes and throughout the year's seasons (Ruddiman, 2008). Changes in precession mainly affect the seasonal insolation at low and mid-latitudes whereas changes in obliquity mostly affect high latitudes (Ruddiman, 2008). The summer insolation received at 65°N is crucial in terms of glacial-interglacial cycles (Maslin, 2013). At this latitude, increased or decreased insolation leads to respectively higher melt rates or growth of the Northern Hemisphere ice sheets (Figure 1) (Imbrie et al., 1993).

DO events

The last glacial period (~120-14 ka) comprises Marine Isotope Stages 4-2 (MIS4-MIS2) (Figure 1). The glaciation period started at the beginning of MIS4 and continued towards the beginning of MIS2, ending with the LGM. While, MIS4 and MIS2 were quite stable cold periods, indicated by the lowest summer insolation throughout the last 70 kyrs (Figure 1), MIS3 was interrupted by frequently recurring climate oscillations.

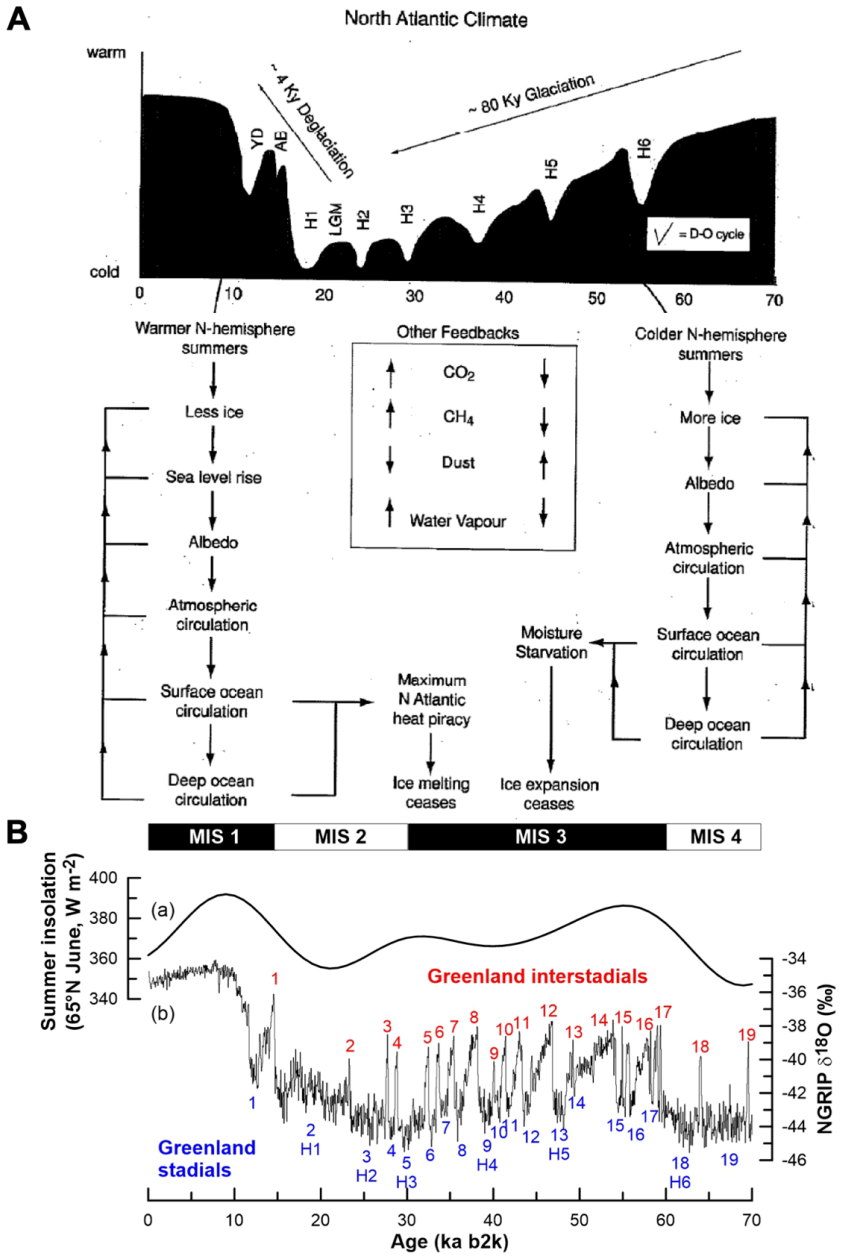

Figure 1: North Atlantic climate variability throughout the last 70 kyrs. A) Feedback mechanisms that cause glacial-interglacial cycles (modified after Maslin (2013)). B) (a) Summer insolation at 65°N (a-d, Berger & Loutre, 1999). (b) Stable oxygen isotope ($\delta^{18}O$) record from the North Greenland Ice core Project (NGRIP, Seierstad et al., 2014) documents Dansgaard-Oeschger (DO) events 19-1, numbers differentiate between colder Greenland Stadials (blue) and warmer Greenland Interstadials (red). H: Heinrich event, indicating Northern Hemisphere ice sheet collapses. LGM: Last Glacial Maximum. AB: Allerød-Bølling. YD: Younger Dryas.

The special character of MIS3 was first identified in stable oxygen isotope ($\delta^{18}O$) records from Greenland ice cores by Willi Dansgaard and Hans Oeschger (Dansgaard et al., 1993a; Rasmussen et al., 2014) (Figure 1). Hence, the abrupt climate oscillations are called Dansgaard-Oeschger (DO) events. Each DO event lasts on average 1470 ± 500 years and comprises a warm interstadial and a cold stadial phase (Dansgaard et al., 1993a; Rasmussen et al., 2014) (Figure 1). Based on the $\delta^{18}O$ records, calibrated with the use of N-isotope studies in the trapped air bubbles, temperature changes above the Greenland Ice Sheet are reconstructed (Huber et al., 2006; Kindler et al., 2014). The abrupt increase of $\delta^{18}O$ values at the onset of a DO event hereby indicates an atmospheric warming of up to 15.5 °C in less than a decade (Kindler et al., 2014). The high amplitude DO events are not only evident in Greenland ice cores. They had global repercussions and are recorded in many different archives, e.g. marine sediment cores (Jansen et al., 2020; Voelker, 2002). In particular, marine sediment cores from the North Atlantic and the Nordic Seas play a crucial role as archives of DO events, and the identification of the mechanisms controlling DO events.

1.3 The North Atlantic Region today and during MIS3

Modern hydrography

The North Atlantic between 80 and 50°N comprises the Nordic Seas (Greenland, Iceland and Norwegian Sea) and the Labrador Sea (Figure 2A). The Nordic Seas are confined to the north by the Fram Strait and the Barents Sea, and to the south by the Greenland Scotland Ridge (GSR) (Drange et al., 2005). The inflow and outflow of the Nordic Seas occur mainly via two pathways: the Faroe-Shetland Channel and the Denmark Strait. Through the Faroe-Shetland Channel, warm Atlantic Water is flowing in via the North Atlantic Current (NAC) and cooler intermediate water masses of the Arctic Ocean flow out as Iceland Scotland Overflow Water (ISOW) (Daniault et al., 2016; Hunter et al., 2007; Straneo et al., 2012). Through the Denmark Strait, warm surface water is entering the Nordic Seas transported by the Irminger Current (IC). The outflow water is called Denmark Strait Overflow Water (DSOW). ISOW and DSOW are mixing with Labrador Sea Water along the East Greenland margin and form the Deep Western Boundary Current (DWBC), which enters the North Atlantic as North Atlantic Deep Water (NADW) (Hunter et al., 2007; Straneo et al., 2012). The DWBC

currently resides between 1900 and 3000 m water depth and can also contain Antarctic Bottom Water (Hunter et al., 2007; McCave & Tucholke, 1986). As the DWBC passes the southern tip of Greenland towards the Labrador Sea, it slows down and suspended sediments are deposited at the Eirik Drift (Hunter et al., 2007; McCave & Tucholke, 1986). At the Eirik Drift, the East Greenland Current (EGC), which exports Arctic freshwater and sea ice through the Denmark Strait (Hopkins, 1991), turns northwards following the West Greenland margin as the West Greenland Current (WGC). From the northern limit of the Baffin Bay, the Labrador Current (LC) transports cold and fresh surface water along the Canadian Shelf towards the subpolar gyre into the North Atlantic (Daniault et al., 2016; Lazier, 1973). The subpolar gyre plays a crucial role for the water mass distribution in the North Atlantic (Figure 2A): warmer, saltier water from the Atlantic is advected northwards into the Nordic Seas (NAC) and westwards into the Labrador Sea (IC); in turn, freshwater from the Arctic (EGC) and from the Baffin Bay (LC) is exported into the northern North Atlantic (Born & Mignot, 2012; Hátún et al., 2005; Huck, 2010).

Paleoceaongraphy

Compared to present-day conditions, large parts of the Baffin Bay and the Nordic Seas were covered by sea ice. North America, Greenland, Eurasia and Iceland were covered by continental ice sheets during MIS3 (Figure 2B). Therefore, the oceanographic conditions of the North Atlantic and the Nordic Seas were highly variable and changes are associated with the climate states of the DO events.

Model and proxy studies suggest that the Atlantic Meridional Overturning Circulation (AMOC) had three modes during the DO events of the last glacial period: A) active deep-water convection in the Nordic Seas and the Labrador Sea during interstadials B) deep-water formation was reduced and shifted towards south of Iceland during stadials (Figure 2B) and C) an off-mode during exceptionally long and cold stadials (i.e. Heinrich Stadials) that occurred every 7 to 15 kyrs (Figure 1B) (e.g. Böhm et al., 2015; Henry et al., 2016; Rahmstorf, 2002). The different modes of AMOC were most likely freshwater-induced (Ganopolski et al., 2010; Rahmstorf, 2002).

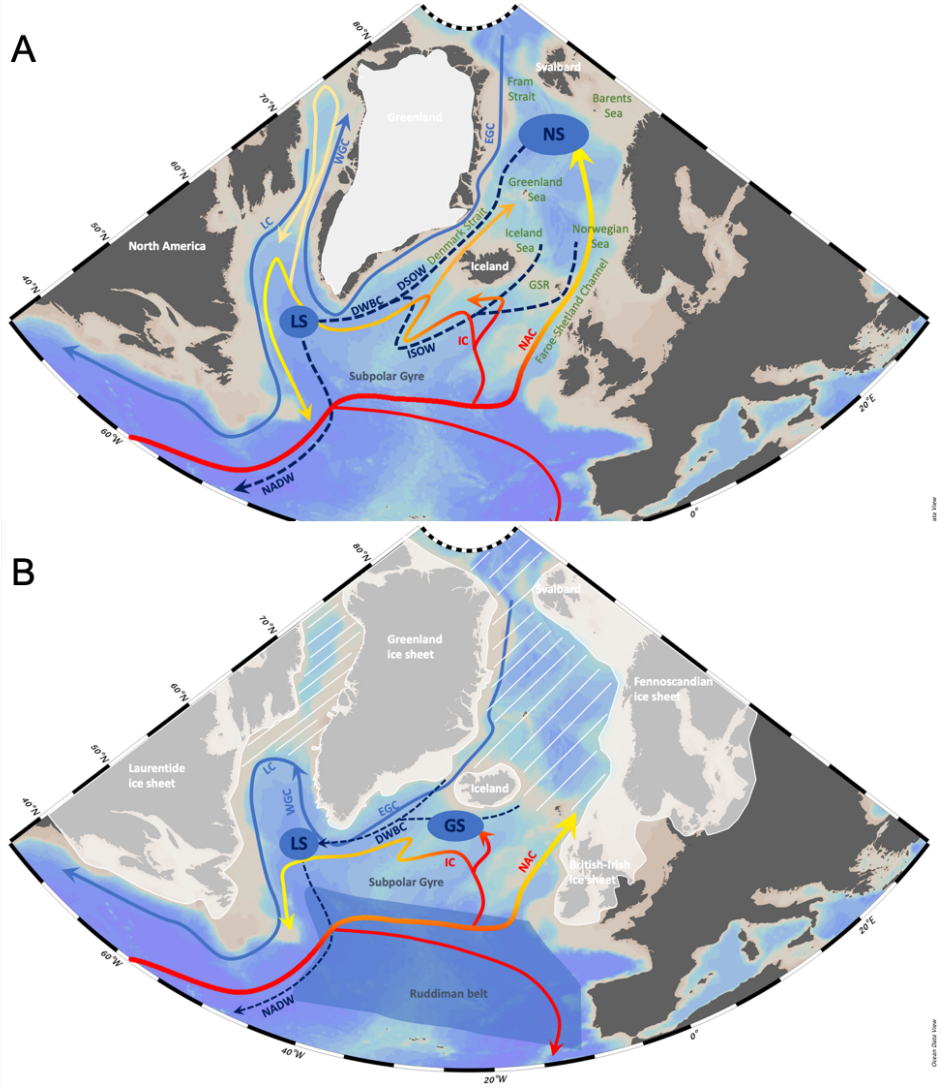

Figure 2: Map of the northern North Atlantic under A) modern and B) glacial conditions (Ocean data view, Schlitzer, 2015) including surface (solid lines) (Straneo et al., 2012 and references therein) and deep-water currents (dashed lines, Hunter et al., 2007), the late MIS3 extent of the Greenland, Laurentide, Eurasian and Iceland ice sheets (modified after Patton et al., 2016 and references therein), and location of the Ruddiman Belt during MIS3 (shaded blue area 40-55°N, Ruddiman, 1977). White lines indicate potentially sea-ice covered areas (de Vernal et al., 2000; Müller et al., 2009; Sadatzki et al., 2019). Areas mentioned in the text (green, GSR: Greenland-Scotland Ridge) and locations of deep-water formation are indicated (blue shaded areas, LS: Labrador Sea; NS: Nordic seas; GS: Greenland Sea). Warm and saline surface currents: North Atlantic Current (NAC) and Irminger Current (IC). Cold and fresh surface currents: East Greenland Current (EGC), Labrador Current (LC) and West Greenland Current (WGC). Deep-water currents: North Atlantic Deep Water (NADW), Deep Western Boundary Current (DWBC), Denmark Strait Overflow Water (DSOW) and Iceland Scotland Overflow Water (ISOW). Arrows indicate flow direction.

Potential mechanisms controlling rapid climate shifts during glacial time

A) Freshwater dynamics

The salt oscillator hypothesis was first identified as a potential mechanism controlling DO events and eventually led to many climate modeling studies using freshwater hosing experiments to force abrupt climate change (Barker et al., 2015; Schmidt & Hertzberg, 2011). According to the salt oscillator hypothesis, melting of the Northern Hemisphere ice sheets (Figure 2B) occurred mainly during warm, interstadial conditions. The meltwater lowered the sea surface salinity in the North Atlantic and hence reduced the Atlantic meridional density gradient between high and low latitudes. In turn, less heat was transported northwards and the climate shifted to cold stadial conditions. Cooler temperatures, and less meltwater allowed for an increase in North Atlantic surface salinity, which in turn strengthened the AMOC leading to interstadial conditions (Schmidt & Hertzberg, 2011).

During interstadials, the Nordic Seas freshened due to melting and calving of the nearby Greenland and Fennoscandian ice sheets (Dokken et al., 2013; Rasmussen & Thomsen, 2013; Sessford et al., 2019). Nonetheless, the largest amount of freshwater was induced during Heinrich Stadials. Sediment core records from the Nordic Seas (Rasmussen et al., 1997; Voelker et al., 1998) and in particular from the Ruddiman Belt, located between 40 and 55°N in the North Atlantic (Figure 2B), reveal large meltwater peaks associated with Heinrich Stadials (Vidal et al., 1997). These meltwater events were caused by the collapse of Northern Hemisphere Ice Sheets, especially the Laurentide Ice Sheet that covered North America during MIS3 (Heinrich, 1988; Hemming, 2004; Rashid et al., 2003). The mechanisms behind the ice sheet collapse remain a matter of debate and comprise binge-purge mechanisms, sea level rise and subsurface warming (Hemming, 2004; Levine & Bigg, 2008; Peck et al., 2007; Scourse et al., 2009). Modeling studies demonstrate that warming of a subsurface layer is one dominating explanation for ice sheet collapse (Alvarez-Solas et al., 2013; Marcott et al., 2011). However, Barker et al. (2015) demonstrated that icebergs are not the trigger for stadial conditions. Instead, the Norwegian Sea or North Atlantic sea ice cover might have been one of the major drivers of DO events, in particular towards the abrupt nature of the changes (e.g. Dokken et al., 2013; Gildor & Tziperman, 2003; Jensen et al., 2016; Li et al., 2010; Sadatzki et al., 2019; Vettoretti & Peltier, 2018).

B) Sea ice dynamics

Marine records reveal that the abrupt transitions from stadial to interstadial conditions are marked by the retreat of sea ice, which is caused by a temperature overshoot in the subsurface of the Nordic Seas (Sadatzki et al., 2019; Sessford et al., 2019; Sessford et al., 2018). Climate models provide additional evidence of sea ice acting as a key mechanism for triggering DO events. For example, the model of Li et al. (2010) shows that, when heat is released from the ocean, the retreat of the Nordic Seas sea ice cover can result in abrupt atmospheric warming over Greenland. However, an extensive sea ice can prevent heat- and moisture loss to the atmosphere (Figure 3), and thereby cause a positive feedback mechanism. When heat is trapped below the sea ice, it accumulates in the ocean below the ice while the atmosphere cools. Above the warm subsurface layer, a strong salinity gradient (halocline) develops (Figure 3B). The halocline marks the boundary between the cold and fresh surface water mass and the warm and salty Atlantic Water mass below that enters the Nordic Seas at the subsurface (Dokken et al., 2013; Ezat et al., 2014). Above the halocline, a fresh surface water layer maintains the insulating character of the sea ice, similar to conditions in the Arctic Ocean today (Dokken et al., 2013; Rasmussen & Thomsen, 2004). Additionally, the surface albedo of ice is much higher compared to the ocean´s, and thus enhances the cooling effect during stadials.

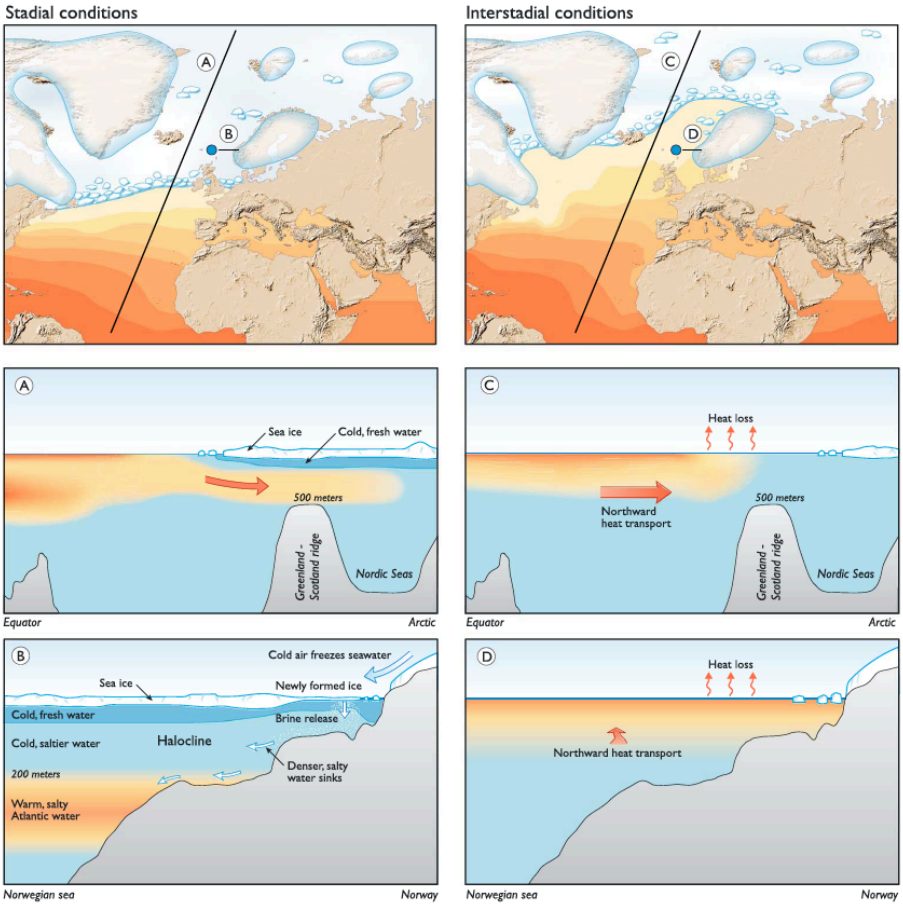

Figure 3: Schematic from Dokken et al. (2013) showing the role of the Nordic Seas sea-ice cover for water column stratification as well as heat and moisture supply to the atmosphere during Greenland Stadial (left) and Interstadial (right) conditions of MIS3.

During interstadials, sea ice can trigger negative feedback mechanisms. When the sea ice cover in the Nordic Seas retreats, the ocean surface can absorb more solar radiation leading to warmer surface water temperatures (Dokken et al., 2013; Ezat et al., 2014). The water column becomes less stratified and the warm subsurface layer shoals, allowing for vertical mixing (Dokken et al., 2013; Sessford et al., 2018). Heat is transported further northward to the Arctic Ocean and moisture can evaporate from the ocean´s surface, providing a source of precipitation towards the Greenland Ice Sheet (Li et al., 2010; Masson-Delmotte et al., 2005; Sadatzki et al., 2019).

During the interstadials of MIS3, oceanographic conditions in the Nordic Seas were most similar to those of today (Sessford et al., 2018). Although it was colder, the Norwegian Sea was seasonally ice-free (Dokken et al., 2013; Sadatzki et al., 2019) (Figure 3). During Greenland Stadials, however, large parts of the Nordic Seas were covered by a year-round (perennial) sea ice (Dokken et al., 2013; Sadatzki et al., 2019) (Figure 3).

1.4 The Northern Hemisphere Ice Sheets: MIS4 to MIS2

From MIS4 to the end of MIS2 (ca. 120-14 ka), Greenland, North America, large parts of Eurasia, and Iceland were covered by ice sheets. During the LGM (26-19 ka), the Eurasian Ice Sheet comprised the Fennoscandian Ice Sheet, the Svalbard-Barents-Kara Sea Ice Sheet and the British-Irish Ice Sheet (Figure 2B). Changes in the ice volume of the Northern Hemisphere Ice Sheets are associated with changing climatic conditions (Figure 4), and can be estimated from global mean sea level reconstructions. During the LGM, the sea level was ca. 120 m lower compared to present day climate conditions (Lambeck et al., 2014; Ruddiman, 2008; Siddall et al., 2003; Waelbroeck et al., 2002). At the same time, iceberg flux was roughly 20 times higher (4196 km^3/yr) than present day iceberg flux (225 km^3/yr) (Levine & Bigg, 2008). In the Northern Hemisphere today, icebergs are mainly discharged from the Greenland Ice Sheet. However, it remains a key challenge to differentiate the evolution of each individual ice sheet, and hence their contribution and sensitivity to climatic changes. One major limitation for the reconstruction of paleo-ice sheet configurations is that terrestrial and marine evidence was eroded or overprinted during the maximum ice extent of the LGM (Patton et al., 2016).

During the LGM, all ice sheets listed above had expanded far out to the shelf edge, making them more vulnerable to climate and sea level changes (Batchelor et al., 2019). Mechanisms such as a rising sea level or warmer ocean temperatures can destabilize marine ice shelves leading to increased iceberg calving events similar to calving events seen at the West Antarctic Ice Sheet today (Joughin & Alley, 2011). Modelling studies and observations show that the loss of a marine ice shelf can decrease buttressing, and thus increase ablation flow rates of the grounded ice sheet (Gudmundsson, 2013;

Joughin & Alley, 2011; Mouginot et al., 2015; Scambos et al., 2004). The grounded ice erodes the underlying bedrock, and icebergs transport the eroded material to the open ocean where it contributes to marine IRD deposits. The origin of IRD can be traced through geochemical fingerprinting (Andrews et al., 2014; Gwiazda et al., 1996; Hemming et al., 2000; White et al., 2016). This sedimentological evidence of past ice sheet growth and decay can, combined with terrestrial evidence (e.g. dating of moraines and other glacial deposits) and model simulations, give insights into the individual history of each ice sheet, and hence their sensitivity to climate change (Batchelor et al., 2019; Hesse, 2015; Hillaire-Marcel et al., 1994; Hughes et al., 2016; Stoner et al., 1998).

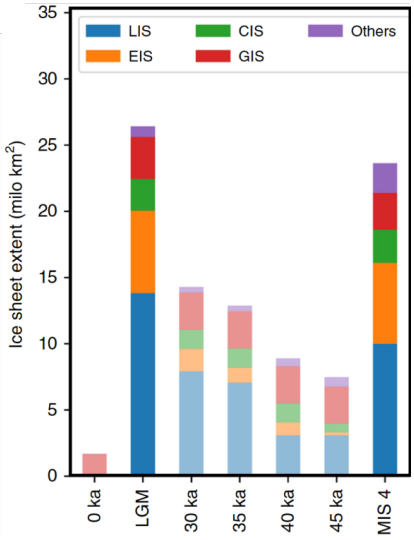

Figure 4: Bar chart of Northern Hemisphere Ice Sheet extent at seven time-slices through the last glacial cycle from Batchelor et al. (2019) with each bar comprising the Laurentide Ice Sheet (LIS), European Ice Sheet (EIS), Cordilleran Ice Sheet (CIS), Greenland Ice Sheet (GIS) and others. The low-saturation colored bars indicate MIS3 and modern-day time slices.

Laurentide Ice Sheet (LIS)

The LIS was the largest ice sheet (Figure 4, blue) in the Northern Hemisphere during MIS4, late MIS3 and during the LGM (Batchelor et al., 2019). During early MIS3 (50-42 ka), large parts of the eastern and central North American continent deglaciated, including the area around Hudson Bay, while the central and western regions remained glaciated (Dalton et al., 2016). Hence, the surrounding areas west and northeast of the Hudson Bay might have been the main contributing areas to the Ruddiman Belt

Heinrich (H) layers H5 and H4 (Dalton et al., 2019). Substantial continental glaciation started between 44 and 42 ka, just prior to H4, and was probably caused by atmospheric circulation changes (Dalton et al., 2016; Pico et al., 2018). Although the Hudson Bay remained ice-free between ~43.7 and 35 ka (McMartin et al., 2019), the LIS might have reached LGM limits between 40 and 30 ka possibly with a brief retreat between 30 ka to 27 ka (Dyke et al., 2002). The maximum extent of the LIS was reached between 24 and 23 ka in the northwest, south and northeast, and between 21 and 20 ka in the far north and southwest. The onset of substantial retreat started at ca. 14 ka in the northwest, southwest and southeast, and ca. 3 kyrs later in the northeast (Dyke et al., 2002).

During the period of substantial ice sheet growth between 45 and 28 ka, five LIS meltwater events are recorded in the Gulf of Mexico, that are interpreted as summer melting associated with warming in the Antarctic (Hill et al., 2006). During the LGM and the deglaciation, the Gulf of Mexico, the Arctic Ocean and the North Atlantic including the Labrador Sea were the main drainage areas for meltwater and icebergs. Margold et al. (2015) found 117 ice streams of which ~20 were located along Baffin Bay (including Hudson Strait) and ~13 along the Labrador Peninsula (including the Gulf of St. Lawrence). The Hudson Strait and the Gulf of St. Lawrence are the two most prominent sources for Ruddiman Belt Heinrich Layers (Hemming, 2004). Major calving events of the LIS occurred every seven kyr-cycle during Heinrich Stadials rather than during DO oscillations (MacAyeal, 1993). However, iceberg calving of the north-eastern LIS occurred on millennial time scales (Andrews & Barber, 2002; Simon et al., 2014).

Greenland Ice Sheet (GrIS)

While the GrIS is the largest ice sheet in the Northern Hemisphere today (Figure 4, red), it was only the third largest during MIS4 and the LGM, and the second largest during MIS3 (Batchelor et al., 2019). The model output of Batchelor et al. (2019) suggests a relatively stable extent of the GrIS for the time period from MIS4 to MIS2. However, Greenland was not equally covered by ice and the ice margins were highly sensitive to rapid climate oscillations, especially at the ice-ocean-interface (Alley et al., 2010; Bradley et al., 2018; Vasskog et al., 2015). Hence, calving events or deglacial

retreat of Greenland margins are often associated with sea level changes or subsurface warming (Knutz et al., 2011; Simon et al., 2014). During MIS4, when the sea level was approximately 80 m below present values (Ruddiman, 2008; Siddall et al., 2003; Waelbroeck et al., 2002), the eastern and southwestern margins probably extended beyond the continental shelf edge, reaching an extent comparable to the LGM (Hansen et al., 1999; Seidenkrantz et al., 2010). After a phase of ice sheet decay, a slow but constant growth of the GrIS was suggested to have occurred during MIS3 (Alley et al., 2010; Ganopolski et al., 2010). Consequently, the continental shelf was reached a second time at ca. 31 ka in the north and southeast, and around 21 ka in the southwest to northwest (Funder et al., 2004). The deglaciation of the GrIS started at ~20 ka in the northeast, and at ~16 ka in the southern Greenland fjords (Funder et al., 2011).

Outlet glaciers in Greenland fjords are a major source for icebergs, and thereby also for IRD. During the last glacial period, the GrIS had five major drainage areas, three along the western margin and two along the eastern margin (Andrews, 2000). Today, two major iceberg calving areas remain: Scoresby Sund (70°N) in East Greenland and Disko Bay (70°N) in West Greenland (White et al., 2016).

Eurasian Ice Sheet (EIS)

During MIS4 and the LGM, the EIS was the second largest ice sheet in the Northern Hemisphere (Figure 4, orange) (Batchelor et al., 2019). During MIS4, the northern and western Eurasian continental margins were most likely ice covered, while southern Scandinavia and the Barents and Kara Seas were ice-free (Siegert et al., 2001). In the beginning of MIS3 (at 56 and 50 ka), the EIS was separated into several different ice sheets. The Scandinavian part of the EIS, for example, had probably retreated to a large extent while the British Irish Ice Sheet was at moderate size, and the ice sheet that covered Svalbard remained comparable to present-day conditions until ca. 30 ka (Hughes et al., 2016; Peck et al., 2007; Scourse et al., 2009; Siegert et al., 2001). From ca. 40 ka these ice sheets grew and developed a joint ice margin between 29 and 25 ka, which reached from Ireland to Svalbard (Sejrup et al., 2009). At that time, the EIS consisted of the Fennoscandian, Svalbard-Barents-Kara Sea, and British-Irish Ice Sheets. The westernmost EIS reached the continental shelf between 27 and 26 ka, and the eastern part between 20 and 19 ka. The Fennoscandian and British-Irish Ice Sheets

merged at ca. 27 ka, and the gap to the Svalbard-Barents-Kara Sea complex was closed at ca. 24 ka. The EIS reached its maximum extent between 23 and 21 ka (Hughes et al., 2016; Patton et al., 2016). The subsequent retreat was complex and highly asynchronous controlled by internal dynamics and response-mechanisms to changes in oceanic conditions and climate (Patton et al., 2017a). As a result, the North Sea and Atlantic margins were already retreating during maximum ice sheet extent while the ice sheet along the eastern margins was still advancing until ca. 20 ka (Patton et al., 2016). The Barents Sea complex experienced the most rapid retreat afer 18 ka, whereas the other parts of the EIS most likely melted equally from around 15 ka. The complex topography of north-western Eurasia caused the development of several patchy ice sheets, similar to the conditions during early MIS3 (Hughes et al., 2016; Patton et al., 2017a).

Iceland Ice Sheet (IIS)

Due to its location on an active mantle plume and its ocean proximity, the IIS is a relatively fast and dynamic ice sheet (Andrews, 2008). Most likely, the IIS was larger during MIS4 compared to MIS3 (Andrews, 2008). Empirical data and modelling approaches suggest that the IIS reached the continental shelf prior to the onset of the LGM, at ca. 28 ka, and had an active calving margin (Hubbard et al., 2006; Patton et al., 2017b). The retreat of the marine ice shelf, which was triggered by climate warming, started at ca. 21.8 ka and took just 5 kyrs. The retreat was subsequently followed by a 2 kyr-period of stable mass balance until a second major collapse occurred around 15 ka, where the remaining onshore ice disappeared (Andrews, 2008; Patton et al., 2017b). Largely ice-free inner shelves in North and West Iceland during the deglacial were also documented by AMS ^{14}C dates (Andrews et al., 2000).

1.5 Proxy Overview

In paleoceanography, the use of proxies and archives is essential to reconstruct the Earth´s climate of the past. In order to study ocean-ice-atmosphere interactions multiple proxies and archives need to be combined (Figure 5). For example, the $\delta^{18}O$ signature in ice cores from the Greenland Ice Sheet as well as in the water column of the Nordic Seas is more negative during the stadials than during the interstadials of

MIS3. The oscillations of $\delta^{18}O$ values in Greenland ice cores can be aligned to the oscillations observed in the North Atlantic, helping us to constrain age models for marine sediment cores. Proxies such as planktic foraminifer and IRD concentrations as well as biomarkers can be used to reconstruct past sea ice extent thereby suggesting that interaction between the ocean and the atmosphere at high latitudes was most likely reduced during stadials (Dokken et al., 2013; Elliot et al., 1998; Sadatzki et al., 2019; Voelker et al., 1998). This reduction was caused by extensive sea ice (Figure 5). During interstadials, atmospheric temperatures were warmer than during stadials (Huber et al., 2006) and sea ice proxies suggest that Atlantic Water was advected to high latitudes and heat from the ocean was released to the atmosphere (Dokken & Jansen, 1999; Sessford et al., 2019). Past sea surface and atmospheric conditions in the North Atlantic region can be reconstructed by combining quantitative and qualitative measuring approaches.

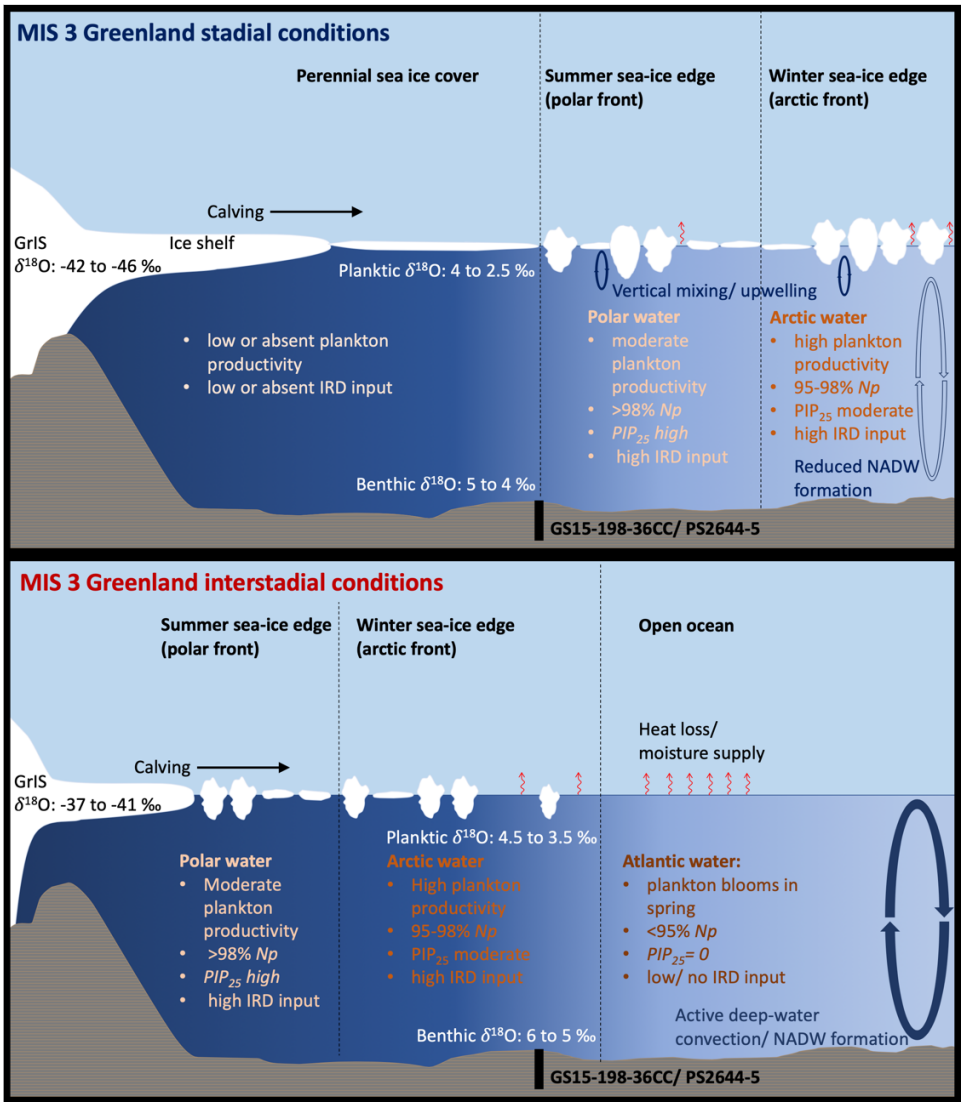

Figure 5: Schematic illustration of ocean-ice-atmosphere interactions east of Greenland during Greenland Stadials (GS, top) and Interstadials (GI, bottom) throughout Marine Isotope Stage 3 (MIS3). Range of oxygen isotope ratios refers to NGRIP (NGRIP, 2004), GS15-198-36CC (Sessford et al., 2018) and PS2644-5 (Voelker et al., 1998) for ice ($\delta^{18}O$ SMOW), benthic and planktic foraminifers ($\delta^{18}O$ VPDB), respectively. Location of oceanic fronts, strength of convection, levels of phyto- and zooplankton productivity inferred from brassicasterol, dinosterol, foraminifers and diatom flux after (Griem et al., 2019; Hoff et al., 2016; Johannessen et al., 1994; Müller et al., 2011). During GS the ocean surface is mainly influenced by the cold, fresh East Greenland Current (polar water) while during GI the influence of the warmer, saltier Irminger Current increases resulting in Arctic and Atlantic Water masses. GrIS: Greenland Ice Sheet; IRD: ice-rafted debris; NADW: North Atlantic Deep Water; Np: planktic foraminifer species Neogloboquadrina pachyderma.

Stable isotope composition of foraminifer tests (Paper I-III)

The planktic $\delta^{18}O$ signal is a function of salinity and temperature with low values indicative of warmer or fresher water masses (Johannessen et al., 1994). Oscillations in planktic $\delta^{18}O$ values reflect climate forcing and ice sheet response (Alley et al., 2010). Planktic $\delta^{13}C$ is a proxy for changes in productivity whereby low values refer to glacial periods. While benthic $\delta^{18}O$ records document changes in global sea level and ice volume (Lambeck & Chappell, 2001), benthic $\delta^{13}C$ is often used as a proxy for ventilation changes of deep-water masses.

Concentration and flux of foraminifers (Paper I & III)

The planktic foraminifer concentration is a proxy for sea surface productivity. The abundance of planktic foraminifers at high and mid-latitudes is mainly driven by nutrient supply and light. Light is not only influenced by the seasons but also by the thickness of the local sea ice cover. Highest concentrations of planktic foraminifers appear in upwelling regions (i.e. along the summer or winter sea ice edge, in polynyas or close to large icebergs) (e.g. Kohfeld et al., 1996; Ramseier et al., 2001; Smith et al., 2007) (Figure 5). Ice-free waters off the sea ice margin can also contain high concentrations of planktic foraminifers although food availability is often limited. Absence of planktic foraminifers in the sediment is most likely characteristic for a perennial sea ice cover due to the lack of nutrients and light (Dowdeswell et al., 1998). Flux rates are calculated from the foraminifer concentrations by correcting for changes in sedimentation rates.

Planktic foraminifer assemblage (Paper I)

At high to mid-latitudes, the assemblage of planktic foraminifers is mainly driven by the sea ice extent, salinity and temperature of the water masses (Figure 5). For the coldest water masses (Polar Water) close to the summer sea ice edge (polar front), which are covered by sea ice throughout most of the year, the assemblage consists almost entirely of the species *N. pachyderma* (formerly referred to *N. pachyderma* sinistral) (Johannessen et al., 1994; Pflaumann et al., 1996; Simstich et al., 2003). The oceanic polar front reflects the boundary between low salinity Polar and saltier Arctic Water masses (Johannessen et al., 1994). For Arctic Waters in the movement area of the winter sea ice edge (arctic front), the planktic foraminifer assemblages are

dominated by species *N. pachyderma* (Figure 5), however *N. incompta* (formerly referred to as *N. pachyderma* dextral) is a common species as well in the assemblage representative of Arctic Waters (Johannessen et al., 1994; Pflaumann et al., 1996). The boundary between cold Arctic and warm Atlantic Water masses is defined as the arctic front (Johannessen et al., 1994). In Atlantic Water, the presence of sub-arctic species like *N. incompta*, *Turborotalita quinqueloba*, *Globigerina bulloides* or *Globigerinita uvula* increases (Johannessen et al., 1994; Pflaumann et al., 1996).

Concentration and flux of IRD and petrologic tracers (Paper I-III)

In general, IRD (mineral grains >150 μm) can be used as a proxy for iceberg discharge from continental ice sheets. The IRD input is dependent on the number of icebergs that are transported to, and the melting at a specific core location as well as on the load of sediment in the ice (Reeh, 2004). Iceberg routes and travel distances are controlled by sea surface temperature, sea ice thickness and extent, surface currents and wind stress (Reeh, 2004). Reeh (2004) suggests the following interpretations of higher IRD concentrations: 1) faster flow of ice from an adjacent ice sheet; 2) flow of ice containing more clasts; 3) loss of an ice shelf which would allow calving of icebergs bearing more debris; 4) cooling of ocean waters that allows icebergs and their debris to be transported longer distances; 5) loss of extensive coastal sea ice that allows icebergs to reach sites more rapidly; and 6) alterations in currents or winds that control iceberg drift tracks. Proximal iceberg sources are more likely, compared to distant ones, to dominate the IRD provenance (Andrews et al., 2017; Andrews & Vogt, 2014; Andrews et al., 2014; Bigg et al., 1996). Still, a precise distinction between IRD transported by sea ice or by icebergs remains open. Nonetheless, the majority of the material transported by sea ice seems to be finer grained (Goldschmidt et al., 1992; Lisitzin, 2012; Nürnberg et al., 1994).

Besides high concentrations of IRD in the Ruddiman Belt, the Heinrich layer deposits have other distinct features: (1) The layers are diluted in foraminifer content due to low productivity in the surface water; (2) the foraminifer assemblages are dominated by polar species *N. pachyderma;* (3) relatively high magnetic susceptibility due to large average grain sizes; (4) relatively low sea surface temperatures; and (5) the debris is dominated by detrital carbonate (Heinrich, 1988; Hemming, 2004; Hillaire-Marcel et

al., 1994). Analyzing the provenance of the deposited grains allows fingerprinting of the grains to their respective origin. Detrital carbonate is associated with icebergs derived from North America while volcanic grains or hematite-stained quartz can be used as petrological tracers for IRD from Iceland and the circum-Arctic region (e.g. Svalbard) (Verplanck et al., 2009). Possible source areas can also be investigated by analyzing certain XRF ratios (e.g. Ca/Sr) or geochemical tracers (Pb-isotopes, Sm-Nd etc.) (Channell & Hodell, 2013; Farmer et al., 2003; Gwiazda et al., 1996; Hemming et al., 2000; Innocent et al., 2000).

Pb-isotopes (Paper II)

The isotopic composition of $^{207}Pb/^{204}Pb$ and $^{206}Pb/^{204}Pb$ ratios measured in single-grain K-feldspars allows for a differentiation between several bedrock provinces (Gwiazda et al., 1996; White et al., 2016). Following Gwiazda et al. (1996) and White et al. (2016), $^{206}Pb/^{204}Pb$ isotope ratios can be roughly classified as Archean, Proterozoic and Caledonian terrains when ratios are <14.5, ~14.5-18 and >18, respectively.

Biomarkers (Paper III)

Biomarkers such as IP_{25} can be used as a direct proxy for sea ice extent (Belt et al., 2007). IP_{25} is a highly branched isoprenoid monoene that is produced during spring by specific sea ice diatoms (*Haslea* and *Pleurosigma*) (Belt et al., 2007). While an increased abundance of IP_{25} in the sediment reflects a seasonal sea ice cover at the core site (Figure 5), absent IP_{25} can be interpreted as open ocean conditions or perennial sea ice cover (Belt et al., 2007; Belt & Müller, 2013). To improve the ambiguity of IP_{25}, the proxy is often combined with the open-water phytoplankton biomarkers dinosterol (produced by marine dinoflagellates) and brassicasterol (produced by marine, freshwater and sea-ice diatoms and coccolithophores) (e.g. Belt et al., 2013; Fahl & Stein, 2012; Müller et al., 2009; Sadatzki et al., 2019; Volkman et al., 1993). This combination allows for a semi-quantitive sea ice reconstruction and is refered to as the phytoplankton-IP_{25} index (PIP_{25}, Müller et al., 2011). PIP_{25} values vary between 0 and 1, with 0 indicating open-ocean conditions and 1 indicating a perennial sea ice cover.

Deuterium-excess (Paper III)

D-excess of water/ice is a proxy for moisture source conditions as a result of kinetic effects occuring during evaporation. Relative humidity with respect to sea surface

temperatures at the moisture source location is the dominant control mechanism (Steen-Larsen et al., 2014). A retreat of sea ice in the high-latitude Northern Hemisphere could therefore create local moisture sources for the Greenland Ice Sheet which could be reflected in the d-excess and $\delta^{18}O$ records in Greenland ice cores (Klein et al., 2015; Kopec et al., 2016).

2 Thesis Approach and Objectives

This thesis is part of the multi-disciplinary ERC Synergy project Ice2Ice. A major focus of this project lays in the Arctic and subarctic sea ice and Greenland Ice Sheet sensitivity to past abrupt climate variability, and whether these changes were similar to the modern anthropogenically forced changes. The approach of this thesis changed across the duration of the study period due to various difficulties that arose. Therefore, the section is divided into the initial and revised thesis approach.

Initial thesis approach

During the last decades the Earth´s atmosphere and the ocean´s surface have warmed by 0.85 °C (2003-2012) and 0.11 °C per decade (1971-2010), respectively (IPCC, 2013). Consequently, the annual mean Arctic sea ice extent decreased by up to 4.1 % per decade (1979-2012) and the Greenland Ice Sheet lost ~215 Gt yr^{-1} of ice between 2002 and 2011 (IPCC, 2013). This loss of continental ice not only contributes to sea level rise, it may also alter ocean circulation and global climate (Rahmstorf, 2003). Rahmstorf et al. (2015) hypothesized a cooling trend during the late 20th and early 21st centuries in the North Atlantic that might have been triggered by a reduction in the AMOC, especially after 1970. If it exists, an enhanced flux of meltwater from sea ice and the Greenland Ice Sheet into the Nordic Seas and the Labrador Sea is the most likely driver of AMOC weakening (Figure 2). The latter areas are also the key areas for deep-water formation in the North Atlantic (Rahmstorf et al., 2015; Thornalley et al., 2018). However, whether this reduction is a reality, and its potential relation to anthropogenic warming, remains a matter of debate (Thornalley et al., 2018). The time period covered by observations is too short to investigate variabilities of longer timescales or for the development of climate models with a high confidence level in future scenarios (IPCC, 2013). In order to be able to explain the dynamics (triggers and consequences) of abrupt climate changes, and thus improve climate model predictions, paleoceanographic data from key locations is required.

The present abrupt climate change may be similar to the DO events (IPCC, 2013), which occurred during the last glacial period and were particularly pronounced during late MIS3 due to the demise of sea ice cover (Jansen et al., 2020). As part of this thesis,

multi proxy records were generated covering the time interval from late MIS4 to the Holocene using sediment cores from the Greenland margin and rise (section 0). By analyzing stable isotopes in benthic foraminifers ($\delta^{18}O$ and $\delta^{13}C$) combined with benthic foraminifer assemblages and grain size-related proxies (sortable silt and magnetic susceptibility) we aim to reconstruct the strength and composition (ISOW & DSOW, section 1.3) of the DWBC over several DO events. Hodell et al. (2010) suggest that during Greenland Interstadials that followed Heinrich Stadials, the ISOW and hence DWBC were stronger than during stadials. The higher current strength indicates an enhanced deep-water formation/strong AMOC. A strong DWBC is characterized by high benthic $\delta^{13}C$ values, increased grain size and high magnetic susceptibility due to increased ventilation, higher current velocity, and hence increased remobilization of magnetic material from the Reykjanes ridge south of Iceland (Hodell et al., 2010; Kissel et al., 1999; Kissel et al., 2008; Stoner et al., 1998).

Additionally, as different foraminiferal species prefer different environmental conditions, the faunal distribution of benthic foraminifers can indicate past bottom current characteristics. For example, high concentrations of the foraminifer species *Uvigerina* were proposed as a proxy for low oxygen levels (Ledbetter & Balsam, 1985). Likewise, a dominance of agglutinated foraminifers can be indicative of corrosive bottom waters (Seidenkrantz, 2013). It was suggested that the presence of species that respond to nutrient availability may be linked to sea ice margins (Figure 5) that are associated with high productivity (e.g. Kohfeld et al., 1996; Ramseier et al., 2001; Seidenkrantz, 2013; Smith et al., 2007).

However, the sediment deposited on the Greenland Rise during MIS3 contained many different benthic foraminifer species but too few specimens (Supplementary material, Table 2) for the reconstruction of the changing environmental conditions during DO events. Where applicable, in order to investigate the relationship between deep-water formation and changes in bottom water temperatures, benthic isotopes were measured and combined with benthic Mg/Ca measurements (Supplementary material, Figure 10). Sortable silt and magnetic susceptibility measurements, performed on the same sediment samples, turned out to be mostly affected by the trends of IRD input (Supplementary material, Figure 8). Therefore, both proxies were unsuitable for

reconstructing current speed variability. Additionally, very low amounts of biomarkers did not allow for a qualitative reconstruction of past sea ice variability (data from Henrik Sadatzki, personal communication (Supplementary material, Figure 8)). Due to the mentioned difficulties, the focus of this thesis shifted to the reconstruction of sea surface conditions.

Revised thesis approach

The multi-proxy approach of this thesis aims to improve our knowledge about the variability of sea ice extent, oceanic frontal systems, iceberg trajectories and meltwater input in the Labrador and Nordic Seas in correspondence to DO events. In Paper I, we use planktic stable isotope measurements, foraminifer and IRD fluxes combined with planktic foraminifer assemblages in order to reconstruct meltwater events, calving events, sea ice variability and corresponding changes of sea surface temperature in the northeastern Labrador Sea. We cover a time interval of ca. 40 kyrs (~65-25 ka b2k) with a 200-year resolution including 17 DO cycels and four Heinrich Stadials. Furthermore, to evaluate changes in surface circulation and oceanic frontal systems, we compare our results to published data from the East-Greenland margin. In Paper II, we analyze the IRD record from the northeastern Labrador Sea (Paper I) in great detail by investigating varying concentrations of different petrological tracers (carbonate concentration, hematite stained quartz and volcanic grains) and single grain K-feldspar Pb-isotope analyzes of each IRD peak. Paper II aims to identify the origin of the deposited IRD during Greenland Stadials and Interstadials between 65 and 25 ka b2k, and to discover any trends in iceberg trajectories or changing meltwater contributions of the Northern Hemisphere Ice Sheets. Paper III uses the data of Paper I, complemented by new data from the Greenland margin (stable isotopes, IRD and foraminifer concentrations), from several other proxy records from the North Atlantic, and from the GRIP ice core. The investigations focus on the DO events of late MIS3 (41-26 ka b2k) and the LGM (26-19 ka b2k). Altogether, data of 17 marine sediment cores from the Labrador Sea, the Nordic Seas and the subtropical North Atlantic are put into context of the GRIP ice core $\delta^{18}O$ and deuterium-excess records. The aim is to identify potential links between the GRIP deuterium-excess record and sea ice extent in the Nordic Seas and North Atlantic during the MIS3 DO events and the LGM.

Objectives

The multi-proxy approach presented here, aims to provide new insights into Arctic sea ice and Greenland Ice Sheet variability during past abrupt climate changes. The main focus lays on oceanographic changes in the northeastern Labrador Sea between late MIS4 and MIS2 (~65-19 ka b2k). In order to set this high-resolution attempt into a wider context, proxy records from ice cores as well as several marine sediment cores from the northern North Atlantic are used for comparison to our results. This comparison sheds light on the climate dynamics driving or driven by the DO oscillations during the last glacial period. The objectives of this thesis are:

(1) Describe the calving processes, freshwater input and sea ice cover in the northeastern Labrador Sea during the DO events between 65 and 25 ka by combining high-resolution stable isotope measurements, foraminifer and IRD concentration records, and planktic foraminifer assemblage counts.

(2) Try to connect the millennial-scale climate sensitivity of the Eurasian, Icelandic and Greenland Ice Sheets to the large collapsing events of the Laurentide Ice Sheet that occurred every 7-15 kyrs. Furthermore, to test whether those calving processes have a common underlying mechanism. To investigate this, we perform a provenance study of our high-resolution IRD record from the northeastern Labrador Sea.

(3) Refine the variability of the oceanic frontal systems along the East Greenland margin and in the Nordic Seas during Greenland Stadials, Greenland Interstadials and the LGM to evaluate changes in moisture sources for ice sheet growth in the Northern Hemisphere.

(4) Synergize sea surface conditions using indirect (i.e. foraminifer and IRD abundance, stable isotope measurements) and direct sea ice proxies (biomarkers) from sediment cores located in the North Atlantic and Nordic Seas. In order to investigate potential links between ice and sediment core records, we compare the findings to the deuterium-excess from the GRIP ice core.

3 Material and Methods

The multi-proxy approach of this thesis was conducted using two sediment cores: GS16-204-18CC (hereafter 18CC) from the Irminger Sea and GS16-204-22CC-A (hereafter 22CC) from the northeastern Labrador Sea. Magnetic susceptibility (MS) and X-ray fluorescence (XRF) was performed on both cores for the entire core length. Furthermore, stable isotope measurements, radiocarbon dating, foraminifer and IRD abundance counts and sortable silt (SS) were performed whereby the same methods were applied but depth intervals and resolutions differ for the sediment cores. In core 22CC benthic and planktic foraminifer assemblages were counted, stable isotopes and Mg/Ca ratios in benthic foraminifers were measured and Pb-isotopes as well as Scanning Electron Microscope (SEM) measurements were analyzed using selected samples.

Paper I contains stable isotope measurements, planktic foraminifer and IRD concentrations as well as planktic foraminifer assemblage counts covering the depth interval between 200 and 530.5 cm of core 22CC. In Paper II, an IRD provenance study of the IRD peaks observed in the same depth interval was performed using results from XRF analyzes, Pb-isotope measurements and SEM. Paper III comprises IRD and planktic foraminifer concentration counts analyzed in depth interval 170-314 cm in core 22CC and 45-410 cm in core 18CC.

The data that is not part of the papers are shown in the Supplementary material of this thesis (sortable silt: Figure 8; Mg/Ca and benthic isotopes: Figures 9 and 10, radiocarbon dates: Table 1; benthic foraminifer assemblage counts: Table 2). The MS, XRF and Mg/Ca ratios will be made available at the Pangaea data base.

Sediment core locations

Both deep-sea sediment cores 18CC and 22CC were retrieved in 2016 with research vessel R/V *G.O. Sars* (ice2ice, 2016). Core 22CC (58° 02.83 N, 47° 02.36 W) is located on the Greenland Rise, ca. 290 km off Cape Farewell, as part of the Eirik Drift, whereas core 18CC (60° 01.84 N, 40° 33.45 W) is located further to the NE on the East Greenland margin (Figure 6). Under modern conditions, both locations are influenced by the same water masses (section 1.3), outside the winter sea ice extent, and south of

the polar front (Figure 6B). At the surface, the water mass characteristics are influenced by the cold, fresh East Greenland Current and the warm, saline Irminger Current (Figure 6A, C). The Labrador Sea Water (LSW; ~3-4°C; ~34.85 psu; 27.74–27.80 kg/m^3; 4-8 Sv) represents the major intermediate water mass and below, a mixture of Denmark Strait Overflow Water (<1.5°C; ~34.9 psu; >27.88 kg/m^3; 2.9-10 Sv) and Iceland Scotland Overflow Water (~-0.5°C; ~34.92 psu; 28.07 kg/m^3; 2-3 Sv) forms the Deep Western Boundary Current (Hunter et al., 2007). Due to deeper water depths in core 22CC, this site can also be influenced by Antarctic Bottom Water (AABW: ~2°C; ~46 kg/m^3; low O_2 ;high Si; 1-2 Sv).

The conductivity-temperature-density (CTD) measurements, which were taken simultaneously to the sediment core recovery, show a temperature range between 10 °C and 8.8 °C, salinities vary between 34.83 psu and 34.6 psu at the surface of sites 18CC and 22CC, respectively (Figure 7). Stoner et al. (1998) suggested sedimentation rates of >30 cm/kyr during the Holocene and 7-10 cm/kyr during glacial periods for the Greenland Rise (22CC). This makes the retrieved core at the Greenland Rise highly suitable for high-resolution investigations of MIS3 DO events.

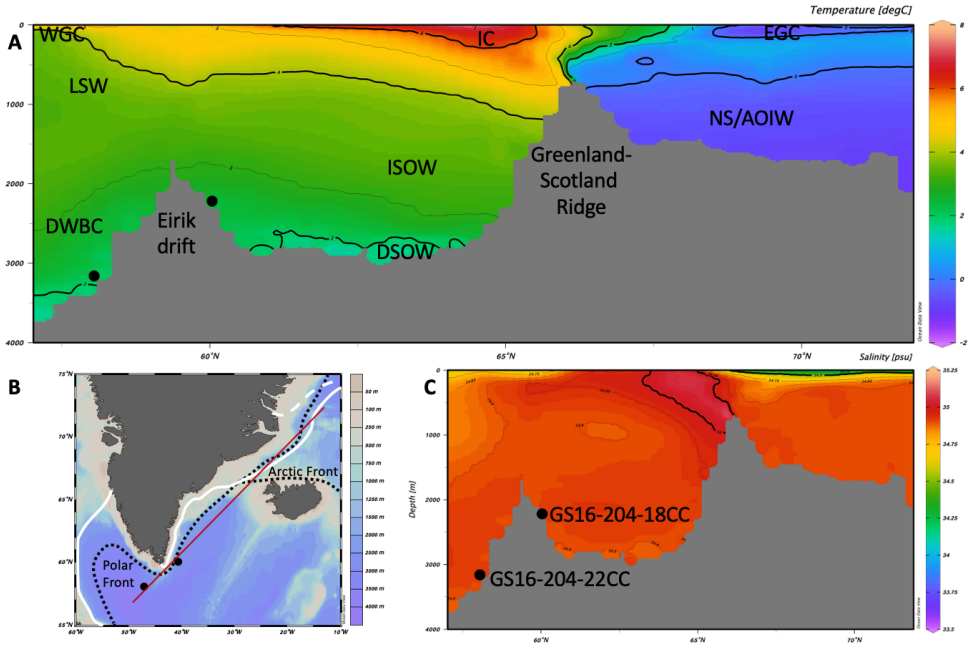

Figure 6: Transect (red line) along the East Greenland Margin (Ocean Data View, Schlitzer, 2015) covering the core locations (black dots) of GS16-204-22CC-A and GS16-204-18CC. A) Water temperature with the names of the main currents and water masses (Hunter et al., 2007): East Greenland Current (EGC), Norwegian Sea/Arctic Ocean Intermediate Water (NS/AOIW), Irminger current (IC), Iceland Scotland Overflow Water (ISOW), Denmark Strait Overflow Water (DSOW), West Greenland Current (WGC), Labrador Sea Water (LSW) and Deep Western Boundary Current (DWBC). B) Map of study area with the location of the March (white line) and September (white dashed line) sea ice extent and arctic and polar front (black dotted line) from (Fetterer, 2017). C) Salinity profile throughout the water column.

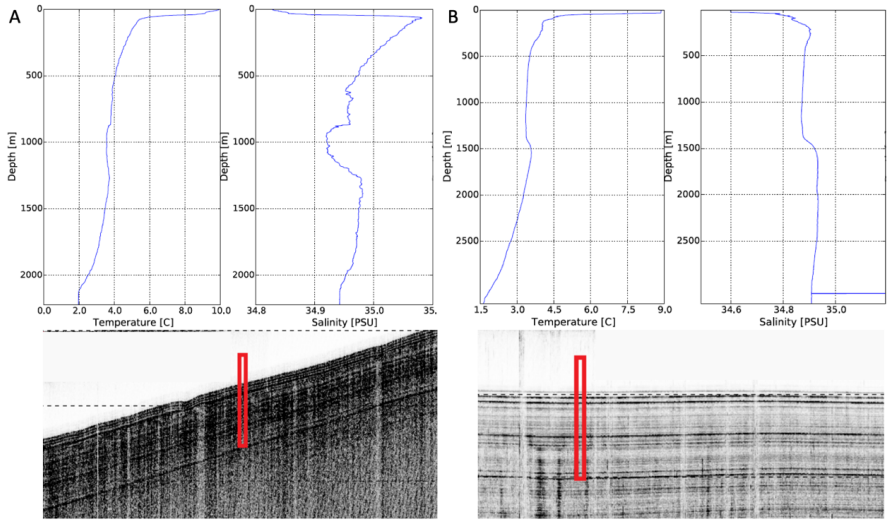

Figure 7: CTD and seismic profiles (ice2ice, 2016) for core sites GS16-204-18CC (A) and GS16-204-22CC-A (B).

Sediment description, sampling, sample preparation and analysis of fine fraction

Calypso core 22CC recovered 1964 cm of sediment from the Greenland Rise (Figure 6) and spans a time range from the early Holocene to approximately late MIS5. The approximate age of the oldest sediment of core 22CC is based on a distinct red layer at 1670 cm which probably points to the Eemian. This presumption is based on previous works which define this red layer in sediment cores from the Labrador Sea and Orphan Knoll (e.g. Nicholl et al., 2012). The sediment texture varies between layers of brownish silty sand and grey colored sandy silt or silty clay. The transitions between these layers are gradual and show signs of bioturbation. Some dark grey lines and larger gravel of up to 2 cm in size were observed, indicating iceberg transport. The water content varies between 37 and 56 % between 0-200 cm and 24 and 66 % between 200 and 530.5 cm in 22CC. The lowest values are associated with the highest number of iceberg-transported material.

The 1861 cm long calypso core 18CC (Figure 6) most likely has a similar resolution as 22CC, although it does not cover the Holocene. In the analyzed core sections (0-700 cm) sediment packages alternate between brown silty clay and gray, coarser material with drop stones, partly consolidated with a higher water content. The water content between 0 and 500 cm has a range of 22 to 53 %.

Both cores were sampled with a sample width of 0.5 cm, following the same strategy. From 0-200 cm, 18CC and 22CC were sampled every 5 cm and at 0.5 cm steps between 200-500 cm for 18CC and 200-530.5 cm for 22CC. Each sample was split into one-third for tephra analyzes (not this study) and benthic assemblage counts and two-thirds for stable isotope analyzes, abundance counts etc. (see methods below). The bulk samples for the latter methods were weighed before and after freeze drying and wet sieved over a 63 µm-sieve, whereby the fine fraction was captured. The coarse fraction was dry sieved into size fractions 63-106 µm, 106-150 µm, 150-500 µm, 500-1000 µm and >1mm. The weight of drop stones >5 mm was documented separately. The sampling interval is 10 cm between 500 and 700 cm for core 18CC and between 530.5 and 1300 cm for core 22CC. The latter intervals were used for planktic stable isotope analyzes and radiocarbon dating only.

In order to investigate the strength of deep-water currents during the DO events of late MIS3, the proxy sortable silt was tested at EARTHLAB, University of Bergen, Norway. The test included the fine fractions (10-63 µm) between 212 and 264 cm (22CC), and between 210 and 246 cm (18CC) at a step size of 4 cm, following McCave et al. (1995), Bianchi et al. (1999) and Tegzes et al. (2015). After all organic components were removed, the sediment grains are counted with the help of a sedigraph (Supplementary material, Figure 8).

Physical and geochemical properties: MS and XRF

Sediment color reflectance and MS (Figure 8) of core 22CC and 18CC were measured on board of the research vessel. The latter was performed for the whole length of each core, at intervals of 1 cm, using a spectrophotometer and a hand-held Bartington MS3 Magnetic Susceptibility meter with a MS2E surface scanning sensor. MS measurements are often used to analyze changes in grain sizes according to bottom current speeds and magnetization of mineral grains. It was suggested by Kissel et al. (1999) that more magnetic mineral grains are eroded from Reykjanes Ridge during MIS3 interstadials. Hence, MS is a useful tool for sediment chronology.

Microradiographic images were taken and XRF scans were performed at intervals of 0.2 cm using the ITRAX core scanner at EARTHLAB, University of Bergen, Norway. Certain element ratios (e.g. Calcium-Strontium (Paper II)) can be used for sediment

provenance studies because high amounts of detrital carbonate in North Atlantic sediments are characteristic of material eroded by the Laurentide Ice Sheet (Channell & Hodell, 2013; Hodell et al., 2008).

Radiocarbon dating

Radiocarbon dating was performed at Beta Analytic Inc., Miami, US and at W. M. Keck Carbon Cycle Accelerator Mass Spectrometry Facility of University of California, Irvine, US (KCCAMS/UCI). Eleven samples of surface-dwelling polar species *N. pachyderma* (150-500 µm) were dated for 22CC (Paper I), and twelve samples using the same species for core 18CC (Table 1, PhD thesis, Sadatzki 2019, p. 160-161, https://bora.uib.no/handle/1956/19239). All calibrated AMS ^{14}C ages, reported in BP (before present=1950 AD, Reimer et al., 2013), were converted to ka b2k (thousand years before 2000 AD) ages by adding 50 years in order to be comparable to ice core data.

Table 1: AMS ^{14}C ages for marine sediment core GS16-204-18CC.

Core depth (cm)	Lab ^{14}C age (BP)	Laboratory	Analysis number
100 - 100.5	18880 ± 80	Keck/ UCIAMS	182310
185.5 - 186	23350 ± 70	Keck/ UCIAMS	
200 - 200.5	24190 ± 110	Keck/ UCIAMS	182311
250 - 250.5	25290 ± 100	Keck/ UCIAMS	184070
286 - 286.5	28190 ± 100	Keck/ UCIAMS	
310 - 310.5	28910 ± 120	Keck/ UCIAMS	184071
350 - 350.5	31180 ± 260	Keck/ UCIAMS	184072
380.5 - 382.5	30180 ± 130	Keck/ UCIAMS	
400 - 400.5	31590 ± 190	Keck/ UCIAMS	184073
450 - 450.5	42190 ± 830	Keck/ UCIAMS	184074
500 - 500.5	44700 ± 1600	Keck/ UCIAMS	182312
800 - 800.5	52700 ± 3600	Keck/ UCIAMS	182314

Stable isotope measurements

Planktic stable isotope analyzes were performed on foraminifer species *N. pachyderma* for cores 18CC and 22CC at different resolutions. For core 18CC the measurement resolution is as follows: 5 cm between 0 and 200 cm, 2 cm between 200 and 500 cm, and 10 cm between 500 and 700 cm. For core 22CC planktic stable isotope measurements were performed at intervals of 5 cm between 0 and 200 cm, 2 cm between 200 and 600 cm, and 10 cm between 600 and 1300 cm. Where applicable, the resolution was increased to 1 cm in 22CC for the interval between 210-330 cm. Benthic

stable isotope measurements were performed for 22CC between 210 and 313.5 cm at the highest possible resolution (Supplementary material, Figure 10). Therefore, all *Uvigerina* spp. (0-42) and *Melonis pompiloides* (0-26) from size fraction 150-500 μm were selected following the same cleaning and measuring protocol as for the planktic foraminifers. Where applicable replicates for the same samples were measured.

Measurements were carried out in the laboratory facilities of FARLAB at the Department of Earth Sciences, University of Bergen, Norway using a ThermoFinnigan MAT253 gas source isotope ratio mass spectrometer. For details about standards and analytical precision we refer to the Method section of Paper I.

Ice-rafted debris and foraminifer counts

IRD and foraminifers were counted at 2-5 cm resolution (22CC: 0-530.5 cm; 18CC: 0-398.25 cm) in size fractions 150-500 μm, 500-1000 μm and > 1mm. In size fraction 150-500 μm, a distinction between benthic and planktic foraminifers, lithic, volcanic, and hematite stained quartz grains was made. Whenever biogenic material appeared in the samples (e.g. ostracods, worm tubes, shells, diatoms etc.), it was noted. For details about the method used for calculating IRD and foraminifer concentrations and fluxes, we refer to the method section of Paper I. Paper I also includes details about the planktic foraminifer assemblage counts that were performed for selected samples in core 22CC.

Benthic foraminifer assemblage counts (Supplementary material, Table 2) were performed on wet samples in size fraction >63 μm (Lloyd, 2006; Perner et al., 2016). Although we identified more than 32 different benthic species, the number of specimens per sample was too low to give statistically reliable results. Therefore, this proxy could not be used.

Pb-isotope measurements

Altogether, twenty samples (core 22CC) were selected for Pb-isotope analysis. Measurements were performed at the School of Earth and Environmental Sciences, University of Portsmouth, Portsmouth, UK. We used a SEM in combination with energy dispersive X-ray spectroscopy (EDS). The Pb-isotope composition of the detected K-feldspar grains was then measured by using Laser Ablation multi-collector

Inductively Coupled Plasma-Mass Spectrometry (LA-MC-ICP-MS). For details about sample preparation and standards we refer to the method section of Paper II.

Benthic Mg/Ca measurements

When applicable, trace metal analyzes of benthic foraminifers were performed for the time interval spanning 40-25 ka b2k in sediment core 22CC (Supplementary material, Figure 10). Benthic foraminifer species *M. pompiloides*, *Planulina wuellerstorfi* and *Uvigerina* spp. were selected from the 150-500 µm size fraction and cleaned separately following the protocol for oxidative cleaning described by Barker et al. (2003). This method includes a clay removal step, the oxidation of organic matter and a surface leaching with a weak acid. All samples were dissolved in trace metal pure 0.1M HNO_3 and diluted to a final concentration of 40 ppm of calcium. Analyzes were performed using an Agilent 720 inductively coupled plasma optical emission spectrometer (ICP-OES) at the Trace Element Laboratory (TELab) at the Norwegian Research Centre, NORCE, Bergen, Norway.

Six standards (from 0.5 to 7.66 mmol/mol) with matched calcium concentration to reduce the matrix effects (Rosenthal et al., 1999) have been prepared and used at the TELab. The standards used reach a concentration similar to foraminiferal carbonate. In order to correct for instrumental biases and analytical drift of the instrument, an internal standard solution with a Mg/Ca ratio of 5.076 mmol/mol was measured every eight samples.

Long-term analytical precision, based on standard solution, is 0.016 mmol/mol (1σ standard deviation) or 0.31% (relative standard deviation). The average Mg/Ca of long-term international limestone standard (ECRM752-1) measurements is 3.76 mmol/mol (1σ = 0.07 mmol/mol) with a published value of 3.75 mmol/mol (Greaves et al., 2008). Due to the development of ferromanganese crusts as part of diagenesis after deposition, manganese, iron and aluminum are the most common contaminants of foraminifer tests. The coefficients of determination (R^2) of the regression between Mg/Ca and Fe/Ca, Al/Ca and Mn/Ca for *P. wuellerstorfi* are 0.36, 0.00 and 0.57, respectively (Supplementary material, Figure 9). For *M. pompiloides* the respective R^2 are 0.03, 0.03 and 0.33 and for *Uvigerina* spp. 0.08, 0.01 and 0.02, respectively (Supplementary material, Figure 9). The Fe/Ca and Al/Ca ratios stay below their respective

contamination limits of 0.1 mol/mol and 0.4 mol/mol (Barker et al., 2003) except for two Fe/Ca and three Al/Ca measurements of species *M. pompiloides* (Supplementary material, Figure 9). Most of the Mn/Ca measurements are above the given contamination limit of 0.105 mol/mol (Boyle, 1983) and seem to covary for *P. wuellerstorfi* (57%) and *M. pompiloides* (33%) (Supplementary material, Figure 9), which can indicate that our samples are contaminated by ferromanganese precipitate. This is certainly due to the cleaning method used for these samples. Due to a limited number of foraminifers, an oxidative cleaning was used instead of the most recommended but more aggressive reductive cleaning that is described by Boyle and Keigwin (1985). Although the possibility of contamination cannot be ruled out, we assume that temperature is still the dominant control on Mg/Ca variability.

The bottom water temperature was calculated using the Mg/Ca-temperature calibrations of Tisserand et al. (2013), Hasenfratz et al. (2017) and Elderfield et al. (2006) for *P. wuellerstorfi*, *M. pompiloides* and *U. peregrina*, respectively (Figure 10). *Uvigerina* spp. were only present in the sediment for a very short interval corresponding to Greenland Interstadial 8. The temperatures calculated by using *Uvigerina* spp. are too cold which might be due to the calibration equation for this species does not cover the cold end. Thus, for the temperature record, the calculated values for *P. wuellerstorfi* and *M. pompiloides* were combined (Figure 10). Due to a generally low and discontinuous resolution no firm conclusion from these data was drawn.

4 Summary of Papers

Paper I: Insolation and Glacial Meltwater Influence on Sea-Ice and Circulation Variability in the Northeastern Labrador Sea During the Last Glacial Period

In Paper I we investigate the sea surface conditions in the northeastern Labrador Sea using stable isotope data, IRD, foraminifer abundances and planktic assemblage counts (%Np) from marine sediment core GS16-204-22CC-A. According to our established age model, the high-resolution records cover the time period from late MIS4 to early MIS2 (i.e. 65-25 thousand years ago (ka)). The results of the study provide insight into sea surface productivity and iceberg transport at the Eirik Drift. In combination with the low-resolution %Np record we infer different scenarios of sea ice cover extent with respect to DO events. Based on our proxy evidence we suggest that the surface productivity and iceberg transport at the Eirik Drift was hampered due to near perennial sea ice between 65 and 56 ka. This period of extensive sea ice was followed by ice-free conditions until 49 ka caused by the solar insolation maximum. Subpolar water masses were generally present at the Eirik Drift during the time from 65 to 49 ka. The time period between 49 and 25 ka was characterized by sea surface conditions that change with respect to DO events. During most stadials and interstadials the Eirik Drift was covered by near-perennial and seasonal sea ice with occasional appearance of subpolar water masses, respectively. After 29 ka (H3) surface productivity in the Labrador Sea increased.

The planktic $\delta^{18}O$ record, documents five meltwater events that we associate with Heinrich Stadials. The meltwater most likely led to water column stratification and weakening of the Subpolar Gyre. Our data reveals a unique pattern for each Heinrich Stadial which leads to the conclusion that sea surface conditions and convection at the Eirik Drift were driven by regional mechanisms. The high-amplitude IRD events, documented during H4 and H3, occur prior to the meltwater signal. The comparison of our proxy records to the planktic $\delta^{18}O$, IRD and %Np records from the Irminger Basin (Elliot et al., 1998) and the Greenland Sea (Voelker et al., 1998), document the dominance of the EGC along the East and South Greenland Margin. During interstadials, especially during GI-14, the Subpolar Gyre was more active. Hence, saltier and warmer water masses were advected into the Irminger Sea and Labrador

Sea. In general, we observe a trend from warmer to cooler conditions throughout MIS3. This trend led to an increased sea ice cover and stronger presence of icebergs driven by a high seasonality towards MIS2.

Paper II: Climate and ice sheet responses in northern latitudes during Marine Isotope Stage 3: A provenance study of ice-rafted debris from the Eirik Drift

In Paper II, the multiproxy approach includes Pb-isotope measurements of individual sand-sized K-feldspars, a Ca/Sr record, concentrations of hematite stained quartz and volcanic grains as well as the chemical composition of each sample using X-ray spectroscopy. The IRD and meltwater events recorded by marine sediment core GS16-204-22CC-A from the Eirik Drift during MIS3, that were observed by Griem et al. (2019), were selected for X-ray spectroscopy and Pb-isotope measurements. Altogether, 20 time slices between 63 and 28 thousand years were analyzed in detail, including five Heinrich Stadials, each characterized by increased meltwater input.

The results of the Pb-isotope measurements cover a wide range of ratios typical for Greenland IRD source areas. Hence, we suggest that Greenland was the main source area of the iceberg transported IRD at the Eirik Drift during stadial, interstadials and Heinrich Stadials of MIS3 (59-29 thousand years). During stadials the sea ice extent was generally longer lasting than during interstadials and became progressively more extensive towards late MIS3 in the Labrador Sea. Although extensive sea ice cover could, at times, have hampered iceberg transport we do not observe a specific shift of IRD source areas. However, in order to observe such a shift a higher resolution may be necessary. However, on condition that the Denmark Strait was ice-free, we suggest that most IRD was transported to the Eirik Drift via the EGC. Since the EGC is the dominant surface current for iceberg transport from North and East Greenland but also from Svalbard, those areas serve as the main IRD source areas. However, the occasional transport of icebergs from the Eurasian Ice Sheet via the EGC and potentially the Subpolar Gyre cannot be completely ruled out as some of our Pb-isotope ratios (e.g. during H5.2) could also indicate a Scandinavian instead of a Greenlandic IRD source. The Pb-isotope ratios, chemical composition and the Ca/Sr ratios during H4 are indicative of IRD derived from the Hudson Strait area. Hence, the signal that documents the collapse of the Laurentide Ice Sheet in the Ruddiman Belt is also evident

at the Eirik Drift. Our proxy evidence during H3, point towards Greenland IRD source areas. Since the amplitude of the H3 IRD peak is comparable to the IRD peak recorded during H4, our results may suggest the partial collapse of the Greenland Ice Sheet during H3.

Paper III: Similar conditions in the North Atlantic region during the Last Glacial Maximum and interstadials: Evidence from ice core and sediment core records

Paper III compiles new and previously published foraminifer and IRD abundance records from the Labrador Sea, the Irminger Sea and the Nordic Seas in order to compare sea ice conditions during the DO events of late MIS3 and the LGM (41-19 thousand years). Additionally, previously published sea surface temperature (SST) and biomarker (P_BIP_{25}) records are presented to evaluate the indirect sea ice proxy records. All marine proxy records are presented in comparison to deuterium excess and $\delta^{18}O$ records from the GRIP ice core (Greenland summit). The data compilation including 17 sediment cores from the high to mid-latitude North Atlantic is used to infer potential driving mechanisms of the deuterium excess signal at Greenland summit. While colder stadials are characterized by lower $\delta^{18}O$ and higher deuterium excess, the warmer interstadials are characterized by higher $\delta^{18}O$ and lower deuterium excess. However, during the LGM the $\delta^{18}O$ signal is decoupled from deuterium excess, hence, the driving mechanism during MIS3 DO events and the LGM appear to be different.

Overall, the maximum sea ice extent occurred during stadials with the polar front most likely located south of Iceland. During the LGM and interstadials, the Polar- and the Arctic Fronts were located along the route of the East Greenland Current and in the Norwegian Sea, respectively. Furthermore, the sea surface in the Norwegian Sea, the West Svalbard Margin, the East Greenland Margin and the Labrador Sea was more productive during the LGM than during MIS3 DO events and the surface waters of the subtropical North Atlantic were as warm or warmer during the LGM than during MIS3 interstadials.

Based on these findings we suggest that the GRIP deuterium excess signal has a northern precipitation source during interstadials. Since the deuterium excess record covaries with Norwegian Sea P_BIP_{25} during MIS3 DO events, we argue that the

Norwegian Sea may represent a northern source of precipitation reaching summit on Greenland. The fact that the covariance of Norwegian Sea P_BIP_{25} values and deuterium excess is not observed during the LGM could be caused by the higher elevation of the Laurentide Ice Sheet during the LGM compared to MIS3. Based on our reconstructions of the Arctic- and Polar Fronts, the main source of precipitation at Greenland summit most likely evaporated at mid-latitudes during the LGM and in the subtropical and tropical North Atlantic during late MIS3 stadials.

5 Synthesis and Outlook

The aim of this thesis is to gain knowledge about A) sea surface conditions such as meltwater input and sea ice extent in the Labrador Sea and B) Greenland Ice Sheet sensitivity during past abrupt climate changes. The new insights are used to investigate the Labrador Sea´s role for ocean circulation and ice-ocean-atmosphere-interactions between late MIS4 and MIS2 (~65-19 ka). Hence, this thesis ties the extensive knowledge of sea surface conditions in the Nordic Seas and the Ruddiman Belt together using consistent methods such as IRD, foraminifer concentrations, stable oxygen isotopes. The interpretation and comparison of the comprehensive number of marine records established and synergized in this thesis are linked to ice core records. The results contribute significantly to the general understanding regarding the impact of past climatic changes on environmental conditions in the North Atlantic region. Furthermore, the detailed IRD records of cores 18CC and 22CC led to in-depth studies of tephra horizons (Rutledal et al., 2020a; Rutledal et al., 2020b) as well as to a detailed investigation of H6 to H3 using ancient DNA and dinoflagellate cysts (De Schepper et al., 2020).

Outlook Paper I

In Paper I, a multiproxy approach combined planktic stable isotope, IRD and foraminifer records in order to investigate the sea surface conditions in the northeastern Labrador Sea over the course of several DO events including four Heinrich Stadials. The comprehensive, high-resolution reconstruction of ocean front boundaries, sea ice cover fluctuations and calving events of the Greenland Ice Sheet contributes significantly to our knowledge of this part of the North Atlantic in the past. The detailed investigation of DO events over a time-interval of more than 40 kyrs, clearly demonstrates in particular that the imprint of DO events in the ocean changed throughout MIS3. From late to mid-MIS3 the Labrador Sea was characterized by more extensive sea ice cover. Between H5 and H4, however, the sea ice cover was seasonal and marked by pronounced stadial-interstadial changes of sea ice extent similar to the oscillations in the Norwegian Sea. While an extensive sea ice cover characterized most stadials, the interstadials were seasonally ice-free during late MIS3. This trend towards a more variable sea ice cover is also characteristic for the investigated H-Stadials. Each

H-Stadial is indicated by depleted planktic oxygen isotope values which is interpreted as a result of increased meltwater input. During H6 and H5, iceberg transport, and thus IRD input, in the Labrador Sea was hampered by a near-perennial sea ice cover, whereas H4 and H3 are characterized by a large-scale IRD input.

The observation of the individual character of DO events as well as Heinrich stadials motivated not only the second paper of this thesis but also a study conducted by De Schepper et al. (2020). De Schepper et al. (2020) highlight the difference of the sea surface conditions that characterized H6 to H3 at the Eirik Drift and link the trends to solar insolation. Hence, De Schepper et al. (2020) support our interpretation that the trends of sea ice cover extent throughout MIS3 are driven by insolation changes at 65°N. Furthermore, Paper I documents new evidence that changes in sea surface productivity and iceberg transport record both ice sheet and sea ice response related to DO events. In addition, the findings of Paper I demonstrate that variations in sea surface conditions and convection in the northeastern Labrador Sea are driven by regional mechanisms. The comparison to the IRD and foraminifer records from the Irminger basin and the Greenland Sea leads to the identification of orbital forcing, strength of the Subpolar Gyre, Arctic freshwater/sea ice export as potential trigger mechanisms of the environmental conditions from late MIS3 to early MIS2. These findings serve as a key step to close the gap regarding environmental conditions at the Eirik Drift between the well-studied time intervals MIS5e and the LGM. The results of Paper I provide scenarios and constraints for the evaluation of model simulations that simulate the state of the climate in the region during the individual Heinrich Stadials or a particular sequence of DO events.

Outlook Paper II

Paper II is built upon the IRD record of Paper I. Here, Pb-isotope measurements of sand-sized K-feldspars were performed and combined with X-ray spectroscopy, Ca/Sr and petrologic tracer records. Each Pb-isotope measurement represents one time-interval of increased IRD input with respect to Greenland Interstadials, Stadials or Heinrich Stadials. During most IRD events, we find a mixed signal representing Greenlandic bedrock provinces. When the East Greenland Margin and the core site were ice free, the route via the EGC was the main iceberg trajectory. However, we

suggest an increased contribution of IRD from Europe and North America during H6 and H4, respectively. This most likely indicates iceberg transport by the Subpolar Gyre. As our datasets, to a large extent, comprise Greenlandic sources, it seems possible that, during the high-amplitude IRD peak of H3 at the Eirik Drift, the Greenland Ice Sheet was large enough to partially collapse and deliver sizable amounts of iceberg borne IRD to the study area. Hence, the results of Paper II indicate that the Greenland Ice Sheet played an important role within the climatic dynamics of MIS3. The icebergs that were discharged from the Greenland Ice Sheet may not only have transported IRD and freshwater to the Labrador Sea but also further south into the North Atlantic. If meltwater from the Greenland Ice Sheet reached the Subpolar Gyre, it might have contributed to a weakening of the Subpolar Gyre and thus northward heat transport into the Nordic Seas.

In order to improve our knowledge about the Greenland Ice Sheet´s contribution to the strength of the Subpolar Gyre, and thereby the northward heat advection via the Atlantic Meridional Overturning Circulation, an increased number of measurements is required. Especially, the IRD layer associated with H3 should become a target for future studies. The H3 IRD layer may, for the first time, indicate a collapse of the Greenland Ice Sheet shortly after it had reached the Greenland continental shelf at ca. 31 ka (Funder et al., 2011).

Outlook paper III

Paper III is similar to Paper II, founded on the results of Paper I. More specifically, the sea surface reconstructions from the Labrador Sea are here put into context with IRD and foraminifer records from the Irminger Basin, as well as with previously published records from the Nordic Seas. The cores from the Nordic Seas were retrieved along the East Greenland Margin, along the West Svalbard Margin, and in the Norwegian Sea. The West Svalbard Margin marks the northernmost area of Atlantic Water advection during the investigated time period between 41 and 19 ka. The advection of Atlantic Water is increased during interstadials when the sea ice cover in the eastern Nordic Seas is seasonal. During stadials, the Nordic Seas as well as the Labrador Sea are covered by near-perennial sea ice. By combining the indirect sea ice proxies (i.e. IRD and foraminifer concentrations) with biomarker records, a link between the sea ice

cover in this region and the parameters recorded during DO events in Greenland ice core records are observed. A seasonal sea ice cover, especially in the Norwegian Sea, is interpreted by higher stable oxygen isotopes and lower deuterium excess values in Greenland ice cores. The near-perennial sea ice cover during stadials is linked to lower stable oxygen isotopes and higher deuterium excess values. Furthermore, this link not only exists during the DO events of late MIS3 but also during the LGM. However, since ice-core deuterium excess and $\delta^{18}O$ are decoupled during the LGM, the underlying mechanism driving the changes in deuterium excess must be different from the one during DO events. During the LGM and interstadials, the heat loss, and hence evaporation and subsequent transport of precipitation to Greenland, must have occurred further north than during stadials when the sea ice hampered ocean-atmosphere-interaction. Additionally, the North Atlantic was characterized by a higher primary productivity during the LGM. Sea surface temperature records from the subtropical North Atlantic reveal that the ocean surface during the LGM was as warm as or warmer than during MIS3 interstadials. Here, in the subtropical and tropical North Atlantic lies the source of Greenland precipitation during stadials whereas during the LGM, it was most likely located in the mid-latitude North Atlantic.

Paper III aims to link the sea surface conditions of the Nordic Seas and the North Atlantic to the proxy records on Greenland summit. We find evidence that the Nordic Seas sea ice and the deuterium excess are closely linked during the DO events of MIS3. However, although sea surface conditions during the LGM were comparable to the conditions during interstadial, we suggest that the height of the Laurentide Ice Sheet plays a key role in driving the ice core signals during the LGM instead of the sea ice cover. Although a link between sea ice and deuterium excess has been suggested in previous studies, this is the first time that direct and indirect proxy evidence for sea ice cover is shown in direct comparison to ice core deuterium-excess.

To further investigate the link between sea surface and ice core proxy records, sediment core records with higher resolution and very-well constrained age models using direct sea ice proxies such as biomarkers are needed. The recently published database by Waelbroeck et al. (2019) may be a helpful first step to improve our possibility of a direct but nonetheless independent comparison between ice and sediment core records.

Additionally, to further improve our interpretations, tephrochronological studies such as Berben et al. (2020) and Rutledal et al. (2020a), which provide direct links between marine and ice core records, will serve as key tools to understand the underlying mechanisms driving environmental change in the ocean and in the atmosphere.

Relevance of thesis results

New, high-resolution records that document the variability of the sea surface conditions in the Labrador Sea throughout 20 DO events are established and connected with proxy records from previous studies. The results demonstrate that the ocean along the East and Southeast Greenland Margin is a highly dynamical area where each DO event has its own characteristic sea surface conditions (i.e. sea ice cover, primary productivity and iceberg drift). By combining the results of this thesis with previously published sea surface records from the Nordic Seas and the mid-latitude North Atlantic, we analyzed and subsequently summarized changing sea surface conditions during MIS3 DO events and the LGM. The summarized results illustrate the different oceanographic conditions during Greenland Interstadials and Stadials as well as the LGM. This compilation of datasets using different sea surface proxies from the LGM into MIS3 thus serves as substantial contribution to the knowledge gained from projects such as MARGO or CLIMAP by extending the time period and adding new parameters and core sites.

6 Supplementary Material

Data from initial thesis approach

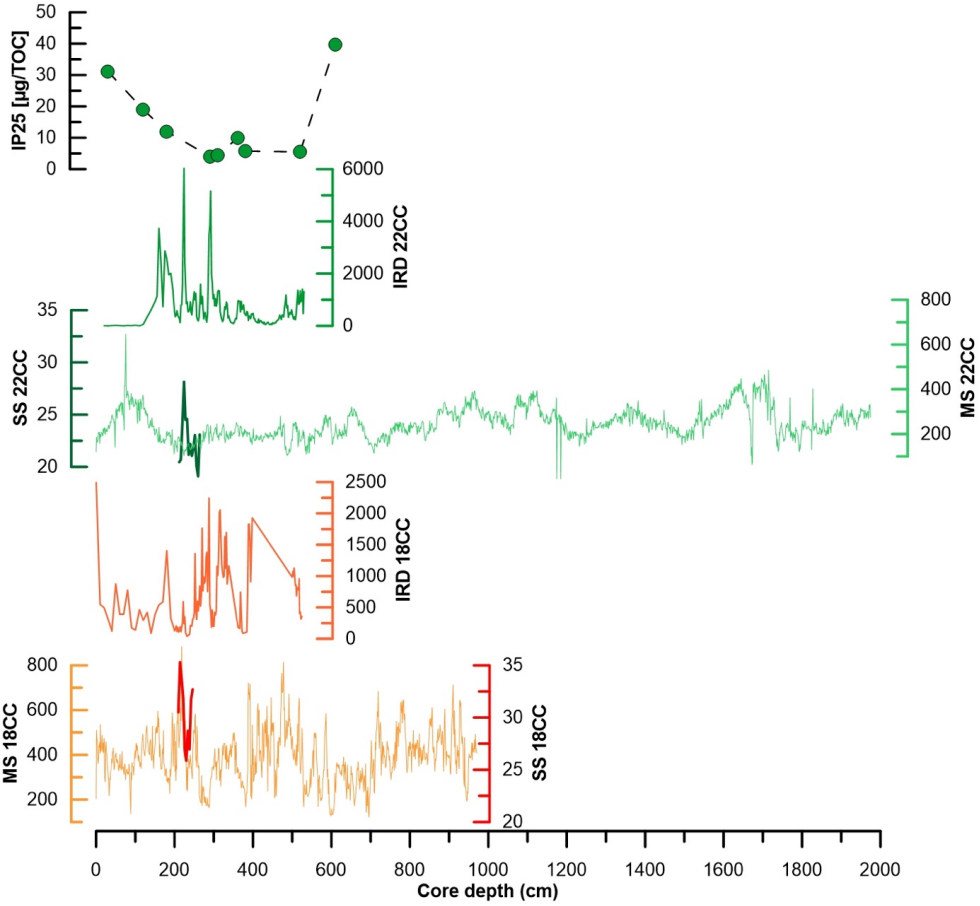

Figure 8: Unpublished Sortable Silt (SS), biomarker (IP_{25}) and Magnetic Susceptibility (MS) data for cores GS16-204-22CC-A and GS16-204-18CC against core depth. GS16-204-22CC-A: IP_{25} (Sadatzki, pers. comm., green dots), ice-rafted debris (IRD>150 µm) concentration (green), SS (dark green) and MS (SI 10^{-5}, light green). GS16-204-18CC: IRD concentration (>150 µm, orange), SS (red) and MS (SI 10^{-5}, light orange).

Table 2: Benthic assemblage counts in size fraction >63 μm in core GS16-204-22CC-A. Red text highlights the core depths where less than 100% of the size fraction was counted.

Mean depth (cm)	270.25	270.75	280.25	280.75	281.25	281.75	282.25	282.75	283.25	283.75	284.25	284.75	285.25	285.75	286.25	286.75	287.25	287.75	288.25	288.75	289.25	289.75	358.25	358.75	397.25	397.75
Wet weight (g)	10.428	7.248	12.179	8.433	11.477	10.540	10.635	10.221	11.644	12.588	7.710	6.257	11.448	11.981	8.572	8.021	10.130	11.960	9.036	14.561	13.932	13.199	14.093	13.277	10.660	9.406
Dry weight (g) >63μm	0.493	0.365	0.154	0.083	0.193	0.145	0.119	0.122	0.168	0.209	0.177	0.280	0.419	0.797	0.475	0.497	1.062	1.768	1.376	1.493	1.939	1.290	0.213	0.261	0.184	0.102
Benthic count (g)	0.493	0.365	0.154	0.083	0.193	0.145	0.119	0.122	0.168	0.209	0.177	0.280	0.419	0.797	0.475	0.497	1.062	1.768	1.376	1.493	1.939	1.290	0.213	0.261	0.184	0.102
Alabaminella weddelensis	17	41	4	1	0	1	2	5	0	16	74	66	92	88	79	76	26	8	5	2	3	17	53	36	31	22
Astrononion gallowayi	2	1	0	0	0	0	0	0	0	0	0	0	1	0	6	9	1	5	2	3	1	0	2	5	3	0
Bolivinita quadrilatera	0	0	0	0	0	0	0	0	0	0	0	0	0	0	0	0	0	0	0	0	1	0	0	1	0	0
Bolivina marginata	0	0	0	0	0	0	0	0	0	0	0	0	0	0	0	2	0	0	2	0	0	0	0	0	0	0
Bolivina pseudopunctata	0	0	0	0	0	0	0	0	0	0	0	0	0	0	0	8	9	0	3	3	0	0	0	0	0	0
Cassidulina neoteretis	0	2	0	0	0	0	1	0	0	1	0	0	0	0	0	0	1	0	0	0	0	0	0	0	0	0
Cassidulina reniforme	1	10	0	0	0	0	0	0	0	0	0	3	3	48	193	330	175	68	84	50	65	112	41	42	1	0
Cibicides lobatulus	1	0	0	0	0	0	0	0	0	0	0	0	1	0	3	3	13	8	5	4	8	2	10	12	0	0
Cibicidoides sp.	0	0	0	0	0	0	0	0	0	0	0	0	0	0	0	0	0	0	0	0	0	0	0	2	0	1
Dentalina spp.	0	0	0	0	0	0	0	0	0	0	0	0	0	0	2	12	1	1	1	3	1	1	0	1	0	0
Discorbis spp.	0	1	0	0	0	0	0	0	0	0	0	0	0	1	0	3	3	0	2	2	1	0	1	1	1	0

Mean depth (cm)	270.25	270.75	280.25	280.75	281.25	281.75	282.25	282.75	283.25	283.75	284.25	284.75	285.25	285.75	286.25	286.75	287.25	287.75	288.25	288.75	289.25	289.75	358.25	358.75	397.25	397.75
Elphidium excavatum	0	1	0	0	0	0	0	0	0	0	0	0	0	0	2	4	5	2	4	5	1	1	2	2	0	1
***Eponides* spp.**	0	2	0	0	0	0	0	0	0	0	0	0	0	3	1	1	6	5	0	0	5	2	0	3	0	0
Epistominella exigua	0	10	0	0	0	0	0	0	0	0	0	1	0	4	8	11	44	4	11	13	24	10	16	14	1	0
Globocassidulina subglobosa	0	0	0	0	0	0	0	0	0	0	0	0	1	2	3	0	0	0	0	0	0	0	0	1	0	2
***Hanzawaia* sp.**	0	1	1	0	0	0	0	0	0	0	0	0	0	3	17	20	22	18	14	13	13	15	41	43	0	0
Islandiella helenae	0	0	0	0	0	0	0	0	0	0	0	0	0	0	0	1	0	3	0	0	0	0	0	0	0	0
Islandiella islandica	0	0	0	0	0	0	0	0	0	0	0	0	0	0	0	1	0	0	0	0	0	0	0	0	0	0
Islandiella norcrossi	0	0	0	0	0	0	0	0	0	0	0	0	0	0	0	0	2	2	2	2	3	3	2	0	0	0
***Lagena* spp.**	1	0	0	0	0	0	0	0	0	2	1	1	0	3	3	6	9	18	13	19	17	23	13	10	0	1
***Lenticulina* spp.**	0	0	0	0	0	0	0	0	0	0	0	0	0	1	0	0	0	0	0	0	0	0	1	3	0	0
Melonis barleanum	25	19	1	1	0	1	1	1	0	3	2	1	2	2	2	7	4	6	3	4	2	0	8	14	5	0
Melonis pompiloides	9	15	0	0	0	0	0	0	1	0	0	3	3	5	12	22	6	9	7	3	4	7	5	5	17	0
Nonionelina iridea	0	0	0	0	0	0	0	0	0	0	0	0	0	0	2	4	1	4	2	0	5	24	2	6	0	0
Oolina hexagona	0	0	0	0	0	0	0	0	0	0	0	0	0	1	2	1	0	0	0	0	0	1	1	1	0	0
Oridorsalis umbonatus	0	0	0	0	0	0	0	0	0	0	0	0	1	0	1	0	3	3	1	2	4	3	1	1	0	0

Mean depth (cm)	270.25	270.75	280.25	280.75	281.25	281.75	282.25	282.75	283.25	283.75	284.25	284.75	285.25	285.75	286.25	286.75	287.25	287.75	288.25	288.75	289.25	289.75	358.25	358.75	397.25	397.75
Pullenia bulloides	1	2	0	0	0	0	0	0	1	2	4	3	10	8	13	15	2	2	1	2	0	0	3	5	4	3
Pullenia osloensis	7	5	0	0	0	0	0	0	1	0	1	1	2	1	17	9	7	13	6	10	5	5	2	8	6	31
Pullenia quinqueloba	28	51	0	0	0	0	0	1	0	1	0	3	2	12	5	12	13	10	10	12	4	3	32	21	33	0
Planulina wuellerstorfi	0	0	0	0	0	0	0	0	0	0	0	0	0	0	0	0	4	7	2	0	4	3	0	11	0	0
Quinqueloculina seminula	0	0	0	0	0	0	0	0	0	0	0	0	0	1	5	14	16	36	48	51	53	36	2	3	1	0
***Rhabdammina/ Reofax* sp.**	0	1	0	0	0	0	0	0	0	0	0	0	0	0	0	0	0	0	0	0	0	0	0	0	0	1
***Rosalina* sp.**	0	0	0	0	0	0	0	0	0	0	0	0	0	0	0	0	1	2	0	0	1	1	0	0	0	0
Stainforthia concava	0	0	0	0	0	0	0	0	0	0	0	0	0	0	3	5	7	3	2	4	1	1	14	11	1	2
Stainforthia fusiformis	0	0	0	0	0	0	0	0	0	0	0	0	0	0	1	1	6	15	10	14	13	8	1	0	0	0
Textularia bocki	0	0	0	0	0	0	0	0	0	0	0	0	0	0	0	0	0	2	0	1	0	0	0	1	1	0
***Textularia* sp.**	0	0	0	0	0	0	0	0	0	0	0	0	0	0	0	0	2	1	1	4	2	2	0	1	0	0
***Uvigerina* spp.**	33	26	2	0	0	0	1	1	7	11	10	4	7	10	1	5	2	2	0	0	0	0	1	1	2	1
Pyrgo	14	11	0	0	0	0	0	0	2	3	1	2	1	6	0	2	0	0	0	1	5	3	7	7	0	0
Unidentified/ juvenile	3	2	0	0	0	0	0	0	0	1	0	0	0	11	29	35	57	159	150	204	162	89	14	3	0	12
No. of specimens	**142**	**201**	**8**	**2**	**0**	**2**	**5**	**8**	**12**	**40**	**93**	**88**	**126**	**210**	**410**	**619**	**448**	**416**	**391**	**431**	**408**	**372**	**275**	**275**	**107**	**77**

Unused data, suitable for future publications

Based on the initial approach of this thesis (see 2), we measured benthic stable isotopes and benthic Mg/Ca using foraminifer species *Uvigerina* spp., *Melonis pompiloides* and *Planulina wuellerstorfi* between 42 and 28 ka (Figure 10). We observe a decrease of benthic $\delta^{18}O$ (*Melonis pompiloides)* simultaneously with the decrease of planktic $\delta^{18}O$ during H4. The temperature increases of the deep-water mass occurs prior to this decrease.

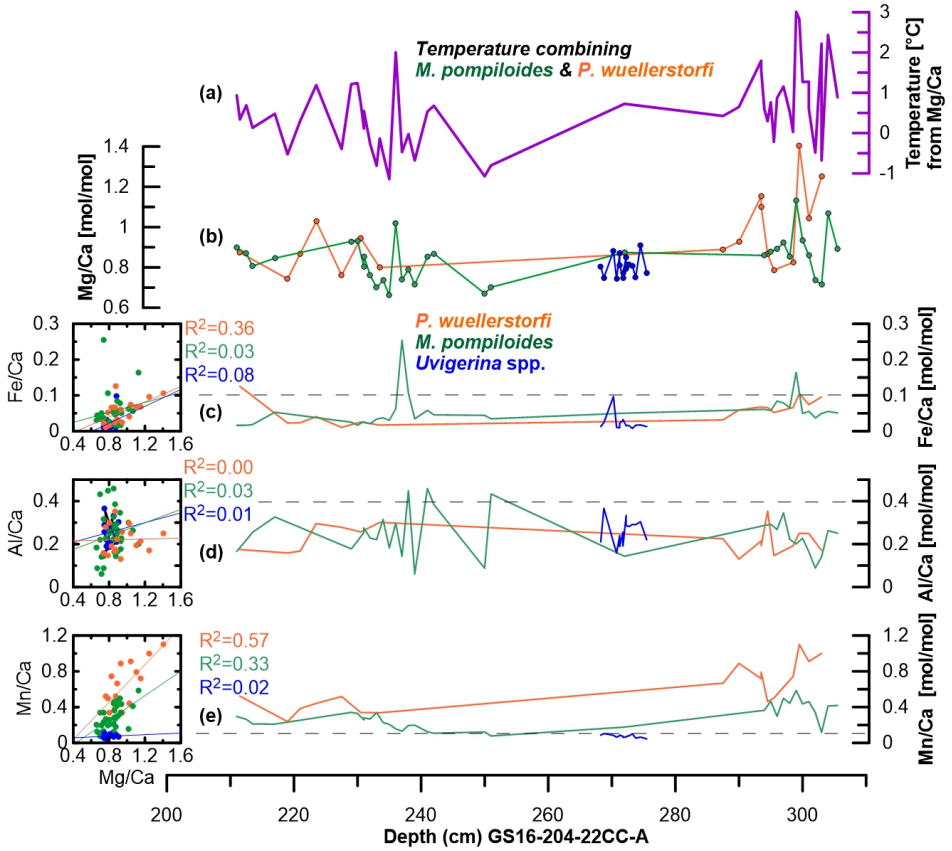

Figure 9: Benthic Mg/Ca records for sediment core GS16-204-22CC-A including selected trace metal-to-calcium ratios to evaluate contamination levels against core depth. (a) Bottom water temperatures were calculated using the Mg/Ca-temperature calibrations of Hasenfratz et al. (2017) and Tisserand et al. (2013) for M. pompiloides and P. wuellerstorfi, respectively, and combined to one record (purple). (b) Mg/Ca ratios, (c) Fe/Ca ratios, (d) Al/Ca ratios and (e) Mn/Ca ratios for P. wuellerstorfi (green), M. pompiloides (orange) and Uvigerina spp. (blue). (d-f) Dashed lines indicate given contamination levels (Barker et al., 2003; Boyle, 1983). Boxes (left) show the regression lines and correlation coefficient (R^2) between Mg/Ca and each selected trace metal (Fe/Ca, Al/Ca, Mn/Ca) for each measured foraminifer species.

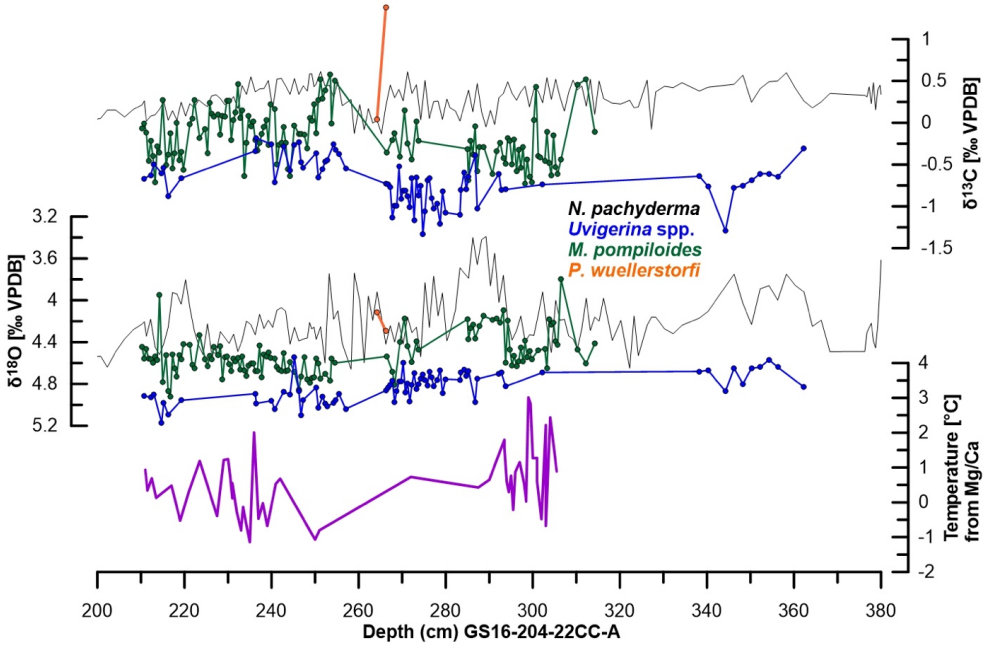

Figure 10: Benthic stable isotope measurements and bottom water temperatures from core GS16-204-22CC-A using the benthic foraminifer species Uvigerina spp. (blue), Melonis pompiloides (green) and Planulina wuellerstorfi (orange) plotted against core depth. The planktic stable isotope record using N. pachyderma is shown for comparison (black). The temperature record (purple) was established by combining the Mg/Ca measurements of species M. pompiloides and P. wuellerstorfi using the calibration of Hasenfratz et al. (2017).

7 References

Alley, R. B., Andrews, J. T., Brigham-Grette, J., Clarke, G., Cuffey, K. M., Fitzpatrick, J., . . . Mitrovica, J. (2010). History of the Greenland Ice Sheet: paleoclimatic insights. *Quaternary Science Reviews, 29*(15-16), 1728-1756.

Alvarez-Solas, J., Robinson, A., Montoya, M., & Ritz, C. (2013). Iceberg discharges of the last glacial period driven by oceanic circulation changes. *Proceedings of the National Academy of Sciences, 110*(41), 16350-16354.

Andrews, J., Dunhill, G., Vogt, C., & Voelker, A. (2017). Denmark Strait during the Late Glacial Maximum and Marine Isotope Stage 3: Sediment sources and transport processes. *Marine Geology, 390*, 181-198.

Andrews, J., & Vogt, C. (2014). Source to sink: statistical identification of regional variations in the mineralogy of surface sediments in the western Nordic Seas (58 N–75 N; 10 W–40 W). *Marine Geology, 357*, 151-162.

Andrews, J. T. (2000). Icebergs and iceberg rafted detritus (IRD) in the North Atlantic: facts and assumptions. *Oceanography*, 100-108.

Andrews, J. T. (2008). The role of the Iceland Ice Sheet in the North Atlantic during the late Quaternary: a review and evidence from Denmark Strait. *Journal of Quaternary Science, 23*(1), 3-20. doi:10.1002/jqs.1142

Andrews, J. T., & Barber, D. (2002). Dansgaard–Oeschger events: is there a signal off the Hudson Strait Ice Stream? *Quaternary Science Reviews, 21*(1-3), 443-454.

Andrews, J. T., Gibb, O. T., Jennings, A. E., & Simon, Q. (2014). Variations in the provenance of sediment from ice sheets surrounding Baffin Bay during MIS 2 and 3 and export to the Labrador Shelf Sea: site HU2008029-0008 Davis Strait. *Journal of Quaternary Science, 29*(1), 3-13.

Andrews, J. T., Hardardóttir, J., Helgadóttir, G., Jennings, A. E., Geirsdóttir, Á., Sveinbjörnsdóttir, Á. E., . . . Thors, K. (2000). The N and W Iceland Shelf: insights into Last Glacial Maximum ice extent and deglaciation based on acoustic stratigraphy and basal radiocarbon AMS dates. *Quaternary Science Reviews, 19*(7), 619-631.

Barker, S., Chen, J., Gong, X., Jonkers, L., Knorr, G., & Thornalley, D. (2015). Icebergs not the trigger for North Atlantic cold events. *Nature, 520*(7547), 333-336. doi:10.1038/nature14330

Barker, S., Greaves, M., & Elderfield, H. (2003). A study of cleaning procedures used for foraminiferal Mg/Ca paleothermometry. *Geochemistry, Geophysics, Geosystems, 4*(9).

Batchelor, C. L., Margold, M., Krapp, M., Murton, D. K., Dalton, A. S., Gibbard, P. L., . . . Manica, A. (2019). The configuration of Northern Hemisphere ice sheets through the Quaternary. *Nature communications, 10*(1), 1-10.

Belt, S. T., Brown, T. A., Ringrose, A. E., Cabedo-Sanz, P., Mundy, C. J., Gosselin, M., & Poulin, M. (2013). Quantitative measurement of the sea ice diatom biomarker IP25 and sterols in Arctic sea ice and underlying sediments: Further considerations for palaeo sea ice reconstruction. *Organic Geochemistry, 62*, 33-45.

Belt, S. T., Massé, G., Rowland, S. J., Poulin, M., Michel, C., & LeBlanc, B. (2007). A novel chemical fossil of palaeo sea ice: IP25. *Organic Geochemistry, 38*(1), 16-27.

Belt, S. T., & Müller, J. (2013). The Arctic sea ice biomarker IP25: a review of current understanding, recommendations for future research and applications in palaeo sea ice reconstructions. *Quaternary Science Reviews, 79*, 9-25.

Berben, S. M., Dokken, T. M., Abbott, P. M., Cook, E., Sadatzki, H., Simon, M. H., & Jansen, E. (2020). Independent tephrochronological evidence for rapid and synchronous oceanic and atmospheric temperature rises over the Greenland stadial-interstadial transitions between ca. 32 and 40 ka b2k. *Quaternary Science Reviews, 236*, 106277.

Berger, A. (1988). Milankovitch theory and climate. *Reviews of Geophysics, 26*(4), 624-657.

Berger, A., & Loutre, M. F. (1999). *Parameters of the Earths orbit for the last 5 Million years in 1 kyr resolution*. Retrieved from: https://doi.org/10.1594/PANGAEA.56040

Bianchi, G., Hall, I. R., McCave, I., & Joseph, L. (1999). Measurement of the sortable silt current speed proxy using the Sedigraph 5100 and Coulter Multisizer IIe: Precision and accuracy. *Sedimentology, 46*(6), 1001-1014.

Bigg, G. R., Wadley, M. R., Stevens, D. P., & Johnson, J. A. (1996). Prediction of iceberg trajectories for the North Atlantic and Arctic Oceans. *Geophysical Research Letters, 23*(24), 3587-3590.

Böhm, E., Lippold, J., Gutjahr, M., Frank, M., Blaser, P., Antz, B., . . . Deininger, M. (2015). Strong and deep Atlantic meridional overturning circulation during the last glacial cycle. *Nature, 517*(7532), 73-76.

Born, A., & Mignot, J. (2012). Dynamics of decadal variability in the Atlantic subpolar gyre: a stochastically forced oscillator. *Climate Dynamics, 39*(1), 461-474.

Boyle, E., & Keigwin, L. (1985). Comparison of Atlantic and Pacific paleochemical records for the last 215,000 years: Changes in deep ocean circulation and chemical inventories. *Earth and Planetary Science Letters, 76*(1-2), 135-150.

Boyle, E. A. (1983). Manganese carbonate overgrowths on foraminifera tests. *Geochimica et Cosmochimica Acta, 47*(10), 1815-1819.

Bradley, S. L., Reerink, T. J., Van De Wal, R. S., & Helsen, M. M. (2018). Simulation of the Greenland Ice Sheet over two glacial-interglacial cycles: investigating a sub-ice-shelf melt parameterization and relative sea level forcing in an ice-sheet-ice-shelf model. *Climate of the Past, 14*(5), 619-635.

Channell, J., & Hodell, D. (2013). Magnetic signatures of Heinrich-like detrital layers in the Quaternary of the North Atlantic. *Earth and Planetary Science Letters, 369*, 260-270.

Dalton, A. S., Finkelstein, S. A., Barnett, P. J., & Forman, S. L. (2016). Constraining the Late Pleistocene history of the Laurentide Ice Sheet by dating the Missinaibi Formation, Hudson Bay Lowlands, Canada. *Quaternary Science Reviews, 146*, 288-299.

Dalton, A. S., Finkelstein, S. A., Forman, S. L., Barnett, P. J., Pico, T., & Mitrovica, J. X. (2019). Was the Laurentide Ice Sheet significantly reduced during Marine Isotope Stage 3? *Geology, 47*(2), 111-114.

Daniault, N., Mercier, H., Lherminier, P., Sarafanov, A., Falina, A., Zunino, P., . . . Huck, T. (2016). The northern North Atlantic Ocean mean circulation in the early 21st century. *Progress in Oceanography, 146*, 142-158.

Dansgaard, W., Johnsen, S., Clausen, H., Dahl-Jensen, D., Gundestrup, N., Hammer, C., . . . Jouzel, J. (1993a). Evidence for general instability of past climate from a 250-kyr ice-core record. *Nature, 364*(6434), 218-220.

Dansgaard, W., Johnsen, S., Clausen, H., Dahl-Jensen, D., Gundestrup, N., Hammer, C., . . . Jouzel, J. (1993b). Evidence for general instability of past climate from a 250-kyr ice-core record. *Nature, 364*(6434), 218.

De Schepper, S., Ray, J. L., Griem, L., Van Nieuwenhove, N., Magann Grant, D., Steinsland, K., . . . Zeeshan Ijaz, U. (2020). *A sedimentary ancient DNA approach to elucidate the Labrador Sea paleoceanography over the last 130,000 years.* Paper presented at the EGU General Assembly Conference Abstracts.

de Vernal, A., Hillaire-Marcel, C., Turon, J.-L., & Matthiessen, J. (2000). Reconstruction of sea-surface temperature, salinity, and sea-ice cover in the northern North Atlantic during the last glacial maximum based on dinocyst assemblages. *Canadian Journal of Earth Sciences, 37*(5), 725-750.

Dickson, B., Yashayaev, I., Meincke, J., Turrell, B., Dye, S., & Holfort, J. (2002). Rapid freshening of the deep North Atlantic Ocean over the past four decades. *Nature, 416*(6883), 832.

Dickson, R. R., & Brown, J. (1994). The production of North Atlantic Deep Water: Sources, rates, and pathways. *Journal of Geophysical Research: Oceans, 99*(C6), 12319-12341. doi:10.1029/94JC00530

Dokken, T. M., & Jansen, E. (1999). Rapid changes in the mechanism of ocean convection during the last glacial period. *Nature, 401*(6752), 458-461.

Dokken, T. M., Nisancioglu, K. H., Li, C., Battisti, D. S., & Kissel, C. (2013). Dansgaard-Oeschger cycles: Interactions between ocean and sea ice intrinsic to the Nordic seas. *Paleoceanography, 28*(3), 491-502. doi:10.1002/palo.20042

Dowdeswell, J., Elverhøi, A., & Spielhagen, R. (1998). Glacimarine sedimentary processes and facies on the Polar North Atlantic margins. *Quaternary Science Reviews, 17*(1-3), 243-272.

Drange, H., Dokken, T., Furevik, T., Gerdes, R., Berger, W., Nesje, A., . . . Østerhus, S. (2005). *The Nordic seas: an overview*: Wiley Online Library.

Dyke, A., Andrews, J., Clark, P., England, J., Miller, G., Shaw, J., & Veillette, J. (2002). The Laurentide and Innuitian ice sheets during the last glacial maximum. *Quaternary Science Reviews, 21*(1-3), 9-31.

Elderfield, H., Yu, J., Anand, P., Kiefer, T., & Nyland, B. (2006). Calibrations for benthic foraminiferal Mg/Ca paleothermometry and the carbonate ion hypothesis. *Earth and Planetary Science Letters, 250*(3-4), 633-649.

Elliot, M., Labeyrie, L., Bond, G., Cortijo, E., Turon, J. L., Tisnerat, N., & Duplessy, J. C. (1998). Millennial-scale iceberg discharges in the Irminger Basin during the last glacial period: Relationship with the Heinrich events and environmental settings. *Paleoceanography, 13*(5), 433-446.

Ezat, M. M., Rasmussen, T. L., & Groeneveld, J. (2014). Persistent intermediate water warming during cold stadials in the southeastern Nordic seas during the past 65 ky. *Geology, 42*(8), 663-666.

Fahl, K., & Stein, R. (2012). Modern seasonal variability and deglacial/Holocene change of central Arctic Ocean sea-ice cover: new insights from biomarker proxy records. *Earth and Planetary Science Letters, 351*, 123-133.

Farmer, G. L., Barber, D., & Andrews, J. (2003). Provenance of Late Quaternary ice-proximal sediments in the North Atlantic: Nd, Sr and Pb isotopic evidence. *Earth and Planetary Science Letters, 209*(1-2), 227-243.

Fetterer, F., Knowles, K., Meier, W. N., Savoie, M., Windnagel, A. K. (2017, updated daily). Sea Ice Index, Version 3. Boulder, Colorado USA. NSIDC: National Snow and Ice Data Center. doi: https://doi.org/10.7265/N5K072F8. (11.09.2019). Retrieved from https://nsidc.org/data/G02135/versions/3

Funder, S., Jennings, A., & Kelly, M. (2004). Middle and late Quaternary glacial limits in Greenland. In *Developments in Quaternary Sciences* (Vol. 2, pp. 425-430): Elsevier.

Funder, S., Kjeldsen, K. K., Kjær, K. H., & Cofaigh, C. Ó. (2011). The Greenland Ice Sheet during the past 300,000 years: A review. In *Developments in Quaternary Sciences* (Vol. 15, pp. 699-713): Elsevier.

Ganopolski, A., Calov, R., & Claussen, M. (2010). Simulation of the last glacial cycle with a coupled climate ice-sheet model of intermediate complexity. *Climate of the Past, 6*(2), 229-244.

Gildor, H., & Tziperman, E. (2003). Sea-ice switches and abrupt climate change. *Philosophical Transactions of the Royal Society of London. Series A: Mathematical, Physical and Engineering Sciences, 361*(1810), 1935-1944.

Goldschmidt, P., Pfirman, S., Wollenburg, I., & Henrich, R. (1992). Origin of sediment pellets from the Arctic seafloor: sea ice or icebergs? *Deep Sea Research Part A. Oceanographic Research Papers, 39*(2), S539-S565.

Greaves, M., Caillon, N., Rebaubier, H., Bartoli, G., Bohaty, S., Cacho, I., . . . Delaney, M. (2008). Interlaboratory comparison study of calibration standards for foraminiferal Mg/Ca thermometry. *Geochemistry, Geophysics, Geosystems, 9*(8).

Griem, L., Voelker, A. H., Berben, S. M., Dokken, T. M., & Jansen, E. (2019). Insolation and glacial meltwater influence on sea-ice and circulation variability in the northeastern Labrador Sea during the last Glacial. *Paleoceanography and Paleoclimatology*.

Gudmundsson, H. (2013). Ice-shelf buttressing and the stability of marine ice sheets. *The Cryosphere, 7*(2), 647-655.

Gwiazda, R. H., Hemming, S. R., & Broecker, W. S. (1996). Tracking the sources of icebergs with lead isotopes: The provenance of ice-rafted debris in Heinrich layer 2. *Paleoceanography, 11*(1), 77-93.

Hansen, L., Funder, S., Murray, A., & Mejdahl, V. (1999). Luminescence dating of the last Weichselian glacier advance in East Greenland. *Quaternary Science Reviews, 18*(2), 179-190.

Hasenfratz, A. P., Schiebel, R., Thornalley, D. J., Schönfeld, J., Jaccard, S. L., Martínez-García, A., . . . Lear, C. H. (2017). Mg/Ca-temperature calibration for the benthic foraminifera Melonis barleeanum and Melonis pompilioides. *Geochimica et Cosmochimica Acta, 217*, 365-383.

Hátún, H., Sandø, A. B., Drange, H., Hansen, B., & Valdimarsson, H. (2005). Influence of the Atlantic subpolar gyre on the thermohaline circulation. *Science, 309*(5742), 1841-1844.

Heinrich, H. (1988). Origin and consequences of cyclic ice rafting in the northeast Atlantic Ocean during the past 130,000 years. *Quaternary research, 29*(2), 142-152.

Hemming, S. (2004). Heinrich events: Massive late Pleistocene detritus layers of the North Atlantic and their global climate imprint. *Reviews of Geophysics, 42*(1).

Hemming, S., Gwiazda, R., Andrews, J., Broecker, W., Jennings, A., & Onstott, T. (2000). 40Ar/39Ar and Pb-Pb study of individual hornblende and feldspar grains from southeastern Baffin Island glacial sediments: Implications for the provenance of the Heinrich layers. *Canadian Journal of Earth Sciences, 37*(6), 879-890.

Henry, L., McManus, J. F., Curry, W. B., Roberts, N. L., Piotrowski, A. M., & Keigwin, L. (2016). North Atlantic ocean circulation and abrupt climate change during the last glaciation. *Science, 353*(6298), 470-474.

Hesse, R. (2015). Ice-proximal Labrador Sea Heinrich layers: a sedimentological approach. *Canadian Journal of Earth Sciences, 53*(1), 71-100.

Hill, H. W., Flower, B. P., Quinn, T. M., Hollander, D. J., & Guilderson, T. P. (2006). Laurentide Ice Sheet meltwater and abrupt climate change during the last glaciation. *Paleoceanography, 21*(1).

Hillaire-Marcel, C., Vernal, A. d., Bilodeau, G., & Wu, G. (1994). Isotope stratigraphy, sedimentation rates, deep circulation, and carbonate events in the Labrador Sea during the last~ 200 ka. *Canadian Journal of Earth Sciences, 31*(1), 63-89.

Hodell, D. A., Channell, J. E., Curtis, J. H., Romero, O. E., & Röhl, U. (2008). Onset of "Hudson Strait" Heinrich events in the eastern North Atlantic at the end of the middle Pleistocene transition (~ 640 ka)? *Paleoceanography, 23*(4).

Hodell, D. A., Evans, H. F., Channell, J. E., & Curtis, J. H. (2010). Phase relationships of North Atlantic ice-rafted debris and surface-deep climate proxies during the last glacial period. *Quaternary Science Reviews, 29*(27), 3875-3886.

Hoff, U., Rasmussen, T. L., Stein, R., Ezat, M. M., & Fahl, K. (2016). Sea ice and millennial-scale climate variability in the Nordic seas 90[thinsp]kyr ago to present. *Nat Commun, 7*. doi:10.1038/ncomms12247

Hopkins, T. S. (1991). The GIN Sea—A synthesis of its physical oceanography and literature review 1972–1985. *Earth-Science Reviews, 30*(3-4), 175-318.

Hubbard, A., Sugden, D., Dugmore, A., Norddahl, H., & Pétursson, H. G. (2006). A modelling insight into the Icelandic Last Glacial Maximum ice sheet. *Quaternary Science Reviews, 25*(17-18), 2283-2296.

Huber, C., Leuenberger, M., Spahni, R., Flückiger, J., Schwander, J., Stocker, T. F., . . . Jouzel, J. (2006). Isotope calibrated Greenland temperature record over Marine Isotope Stage 3 and its relation to CH4. *Earth and Planetary Science Letters, 243*(3-4), 504-519.

Huck, T. (2010). *Recent changes in the North Atlantic circulation.* Paper presented at the Iceland in the Central Northern Atlantic: hotspot, sea currents and climate change.

Hughes, A. L., Gyllencreutz, R., Lohne, Ø. S., Mangerud, J., & Svendsen, J. I. (2016). The last Eurasian ice sheets–a chronological database and time-slice reconstruction, DATED-1. *Boreas, 45*(1), 1-45.

Hunter, S., Wilkinson, D., Louarn, E., McCave, I. N., Rohling, E., Stow, D. A., & Bacon, S. (2007). Deep western boundary current dynamics and associated sedimentation on the Eirik Drift, Southern Greenland Margin. *Deep Sea Research Part I: Oceanographic Research Papers, 54*(12), 2036-2066.

ice2ice. (2016). Ice2Ice Cruise GS16-204, 16. Aug - 5. Sept 2016. Retrieved from https://www.bcdc.no/files/bcdc-theme/documents/GS16-204_cruise%20report.pdf

Imbrie, J., Mix, A., & Martinson, D. (1993). Milankovitch theory viewed from Devils Hole. *Nature, 363*, 10.

Innocent, C., Fagel, N., & Hillaire-Marcel, C. (2000). Sm–Nd isotope systematics in deep-sea sediments: clay-size versus coarser fractions. *Marine Geology, 168*(1-4), 79-87.

IPCC. (2013). *Climate Change 2013: The Physical Science Basis. Contribution of Working Group I to the Fifth Assessment Report of the Intergovernmental Panel on Climate Change*. In T. F. Stocker, D. Qin, G.-K. Plattner, M. Tignor, S.K. Allen, J. Boschung, A. Nauels, Y. Xia, V. Bex and P.M. Midgley (Ed.), (pp. 1535 pp). Retrieved from https://www.ipcc.ch/report/ar5/wg1/

Jansen, E., Christensen, J. H., Dokken, T., Nisancioglu, K. H., Vinther, B. M., Capron, E., . . . Pedersen, R. A. (2020). Past perspectives on the present era of abrupt Arctic climate change. *Nature Climate Change*, 1-8.

Jensen, M. F., Nilsson, J., & Nisancioglu, K. H. (2016). The interaction between sea ice and salinity-dominated ocean circulation: implications for halocline stability and rapid changes of sea ice cover. *Climate Dynamics, 47*(9-10), 3301-3317.

Johannessen, T., Jansen, E., Flatøy, A., & Ravelo, A. C. (1994). The relationship between surface water masses, oceanographic fronts and paleoclimatic proxies in surface sediments of the Greenland, Iceland, Norwegian Seas. In *Carbon cycling in the glacial ocean: constraints on the ocean's role in global change* (pp. 61-85): Springer.

Joughin, I., & Alley, R. B. (2011). Stability of the West Antarctic ice sheet in a warming world. *Nature Geoscience, 4*(8), 506.

Kindler, P., Guillevic, M., Baumgartner, M., Schwander, J., Landais, A., & Leuenberger, M. (2014). Temperature reconstruction from 10 to 120 kyr b2k from the NGRIP ice core. *Climate of the Past, 10*(2), 887-902.

Kissel, C., Laj, C., Labeyrie, L., Dokken, T., Voelker, A., & Blamart, D. (1999). Rapid climatic variations during marine isotopic stage 3: magnetic analysis of sediments from Nordic Seas and North Atlantic. *Earth and Planetary Science Letters, 171*(3), 489-502.

Kissel, C., Laj, C., Piotrowski, A. M., Goldstein, S. L., & Hemming, S. R. (2008). Millennial-scale propagation of Atlantic deep waters to the glacial Southern Ocean. *Paleoceanography, 23*(2).

Klein, E. S., Cherry, J., Young, J., Noone, D., Leffler, A., & Welker, J. (2015). Arctic cyclone water vapor isotopes support past sea ice retreat recorded in Greenland ice. *Scientific Reports, 5*, 10295.

Knutz, P. C., Sicre, M. A., Ebbesen, H., Christiansen, S., & Kuijpers, A. (2011). Multiple-stage deglacial retreat of the southern Greenland Ice Sheet linked with Irminger Current warm water transport. *Paleoceanography, 26*(3).

Kohfeld, K. E., Fairbanks, R. G., Smith, S. L., & Walsh, I. D. (1996). Neogloboquadrina pachyderma (sinistral coiling) as paleoceanographic tracers in polar oceans: Evidence from Northeast Water Polynya plankton tows, sediment traps, and surface sediments. *Paleoceanography, 11*(6), 679-699.

Kopec, B. G., Feng, X., Michel, F. A., & Posmentier, E. S. (2016). Influence of sea ice on Arctic precipitation. *Proceedings of the National Academy of Sciences, 113*(1), 46-51.

Kuhlbrodt, T., Griesel, A., Montoya, M., Levermann, A., Hofmann, M., & Rahmstorf, S. (2007). On the driving processes of the Atlantic meridional overturning circulation. *Reviews of Geophysics, 45*(2).

Lambeck, K., & Chappell, J. (2001). Sea level change through the last glacial cycle. *Science, 292*(5517), 679-686.

Lambeck, K., Rouby, H., Purcell, A., Sun, Y., & Sambridge, M. (2014). Sea level and global ice volumes from the Last Glacial Maximum to the Holocene. *Proceedings of the National Academy of Sciences, 111*(43), 15296-15303.

Lazier, J. R. (1973). *The renewal of Labrador Sea water.* Paper presented at the Deep Sea Research and Oceanographic Abstracts.

Ledbetter, M. T., & Balsam, W. L. (1985). Paleoceanography of the Deep Western Boundary Undercurrent on the North American continental margin for the past 25 000 yr. *Geology, 13*(3), 181-184.

Levine, R. C., & Bigg, G. R. (2008). Sensitivity of the glacial ocean to Heinrich events from different iceberg sources, as modeled by a coupled atmosphere-iceberg-ocean model. *Paleoceanography and Paleoclimatology, 23*(4).

Li, C., Battisti, D. S., & Bitz, C. M. (2010). Can North Atlantic sea ice anomalies account for Dansgaard–Oeschger climate signals? *Journal of Climate, 23*(20), 5457-5475.

Li, C., & Born, A. (2019). Coupled atmosphere-ice-ocean dynamics in Dansgaard-Oeschger events. *Quaternary Science Reviews, 203*, 1-20.

Lisitzin, A. P. (2012). *Sea-ice and iceberg sedimentation in the ocean: recent and past*: Springer Science & Business Media.

Lloyd, J. M. (2006). Modern distribution of benthic foraminifera from Disko Bugt, west Greenland. *The Journal of Foraminiferal Research, 36*(4), 315-331.

MacAyeal, D. (1993). Binge/purge oscillations of the Laurentide ice sheet as a cause of the North Atlantic's Heinrich events. *Paleoceanography, 8*(6), 775-784.

Marcott, S. A., Clark, P. U., Padman, L., Klinkhammer, G. P., Springer, S. R., Liu, Z., . . . Padman, J. (2011). Ice-shelf collapse from subsurface warming as a trigger for Heinrich events. *Proceedings of the National Academy of Sciences, 108*(33), 13415-13419.

Margold, M., Stokes, C. R., & Clark, C. D. (2015). Ice streams in the Laurentide Ice Sheet: Identification, characteristics and comparison to modern ice sheets. *Earth-Science Reviews, 143*, 117-146.

Maslin, M. S., Dan Lowe, John (2013). Synthesis of the Nature and Causes of Rapid Climate Transitions During the Quaternary. In B. J. H. a. M. M. D. Seidov (Ed.), *The Oceans and Rapid Climate Change* (pp. 9-52).

Masson-Delmotte, V., Jouzel, J., Landais, A., Stievenard, M., Johnsen, S. J., White, J., . . . Fuhrer, K. (2005). GRIP deuterium excess reveals rapid and orbital-scale changes in Greenland moisture origin. *Science, 309*(5731), 118-121.

McCave, I., Manighetti, B., & Beveridge, N. (1995). Circulation in the glacial North Atlantic inferred from grain-size measurements. *Nature, 374*(6518), 149-152.

McCave, I., & Tucholke, B. (1986). Deep current-controlled sedimentation in the western North Atlantic. *The Geology of North America, 1000*, 451-468.

McMartin, I., Campbell, J. E., & Dredge, L. A. (2019). Middle Wisconsinan marine shells near Repulse Bay, Nunavut, Canada: implications for Marine Isotope Stage 3 ice-free conditions and Laurentide Ice Sheet dynamics in north-west Hudson Bay. *Journal of Quaternary Science, 34*(1), 64-75.

Milankovitch, M. (1930). Mathematische klimalehre und astronomische theorie der klimaschwankungen. *Handbuch der Klimatologie 1*.

Mouginot, J., Rignot, E., Scheuchl, B., Fenty, I., Khazendar, A., Morlighem, M., . . . Paden, J. (2015). Fast retreat of Zachariæ Isstrøm, northeast Greenland. *Science, 350*(6266), 1357-1361.

Müller, J., Massé, G., Stein, R., & Belt, S. T. (2009). Variability of sea-ice conditions in the Fram Strait over the past 30,000 years. *Nature Geoscience, 2*(11), 772.

Müller, J., Wagner, A., Fahl, K., Stein, R., Prange, M., & Lohmann, G. (2011). Towards quantitative sea ice reconstructions in the northern North Atlantic: A combined biomarker and numerical modelling approach. *Earth and Planetary Science Letters, 306*(3-4), 137-148.

NGRIP, m. N. G. I. C. P. (2004). Ice Core Project members. High-resolution record of Northern Hemisphere climate extending into the last interglacial period. *Nature, 431*, 147-151.

Nicholl, J. A., Hodell, D. A., Naafs, B. D. A., Hillaire-Marcel, C., Channell, J. E., & Romero, O. E. (2012). A Laurentide outburst flooding event during the last interglacial period. *Nature Geoscience, 5*(12), 901.

Nürnberg, D., Wollenburg, I., Dethleff, D., Eicken, H., Kassens, H., Letzig, T., . . . Thiede, J. (1994). Sediments in Arctic sea ice: implications for entrainment, transport and release. *Marine Geology, 119*(3-4), 185-214.

Patton, H., Hubbard, A., Andreassen, K., Auriac, A., Whitehouse, P. L., Stroeven, A. P., . . . Hall, A. M. (2017a). Deglaciation of the Eurasian ice sheet complex. *Quaternary Science Reviews, 169*, 148-172.

Patton, H., Hubbard, A., Andreassen, K., Winsborrow, M., & Stroeven, A. P. (2016). The build-up, configuration, and dynamical sensitivity of the Eurasian ice-sheet complex to Late Weichselian climatic and oceanic forcing. *Quaternary Science Reviews, 153*, 97-121.

Patton, H., Hubbard, A., Bradwell, T., & Schomacker, A. (2017b). The configuration, sensitivity and rapid retreat of the Late Weichselian Icelandic ice sheet. *Earth-Science Reviews, 166*, 223-245.

Peck, V. L., Hall, I. R., Zahn, R., Grousset, F., Hemming, S., & Scourse, J. (2007). The relationship of Heinrich events and their European precursors over the past 60ka BP: a multi-proxy ice-rafted debris provenance study in the North East Atlantic. *Quaternary Science Reviews, 26*(7), 862-875.

Pedersen, R. A., & Christensen, J. H. (2019). Attributing Greenland warming patterns to regional Arctic sea ice loss. *Geophysical Research Letters, 46*(17-18), 10495-10503.

Perner, K., Jennings, A. E., Moros, M., Andrews, J. T., & Wacker, L. (2016). Interaction between warm Atlantic-sourced waters and the East Greenland Current in northern Denmark Strait (68° N) during the last 10 600 cal a BP. *Journal of Quaternary Science, 31*(5), 472-483.

Pflaumann, U., Duprat, J., Pujol, C., & Labeyrie, L. D. (1996). SIMMAX: A modern analog technique to deduce Atlantic sea surface temperatures from planktonic foraminifera in deep-sea sediments. *Paleoceanography, 11*(1), 15-35.

Pico, T., Birch, L., Weisenberg, J., & Mitrovica, J. (2018). Refining the Laurentide Ice Sheet at Marine Isotope Stage 3: A data-based approach combining glacial isostatic simulations with a dynamic ice model. *Quaternary Science Reviews, 195*, 171-179.

Rahmstorf, S. (2002). Ocean circulation and climate during the past 120,000 years. *Nature, 419*(6903), 207-214.

Rahmstorf, S. (2003). Thermohaline circulation: The current climate. *Nature, 421*(6924), 699-699.

Rahmstorf, S., Box, J. E., Feulner, G., Mann, M. E., Robinson, A., Rutherford, S., & Schaffernicht, E. J. (2015). Exceptional twentieth-century slowdown in Atlantic Ocean overturning circulation. *Nature Climate Change, 5*(5), 475.

Ramseier, R. O., Garrity, C., & Martin, T. (2001). An overview of sea-ice conditions in the Greenland Sea and the relationship of oceanic sedimentation to the ice regime. In *The Northern North Atlantic* (pp. 19-38): Springer.

Rashid, H., Hesse, R., & Piper, D. J. (2003). Evidence for an additional Heinrich event between H5 and H6 in the Labrador Sea. *Paleoceanography, 18*(4).

Rasmussen, S. O., Bigler, M., Blockley, S. P., Blunier, T., Buchardt, S. L., Clausen, H. B., . . . Fischer, H. (2014). A stratigraphic framework for abrupt climatic changes during the Last Glacial period based on three synchronized Greenland ice-core records: refining and extending the INTIMATE event stratigraphy. *Quaternary Science Reviews, 106*, 14-28.

Rasmussen, T. L., & Thomsen, E. (2004). The role of the North Atlantic Drift in the millennial timescale glacial climate fluctuations. *Palaeogeography, Palaeoclimatology, Palaeoecology, 210*(1), 101-116.

Rasmussen, T. L., & Thomsen, E. (2013). Pink marine sediments reveal rapid ice melt and Arctic meltwater discharge during Dansgaard–Oeschger warmings. *Nature communications, 4*.

Rasmussen, T. L., Van Weering, T. C., & Labeyrie, L. (1997). Climatic instability, ice sheets and ocean dynamics at high northern latitudes during the last glacial period (58-10 KA BP). *Quaternary Science Reviews, 16*(1), 71-80.

Reeh, N. (2004). Holocene climate and fjord glaciations in Northeast Greenland: implications for IRD deposition in the North Atlantic. *Sedimentary Geology, 165*(3-4), 333-342.

Reimer, P. J., Bard, E., Bayliss, A., Beck, J. W., Blackwell, P. G., Ramsey, C. B., . . . Friedrich, M. (2013). IntCal13 and Marine13 radiocarbon age calibration curves 0–50,000 years cal BP. *Radiocarbon, 55*(4), 1869-1887. doi:10.2458/azu_js_rc.55.16947

Rosenthal, Y., Field, M. P., & Sherrell, R. M. (1999). Precise determination of element/calcium ratios in calcareous samples using sector field inductively coupled plasma mass spectrometry. *Analytical chemistry, 71*(15), 3248-3253.

Ruddiman, W. (2008). Earth's Climate: Past and Future, 2nd edn. ed. *New York*.

Ruddiman, W. F. (1977). Late Quaternary deposition of ice-rafted sand in the subpolar North Atlantic (lat 40 to 65 N). *Geological Society of America Bulletin, 88*(12), 1813-1827.

Rutledal, S., Berben, S. M., Dokken, T. M., Van Der Bilt, W. G., Cederstrøm, J. M., & Jansen, E. (2020a). Tephra horizons identified in the western North Atlantic and Nordic Seas during the Last Glacial Period: Extending the marine tephra framework. *Quaternary Science Reviews*, 106247.

Rutledal, S., Haflidason, H., Berben, S. M., Griem, L., & Jansen, E. (2020b). A continuous tephrostratigraphic record from the Labrador Sea spanning the last 65 ka. *Journal of Quaternary Science*.

Sadatzki, H., Dokken, T. M., Berben, S. M. P., Muschitiello, F., Stein, R., Fahl, K., . . . Jansen, E. (2019). Sea ice variability in the southern Norwegian Sea during glacial Dansgaard-Oeschger climate cycles. *Science Advances, 5: eaau6174*(3). doi:10.1126/sciadv.aau6174

Scambos, T. A., Bohlander, J., Shuman, C. u., & Skvarca, P. (2004). Glacier acceleration and thinning after ice shelf collapse in the Larsen B embayment, Antarctica. *Geophysical Research Letters, 31*(18).

Schlitzer, R. (2015). Ocean Data View. odv.awi.de.

Schmidt, M., & Hertzberg, J. (2011). Abrupt climate change during the last ice age. *Nat Educ Knowl, 3*(10), 11.

Scourse, J. D., Haapaniemi, A. I., Colmenero-Hidalgo, E., Peck, V. L., Hall, I. R., Austin, W. E., . . . Zahn, R. (2009). Growth, dynamics and deglaciation of the last British–Irish ice sheet: the deep-sea ice-rafted detritus record. *Quaternary Science Reviews, 28*(27-28), 3066-3084.

Seidenkrantz, M.-S. (2013). Benthic foraminifera as palaeo sea-ice indicators in the subarctic realm – examples from the Labrador Sea–Baffin Bay region. *Quaternary Science Reviews, 79*, 135-144. doi:http://dx.doi.org/10.1016/j.quascirev.2013.03.014

Seidenkrantz, M.-S., Kuijpers, A., Aagaard-Sørensen, S., Andersson, S., Lindgreen, H., Ploug, J., . . . Ivanov, M. (2010). Glacial ocean circulation and shelf edge glaciation offshore SW Greenland during the past 75.000 years.

Seierstad, I. K., Abbott, P. M., Bigler, M., Blunier, T., Bourne, A. J., Brook, E., . . . Cook, E. (2014). Consistently dated records from the Greenland GRIP, GISP2 and NGRIP ice cores for the past 104 ka reveal regional millennial-scale δ18O gradients with possible Heinrich event imprint. *Quaternary Science Reviews, 106*, 29-46.

Sejrup, H., Nygård, A., Hall, A., & Haflidason, H. (2009). Middle and Late Weichselian (Devensian) glaciation history of south-western Norway, North Sea and eastern UK. *Quaternary Science Reviews, 28*(3-4), 370-380.

Sessford, E., Jensen, M., Tisserand, A., Muschitiello, F., Dokken, T., Nisancioglu, K., & Jansen, E. (2019). Consistent fluctuations in intermediate water temperature off the coast of Greenland and Norway during Dansgaard-Oeschger events. *Quaternary Science Reviews, 223*, 105887.

Sessford, E., Tisserand, A., Risebrobakken, B., Andersson, C., Dokken, T., & Jansen, E. (2018). High-Resolution Benthic Mg/Ca Temperature Record of the Intermediate Water in the Denmark Strait Across D-O Stadial-Interstadial Cycles. *Paleoceanography and Paleoclimatology, 33*(11), 1169-1185.

Siddall, M., Rohling, E., Almogi-Labin, A., Hemleben, C., Meischner, D., Schmelzer, I., & Smeed, D. (2003). Sea-level fluctuations during the last glacial cycle. *Nature, 423*(6942), 853.

Siegert, M. J., Dowdeswell, J. A., Hald, M., & Svendsen, J.-I. (2001). Modelling the Eurasian Ice Sheet through a full (Weichselian) glacial cycle. *Global and Planetary Change, 31*(1-4), 367-385.

Simon, Q., Hillaire-Marcel, C., St-Onge, G., & Andrews, J. T. (2014). North-eastern Laurentide, western Greenland and southern Innuitian ice stream dynamics during the last glacial cycle. *Journal of Quaternary Science, 29*(1), 14-26.

Simstich, J., Sarnthein, M., & Erlenkeuser, H. (2003). Paired δ 18 O signals of Neogloboquadrina pachyderma (s) and Turborotalita quinqueloba show thermal stratification structure in Nordic Seas. *Marine Micropaleontology, 48*(1), 107-125.

Smith, K. L., Robison, B. H., Helly, J. J., Kaufmann, R. S., Ruhl, H. A., Shaw, T. J., . . . Vernet, M. (2007). Free-drifting icebergs: hot spots of chemical and biological enrichment in the Weddell Sea. *Science, 317*(5837), 478-482.

Steen-Larsen, H. C., Sveinbjörnsdottir, A. E., Peters, A., Masson-Delmotte, V., Guishard, M., Hsiao, G., . . . White, J. (2014). Climatic controls on water vapor deuterium excess in the marine boundary layer of the North Atlantic based on 500 days of in situ, continuous measurements. *Atmospheric Chemistry and Physics, 14*(15), 7741-7756.

Stoner, J., Channell, J., & Hillaire-Marcel, C. (1998). A 200 ka geomagnetic chronostratigraphy for the Labrador Sea: Indirect correlation of the sediment record to SPECMAP. *Earth and Planetary Science Letters, 159*(3), 165-181.

Straneo, F., Sutherland, D. A., Holland, D., Gladish, C., Hamilton, G. S., Johnson, H. L., . . . Koppes, M. (2012). Characteristics of ocean waters reaching Greenland's glaciers. *Annals of Glaciology, 53*, 60.

Tegzes, A. D., Jansen, E., & Telford, R. J. (2015). Which is the better proxy for paleo-current strength: Sortable-silt mean size ($\overline{SS}$) or sortable-silt mean grain diameter (dSS)? A

case study from the Nordic Seas. *Geochemistry, Geophysics, Geosystems, 16*(10), 3456-3471. doi:10.1002/2014GC005655

Thornalley, D. J., Oppo, D. W., Ortega, P., Robson, J. I., Brierley, C. M., Davis, R., . . . Spooner, P. T. (2018). Anomalously weak Labrador Sea convection and Atlantic overturning during the past 150 years. *Nature, 556*(7700), 227.

Tisserand, A. A., Dokken, T. M., Waelbroeck, C., Gherardi, J. M., Scao, V., Fontanier, C., & Jorissen, F. (2013). Refining benthic foraminiferal Mg/Ca-temperature calibrations using core-tops from the western tropical Atlantic: Implication for paleotemperature estimation. *Geochemistry, Geophysics, Geosystems, 14*(4), 929-946.

Vasskog, K., Langebroek, P. M., Andrews, J. T., Nilsen, J. E. Ø., & Nesje, A. (2015). The Greenland Ice Sheet during the last glacial cycle: Current ice loss and contribution to sea-level rise from a palaeoclimatic perspective. *Earth-Science Reviews, 150*, 45-67.

Verplanck, E. P., Farmer, G. L., Andrews, J., Dunhill, G., & Millo, C. (2009). Provenance of Quaternary glacial and glacimarine sediments along the southeast Greenland margin. *Earth and Planetary Science Letters, 286*(1), 52-62.

Vettoretti, G., & Peltier, W. R. (2016). Thermohaline instability and the formation of glacial North Atlantic super polynyas at the onset of Dansgaard-Oeschger warming events. *Geophysical Research Letters*.

Vettoretti, G., & Peltier, W. R. (2018). Fast physics and slow physics in the nonlinear Dansgaard–Oeschger relaxation oscillation. *Journal of Climate, 31*(9), 3423-3449.

Vidal, L., Labeyrie, L., Cortijo, E., Arnold, M., Duplessy, J., Michel, E., . . . Van Weering, T. (1997). Evidence for changes in the North Atlantic Deep Water linked to meltwater surges during the Heinrich events. *Earth and Planetary Science Letters, 146*(1-2), 13-27.

Voelker, A. H. (2002). Global distribution of centennial-scale records for Marine Isotope Stage (MIS) 3: a database. *Quaternary Science Reviews, 21*(10), 1185-1212.

Voelker, A. H., Sarnthein, M., Grootes, P. M., & Schleicher, M. (1998). *Correlation of marine 14C ages from the Nordic Seas with the GISP2 isotope record: Implications for 14C calibration beyond 25 ka BP.* Paper presented at the Radiocarbon.

Volkman, J. K., Barrett, S. M., Dunstan, G. A., & Jeffrey, S. (1993). Geochemical significance of the occurrence of dinosterol and other 4-methyl sterols in a marine diatom. *Organic Geochemistry, 20*(1), 7-15.

Waelbroeck, C., Labeyrie, L., Michel, E., Duplessy, J. C., McManus, J., Lambeck, K., . . . Labracherie, M. (2002). Sea-level and deep water temperature changes derived from benthic foraminifera isotopic records. *Quaternary Science Reviews, 21*(1), 295-305.

Waelbroeck, C., Lougheed, B. C., Riveiros, N. V., Missiaen, L., Pedro, J., Dokken, T., . . . Dumoulin, J.-P. (2019). Consistently dated Atlantic sediment cores over the last 40 thousand years. *Scientific data, 6*(1), 1-12.

White, L. F., Bailey, I., Foster, G. L., Allen, G., Kelley, S. P., Andrews, J. T., . . . Storey, C. D. (2016). Tracking the provenance of Greenland-sourced, Holocene aged, individual sand-sized ice-rafted debris using the Pb-isotope compositions of feldspars and 40Ar/39Ar ages of hornblendes. *Earth and Planetary Science Letters, 433*, 192-203.

I

Insolation and Glacial Meltwater Influence on Sea-Ice and Circulation Variability in the Northeastern Labrador Sea During the Last Glacial Period

Lisa Griem, Antje H. L. Voelker, Sarah M. P. Berben, Trond M. Dokken, and Eystein Jansen

Published in Paleoceanography and Paleoclimatology, doi: 10.1029/2019PA003605.

Paleoceanography and Paleoclimatology

RESEARCH ARTICLE
10.1029/2019PA003605

Key Points:
- The sea-ice cover in the northeastern Labrador Sea appears to only have varied on millennial timescales between H5 and H4
- Heinrich-like calving events are only evident related to H4 and H3, not H6 and H5
- Enhanced influence of Atlantic water during Greenland interstadials 14, 12 and 8

Supporting Information:
- Supporting Information S1

Correspondence to:
L. Griem,
lisa.griem@uib.no

Citation:
Griem, L., Voelker, A. H. L., Berben, S. M. P., Dokken, T. M., & Jansen, E. (2019). Insolation and glacial meltwater influence on sea-ice and circulation variability in the northeastern Labrador Sea during the last Glacial period. *Paleoceanography and Paleoclimatology*, *34*, 1689–1709. https://doi.org/10.1029/2019PA003605

Received 12 MAR 2019
Accepted 19 SEP 2019
Accepted article online 19 OCT 2019
Published online 1 NOV 2019

Insolation and Glacial Meltwater Influence on Sea-Ice and Circulation Variability in the Northeastern Labrador Sea During the Last Glacial Period

Lisa Griem[1], Antje H. L. Voelker[2,3], Sarah M. P. Berben[1], Trond M. Dokken[4], and Eystein Jansen[1,4]

[1]Department of Earth Science, University of Bergen, Bjerknes Center for Climate Research, Bergen, Norway, [2]Divisão de Geologia e Georecursos Marinhos, Instituto Português do Mar e da Atmosfera (IPMA), Lisbon, Portugal, [3]Centre of Marine Sciences (CCMAR), Universidade do Algarve, Faro, Portugal, [4]NORCE Climate, NORCE Norwegian Research Centre AS, Bjerknes Center for Climate Research, Bergen, Norway

Abstract The variable amounts of ice rafted debris (IRD) and foraminifers in North Atlantic sediments are related to the abrupt, millennial-scale alteration from Greenland stadials to interstadials during the last glacial period and indicate past ice sheet instabilities, changes in sea-ice cover and productivity. In the Norwegian Sea, Greenland stadials were likely characterized by an extensive, near-perennial sea-ice cover whereas Greenland interstadials were seasonally ice-free. The variability in other areas, such as the Labrador Sea, remains, however, obscure. We therefore investigated deep-sea sediment core GS16-204-22CC retrieved south of Greenland. Using a multiproxy approach, we distinguish two sediment regimes and hence different environmental conditions between ca. 65 and 25 ka b2k. Regime 1 (~65-49 ka b2k) is characterized by the dominance of planktic foraminifers in the sediments. During late MIS4 and early MIS3, the site was covered by near-perennial sea-ice with occasional periods of iceberg discharge. During the younger part of regime 1 the northeastern Labrador Sea was seasonally ice-free with hardly any icebergs melting near the site and long-term environmental conditions were less variable. Regime 2 (~49-25 ka b2k) is characterized by pronounced stadial-interstadial variability of foraminifer and IRD fluxes, suggesting an extensive sea-ice cover during most Greenland stadials and seasonally ice-free conditions during most Greenland interstadials. During MIS2 environmental conditions were very similar to those of the younger part of regime 1. While all Heinrich (H) related Greenland stadials are marked by depleted oxygen isotope values at our core site, only H4 and H3 are associated with pronounced IRD peaks.

Plain Language Summary North Atlantic sediments contain variable amounts of sand-sized mineral grains and microorganism shells. Mineral grains indicate iceberg transport from continental ice sheets, like the Greenland ice sheet (more icebergs/melting sea-ice, more grains). If the sea-ice cover is too thick, no light can penetrate and fewer microorganisms live in the water beneath the ice. Using these indicators, we investigated ocean sediments from south of Greenland covering the time period between ca. 65 and 25 thousand years ago. This time period was characterized by several abrupt changes between cold and warm climates on millennial timescales. We find that the ocean south of Greenland was sea-ice covered for most of the year with occasional time periods of iceberg discharge between 65 to 56 thousand years ago. From 56 to 49 thousand years ago the ice-free season was extended and hardly any icebergs melted near the site. From 49 thousand years ago our study area was covered by sea-ice year-round during cold time intervals whereas warm time intervals were only seasonally sea-ice covered. Continental ice sheets were growing during this time interval and we observed two major calving events related to two of the four very cold climate intervals recorded in the analyzed sediment.

1. Introduction

Freshwater influx sourced from ice-sheet instabilities and melting sea-ice has an impact on surface and deep ocean circulation and hence, on global climate. A key area to investigate such dynamics is the Labrador Sea, as it is both a region susceptible to climate change and the location for several key circulation processes. The Labrador Sea is a locus of deep-water formation and plays a role as conduit for deep sea flows and hosts

interactions between warm and cold surface currents. The region comprises a mix of water masses of distinct origin: warmer and more saline Atlantic water, and cooler and fresher Arctic waters (Dickson et al., 2002).

During the last glacial period the North Atlantic region experienced changes in sea surface hydrology as a response to abrupt climate changes (Cortijo et al., 1997), and consequently expanded sea-ice distribution and drifting ice bergs (Bond, 1997). Abrupt climate changes as recorded in Greenland ice cores (Dansgaard-Oeschger (DO) events, Dansgaard et al., 1993) might have been driven by changes in the Nordic Seas sea-ice extent (Dokken et al., 2013; Hoff et al., 2016; Sadatzki et al., 2019). Reduced sea-ice formation during Greenland interstadials allowed for a northward heat transport and subsequent loss of oceanic heat to the atmosphere, whereas during Greenland stadials, a more extended sea-ice cover resulted in a reduced heat exchange. Thus, it is often assumed by model studies that sea-ice has continuously covered the Labrador Sea and extended as far south as 50°N during both Greenland stadial and interstadial conditions (Vettoretti & Peltier, 2016). Along the ice edge, melting icebergs, originating from the ice stream collapses of the Laurentide and Eurasian ice sheets, delivered pronounced amounts of ice rafted debris (IRD) to an area of the North Atlantic known as the Ruddiman belt (55 to 40°N; Bond et al., 1993; Hemming, 2004; Ruddiman, 1977). Prominent layers of IRD coincide with the coldest Greenland stadials every 7 to 15 ka (Bond et al., 1992; Heinrich, 1988; Rashid et al., 2003b). These IRD events are characterized by collapsing ice sheets and possible reduction in overturning circulation, and are referred to as Heinrich (H) events. Over the last glacial cycle six H-layers (H1 to H6) were identified (e.g. Böhm et al., 2015; Rahmstorf, 2002). The main contributor to the IRD-rich H-layers was the Laurentide ice sheet, except for H3 and H6 where the IRD content potentially had a Eurasian source (Hemming, 2004 and references therein). However, the Greenland ice sheet´s contribution to H-layers and IRD influx in general during MIS3 are still obscure, while proxy evidence from the Labrador Sea is non-existent.

Proxy data from the Labrador Sea is required to evaluate potential future climate responses, including the sensitivity of the Greenland ice sheet to rising Arctic temperatures and the impact of a higher freshwater influx on deep-water formation. Evidence from this region can help improve reconstructions of oceanic front boundaries, sea-ice cover fluctuations and ice sheet instabilities, as well as the similarities and differences between the individual Greenland stadials and interstadials. This knowledge is important for model simulations in order to constrain the boundary conditions of abrupt climate changes and lead to a better understanding of today´s abrupt warming and its consequences. To date, the lack of proxy evidence from the Labrador Sea leads to model simulations of climate parameters like sea-ice extent or sea surface temperatures that cannot be validated (e.g. Bagniewski et al., 2017; Drijfhout et al., 2013; Kleppin et al., 2015).

In addition to the unknown variability of the sea-ice cover and surface hydrography in the Labrador Sea, it also remains uncertain whether the Greenland ice sheet reached the continental shelf edge between MIS6 and MIS2 (Funder et al., 2004; Vasskog et al., 2015). It was suggested that the Greenland ice sheet constantly grew throughout MIS3 whereby rapid responses are limited to the ice margins and were caused by rapid forcings (Alley et al., 2010; Ganopolski et al., 2010). Hereby, the sensitivity of the ice margins to climate changes varies geographically, depending on shelf bathymetry and drainage, sea surface temperatures in the vicinity of the ice sheet, sea-level, sea-ice conditions, etc. (Funder et al., 2011). Marine-geological investigations by Funder et al. (2004) suggested that the Greenland ice sheet reached the northern and southeastern shelves at ca. 31 ka b2k and the southwestern to northwestern shelf ca. 10 ky later. To our knowledge, no proxy evidence supporting a Greenland ice sheet collapse similar to those of the Laurentide or Eurasian ice sheets exists. All MIS3 calving events recorded along the East Greenland margin show a similar amplitude and seem to follow a millennial timescale whereby an enhanced IRD input was observed for both Greenland interstadials and stadials (e.g. Elliot et al., 1998; Elliot et al., 2001; Voelker et al., 1998). However, the IRD input could have been hampered by too cold sea-surface temperatures or sea-ice which, according to Dokken et al. (2013), might have covered the Denmark Strait during both Greenland interstadials and stadials. Contrarily, the Nordic Seas were seasonally ice-free during Greenland interstadials providing a potential moisture source for the Greenland ice sheet to grow during MIS3 (e.g. Dokken et al., 2013; Li et al., 2010).

Since proxy evidence about changes in calving rates, surface hydrography and sea-ice cover are currently missing from the Labrador Sea for MIS3, no conclusions about the effect of abrupt climate changes on deep-water convection or the size of the Greenland ice sheet can be drawn. Most studies from the Labrador Sea focus on either long-term low-resolution records (e.g. Evans et al., 2007; Hillaire-Marcel et al., 1994; Hillaire-Marcel et al., 2011; Hiscott et al., 2001; Hunter et al., 2007; Müller-Michaelis &

Uenzelmann-Neben, 2014) or high-resolution reconstructions restricted to the Eemian or the period between MIS2 and the Holocene (e.g. de Vernal & Hillaire-Marcel, 2000; Galaasen et al., 2014; Irvalı et al., 2016; Moffa-Sánchez et al., 2014). The main reason for this time gap is that Greenland shelf sediments were eroded to a large extent during the last glacial maximum (Funder et al., 2004; Vasskog et al., 2015). MIS3 proxy data from the northern Labrador Sea are highly relevant in order to connect the millennial-scale changes in the Nordic Seas with the events recorded in the Ruddiman belt and fill in the knowledge gaps related to abrupt climate changes in this region.

In this study, we investigate a deep-sea sediment core from the Eirik drift, northeastern Labrador Sea, for a time period between the end of MIS4 (ca. 65 ka b2k) and the beginning of MIS2 (ca. 25 ka b2k). Using a combination of high-resolution stable isotope data, IRD and foraminifer fluxes and low-resolution planktic assemblage counts we aim to (1) close the time gap between MIS5 and MIS2 as well as the geographical gap of proxy evidence between 60 and 55°N in the Northwestern Atlantic, (2) draw conclusions about the sensitivity of the Labrador Sea in terms of sea-ice extent, surface hydrography and iceberg discharge during MIS3, and (3) connect the proxy records along the east-to-south Greenland margin by comparing our data to marine sediment cores PS2644-5 (Voelker et al., 1998) and SU90-24 (Elliot et al., 1998).

2. Oceanographic Setting of the Study Site

Sediment core GS16-204-22CC-A (58° 02.83 N, 47° 02.36 W, water depth 3160 m, Figure 1; hereafter 22CC) was retrieved at the Eirik drift by R/V *G.O. Sars* (ice2ice, 2016). The Eirik drift is an elongated, mounded ridge system in the northeastern Labrador Sea where sediments from the Denmark Strait and the Greenland margin are deposited by the Deep Western Boundary Current. The Deep Western Boundary Current follows the topography of the Greenland margin towards the toe of the Eirik drift crest whereafter it turns towards the western Labrador Sea. In this process the Deep Western Boundary Current slows down at the Eirik drift, whereby its velocity and pathway depend on climatic conditions (Hunter et al., 2007; McCave & Tucholke, 1986). During glacial periods the sedimentation rates were, in general, higher on the Greenland slope (<2500 m water depth) compared to the Greenland rise (>3000 m water depth). Sedimentation rates for the Greenland rise are estimated at ~7-10 cm/ky during glacial intervals and >30 cm/ky during the Holocene (Hillaire-Marcel et al., 1994; Stoner et al., 1998). However, this might have changed on shorter timescales (Hillaire-Marcel et al., 1994). The combination of this location´s climate sensitivity and high sediment accumulation rates make the Eirik drift ideal for high-resolution paleoclimate studies on multi-decadal timescales.

The study location is further characterized by an interplay of several surface currents (Figure 1). First, the East Greenland Current (EGC) exports freshwater and sea-ice from the Arctic Ocean, via the Denmark Strait, into the North Atlantic (Hopkins, 1991). The cold EGC protects the coastal glaciers of Greenland from the warm water masses of the Irminger Current. The latter turns south of Iceland, and flows subsequently southwards parallel to the EGC. Reaching the southern tip of Greenland, the water masses of both surface currents mix and the surface watermass becomes warmer and saltier with temperatures between 3 and 8°C in present conditions. The surface circulation continues counter-clockwise around Greenland as the West Greenland Current although one-third is retroflected southwards into the subpolar gyre (e.g. Daniault et al., 2016; Garcia-Ibanez et al., 2018; Holliday et al., 2007). The subpolar gyre redistributes freshwater from the Hudson Strait via the Labrador Current and the Arctic via the EGC. In turn, it advects warmer, saline water from the Atlantic into the Labrador Sea and the Nordic Seas via the Irminger Current and the North Atlantic Current, respectively (e.g. Born & Mignot, 2012; Hátún et al., 2005; Huck, 2010).

The subpolar gyre may have been important in driving DO-events. Its strength and lateral expansion are dependent on atmospheric winds, surface heat exchange and freshwater input whereby all those mechanisms are influenced by sea-ice (Li & Born, 2019). Following Li and Born (2019), an expanded sea-ice cover at our core location would introduce a freshwater perturbation that would weaken deep-water convection, the subpolare gyre and thus the northward transport of heat and salt into the Labrador Sea and Nordic Seas. Such a weakening was found under present conditions (Rhein et al., 2011; Thornalley et al., 2018) as well as during past warm periods (Born et al., 2011). While the glacial subpolar gyre has played a crucial role for freshwater distribution, it was also important for the dispersal of icebergs. Under favorable sea surface

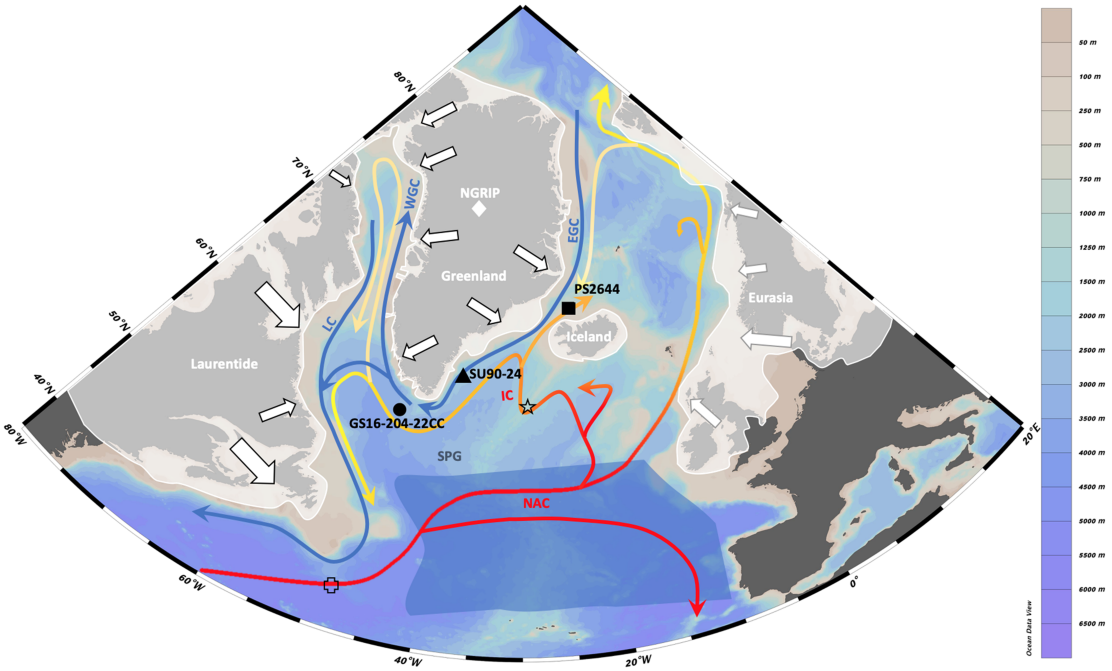

Figure 1. Map of study area from Ocean data view (Schlitzer, 2015) including surface currents (Straneo et al., 2012 and references therein), location of the Ruddiman belt during MIS3 (dark blue shading, Ruddiman, 1977), the late MIS3 ice sheet extent for Greenland, Laurentide, Eurasia and Iceland (modified after Patton et al., 2016 and references therein) and location of sediment cores GS16-204-22CC (this study, circle), PS2644-5 (Voelker et al., 1998, square), SU90-24 (Elliot et al., 1998, triangle), CH69-K09 (Labeyrie et al., 1999, cross), SO82-05 (van Kreveld et al., 2000, star) and ice core NGRIP (white diamond). LC: Labrador Current, WGC: West Greenland Current, EGC: East Greenland Current, IC: Irminger Current, NAC: North Atlantic Current. Arrows indicate flow direction. White arrows indicate major iceberg sources during the last glacial period (Andrews, 2000).

temperature and wind conditions in the North Atlantic, even icebergs from the European ice sheet were transported towards the Labrador Sea (Death et al., 2006).

3. Material and Methods

3.1. Core Description and Sample Preparation

The 1964 cm long calypso core 22CC covers a time interval that spans the early Holocene to approximately the late MIS6. The lower age estimate is based on a distinct red layer at 1670 cm that has previously been observed in other cores from the Labrador Sea and Orphan Knoll and is suggested to have been deposited during early MIS5e (Channell et al., 2012; Nicholl et al., 2012). The core was sampled every 2 cm between 200 and 530 cm with a sample width of 0.5 cm. Bulk sample weights were taken prior to and after freeze-drying. Subsequently, the dried sediment was wet sieved over a 63 μm sieve, whereby the fine fraction was captured. The coarse fraction was dry sieved into size fractions 63-106 μm, 106-150 μm, 150-500 μm, 500-1000 μm and > 1mm, respectively. The weight of drop stones >5 mm was documented separately.

3.2. Radiocarbon Ages

Radiocarbon dating was performed at Beta Analytic Inc., Miami, US and at W. M. Keck Carbon Cycle Accelerator Mass Spectrometry Facility of University of California, Irvine, US (KCCAMS/UCI), respectively. Altogether eleven samples of surface-dwelling polar species *N. pachyderma* (formerly referred to as *N. pachyderma* sinistral, 150-500 μm) were dated. Information regarding the dated material is summarized in Table 1. The AMS ^{14}C ages were calibrated using the Marine13 calibration curve (Reimer et al., 2013) whereby no

Table 1
AMS ^{14}C Ages (Adjusted to b2k by Adding 50 Years) According to the Depths in Sediment Core GS16-204-22CC-A From the Eirik Drift Including, AMS ^{14}C Ages, Calendar Ages, Age Model Ages and the Offset Between the Calendar Age and Our Age Model. In the Right Column the Name of the Laboratory as Well as the Sample Weights are Given

Mean depth (cm)	AMS ^{14}C age (ka b2k)	Calendar age[a] (error 2σ) (ka b2k)	Age model age (ka b2k)	Offset age model from cal. age (ka b2k)	Laboratory (sample weight)
150.5	13.10 ± 0.05	15.09 (14.82 to 15.28)	15.09	0	BETA (5.3 g)
200.25	23.60 ± 0.10	27.49 (27.28 to 27.70)	25.43	-2.06	Keck (7.7 g)
230.25	28.56 ± 0.11	31.89 (31.52 to 32.45)	31.89	0	Keck (9.6 g)
300.25	30.42 ± 0.27	34.10 (33.68 to 34.60)	39.80	5.70	Keck (6.0 g)
370.25	35.48 ± 0.28	39.61 (38.90 to 40.27)	46.04	6.44	Keck (4.9 g)
410.25	48.75 ± 2.50	Outside cal. range	49.62	-	Keck (6.5 g)
450.25	46.98 ± 0.89	Outside cal. range	53.22	-	Keck (9.2 g)
500.5	35.64 ± 0.30	Too young	58.21	-	BETA (6.3 g)
600.25	52.25 ± 1.70	Outside cal. range	Outside investigation period	-	Keck (7.3 g)
640.25	57.55 ± 3.20	Outside cal. range	Outside investigation period	-	Keck (9.5 g)
1000.5	44.60 ± 0.90	Too young	Outside investigation period	-	BETA (5.2 g)

[a]Marine13 (Reimer et al., 2013).

local reservoir corrections were applied. For this study, the calibrated BP (before present=1950 AD) ages were converted to b2k (before 2000 AD) ages by adding 50 years.

3.3. Stable Isotope Measurements

Stable isotope analysis was carried out in the laboratory facilities of FARLAB at the Department of Earth Sciences, University of Bergen, Norway using a ThermoFinnigan MAT253 gas source isotope ratio mass spectrometer. The long-term analytical precision of the instrument is ±0.04‰ and ±0.02‰ for δ^{18}O and δ^{13}C, respectively, based on repeated analysis of in-house standard CM 12 and IAEA standard NBS 18. The results are reported relative to the VPDB scale.

Eight to ten encrusted planktic *N. pachyderma* specimens (50-80 μg) ranging in size from 212 to 250 μm were selected for stable isotope analysis. The foraminifer tests were rinsed with methanol and cleaned in an ultrasonic bath for ten seconds. Isotope measurements were performed on samples between 200 and 600 cm at intervals of 2 cm.

Although the habitat depth of *N. pachyderma* is quite variable and driven by sea-ice and the concentration of chlorophyll (Greco et al., 2019), it is usually concentrated around an isopycnal layer with water densities between 27.7 and 27.8 (σ_τ, Kozdon et al., 2009) at water depths between 70 and 130 m below the fresh EGC. However, depleted planktic δ^{18}O values might indicate a conservative estimate of meltwater input (Simstich et al., 2003). The planktic δ^{18}O signal is a function of salinity and temperature and therefore, depleted planktic δ^{18}O values can also indicate an increased inflow of warm Atlantic water and thus represent a shift between oceanic fronts (Johannessen et al., 1994).

3.4. IRD and Foraminifer Abundances

IRD and foraminifers were counted between 200 and 530.5 cm at 2 cm resolution (total of 166 samples) in the size fractions 150-500 μm, 500-1000 μm and >1mm. In the 150-500 μm fraction about 400 to 1500 grains were counted for both total IRD and foraminifers depending on the number of splits (0-4). The results are reported in number of grains >150 μm g^{-1} dry sediment (combining the three counted size fractions, supporting information and Figure 3) and as fluxes (Figures 4 and 5). Here, IRD consists of the number of lithic grains although volcanic grains were counted separately in order to identify tephra layers. Drop stones (>5 mm) were found throughout the record weighing between 0.2 g and 8.1 g with a size up to 2.5 cm (~38.5 ka b2k). Due to their high impact on the dry bulk sediment weight and their diameter larger than the sample width (0.5 cm), they were not considered for the calculation of IRD and foraminifer abundances. Despite the background noise of IRD throughout the core resulting from the proximity of the Greenland ice sheet, high IRD concentrations occur due to icebergs from calving ice sheets and along the sea-ice edge (Dowdeswell et al., 1998; Ramseier et al., 2001). The lowest IRD concentrations occur during periods of

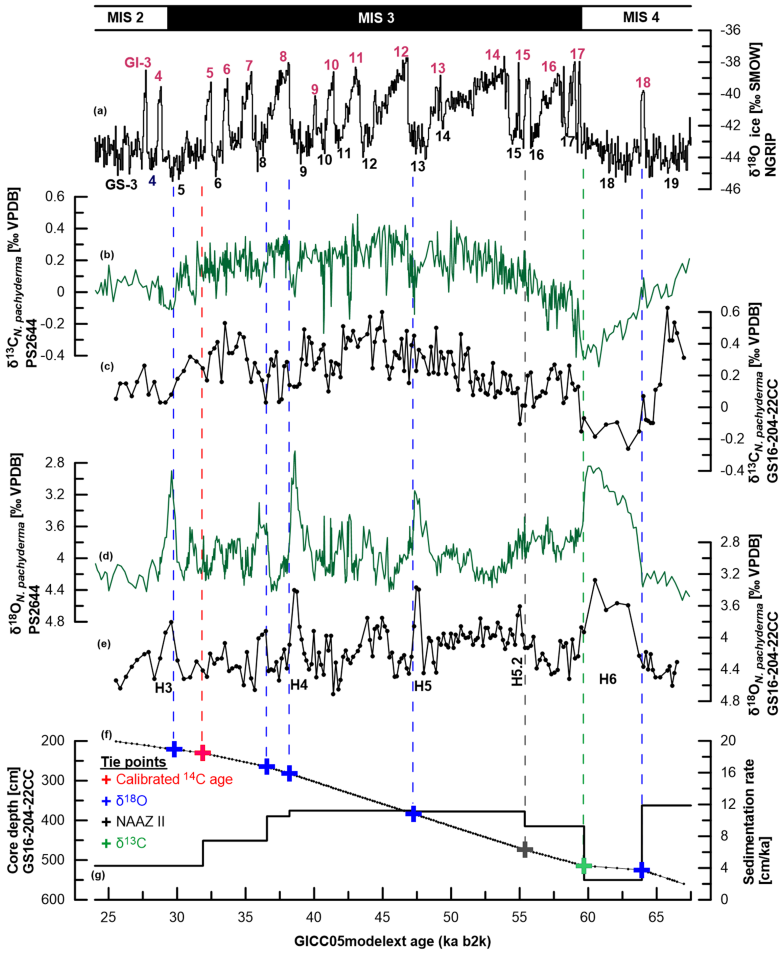

Figure 2. Chronology of core GS16-204-22CC and PS2644-5 (Voelker & Haflidason, 2015a, adjusted to b2k by adding 50 years; Voelker & Haflidason, 2015b) on ka b2k age scale. (a) $\delta^{18}O$ of the NGRIP ice core (Seierstad et al., 2014) with indicated Greenland interstadials (GI, red) and Greenland stadials (GS, black). (b) Planktic $\delta^{13}C$ data of core PS2644-5. (c) Planktic $\delta^{13}C$ data of core GS16-204-22CC. (d) Planktic $\delta^{18}O$ record of core PS2644-5. (e) Planktic $\delta^{18}O$ record of core GS16-204-22CC. (f) Tie-points on age-depth plot: Calibrated ^{14}C age (red cross), $\delta^{18}O$ (blue crosses), North Atlantic Ash Zone (NAAZ) II (gray cross) and $\delta^{13}C$ (green cross). (g) Corresponding sedimentation rates. H3-H6 indicate the corresponding time periods of the depleted $\delta^{18}O$ values.

decreased iceberg discharge or reduced melting, an ice-free ocean or when melting ice does not transport a large amount of coarse debris.

The number of foraminifers consists of benthic and planktic foraminifer tests. The planktic foraminifer abundance (number/g dry sediment) is used as a proxy for sea surface productivity. It is driven by the thickness and extent of the local sea-ice cover controlling the supply of light and nutrients. The highest planktic foraminifer abundances are characteristic for the sea-ice edge, polynyas or large icebergs (e.g. Kohfeld et al., 1996; Ramseier et al., 2001; Smith et al., 2007). Ice-free areas off the sea-

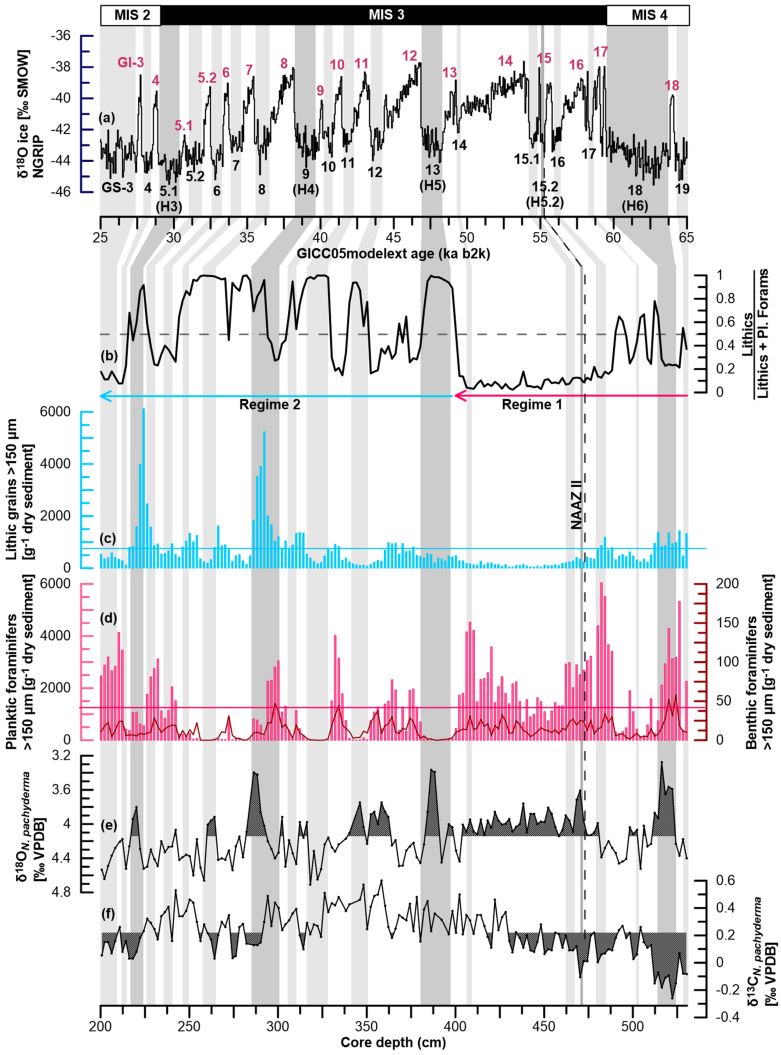

Figure 3. Proxy data of GS16-204-22CC-A versus core depth (bottom) and time (top). All Greenland stadials (GS) are indicated in grey, with a darker grey emphasis on H-associated GS H3-H6. (a) $\delta^{18}O$ of the NGRIP ice core (Seierstad et al., 2014) with indicated Greenland interstadials (GI, red) and GS, (black). (b) Lithics*(Lithics + planktic foraminifers)$^{-1}$ (black), horizontal dashed line indicates the transition between lithic and foraminifer dominated time periods leading to the subdivision of regime 1 and 2. (c) Lithic grain concentration per gram, the blue line indicates the average amount of total IRD. (d) Planktic (pink) and benthic (dark red) foraminifer concentration per gram, the pink line indicates the average amount of total planktic foraminifer concentration. (e) $\delta^{18}O$ of planktic species *N. pachyderma*, filling indicates values lower than the overall average. (f) $\delta^{13}C$ of planktic species *N. pachyderma*, filling indicates values lower than the overall average.

ice margin can also be characterized by high concentrations of planktic foraminifers whereas a perennial sea-ice cover or a lack of nutrients would lead to the absence of planktic foraminifers (Dowdeswell et al., 1998).

Fluxes were calculated by multiplying the respective concentrations with the bulk mass accumulation rate following Peck et al. (2007). Sediment particle, carbonate and water densities of 2.650, 2.730 and 1.025 g cm^{-3} were assumed, respectively. Sedimentation rates used to calculate bulk mass accumulation rates for cores PS2664-5 and SU90-24 were derived from the updated GICC05 related age models, respectively (see subchapter 4, Chronology). The ratio between lithic grains and planktic foraminifers was calculated using the following equation: lithic grains * (total entities)$^{-1}$ (Bond et al., 1992; Heinrich, 1988).

Planktic foraminifer assemblage counts in the 150-500 µm size fraction were performed for 31 samples, spread irregularly through the studied section. Each sample was split until a minimum of 300 specimens was left for counting. The results are given as percentage *N. pachyderma* (%Np). %Np between 90 and 94 % represents the movement of the arctic front whereas values between 94 and 98 % are representative for the location of the polar front (Pflaumann et al., 1996). The fronts divide the North Atlantic into Polar, Arctic and Atlantic waters. Due to the increasing water temperatures, the %Np declines in the direction of Atlantic water (Johannessen et al., 1994).

4. Chronology

The AMS ^{14}C ages below 371 cm are outside of the calibration range (Table 1) and it is known that the reservoir ages of the AMS ^{14}C ages >10 ka BP are highly variable during the glacial period in this region (e.g. Sarnthein et al., 2001; Sarnthein et al., 2015; Waelbroeck et al., 2001) Consequently, we followed a different approach to establish a chronostratigraphy for 22CC. For the final age model, we combined three different types of control points (Figure 2, Table 2). The stratigraphy between 15 and 32 ka b2k is mostly based on two of the calibrated AMS ^{14}C dates, whereas the North Atlantic Ash Zone (NAAZ) II tephra layer provides an independent age control point in early MIS3. NAAZ II (55.38 ± 1.184 ka b2k) is a very well-known volcanic horizon recorded in both marine sediment cores from the North Atlantic (Austin et al., 2004 and references therein) and in Greenland ice cores (e.g. Svensson et al., 2008).

To create a more detailed chronology during MIS3 and MIS4 for core 22CC (Figure 2), we synchronized the planktic $\delta^{18}O$ and $\delta^{13}C$ time series between 22CC and core PS2644-5 (Voelker & Haflidason, 2015a) following Jansen (1989), using the program AnalySeries (Paillard et al., 1996). Core PS2644-5 (hereafter PS2644) was retrieved from the Greenland Sea, off Northwest Iceland (67°52.02′N, 21°45.92′W, 777 m water depth), and has a well constrained chronology based on tuning between the planktic $\delta^{18}O$ and the ice core GISP2 $\delta^{18}O$ record (GISP2 ages converted to GICC05, Voelker & Haflidason, 2015a). The tuning approach is supported by independent time markers including AMS ^{14}C dates, tephra horizons and geomagnetic data (Voelker et al., 1998; Voelker et al., 2000; Voelker & Haflidason, 2015a).

The synchronization between 22CC and PS2644 is based on three assumptions. First, we assume that the near-surface oceanographic changes at the two sites occur virtually synchronously with regard to the age resolution of the cores. Second, the $\delta^{18}O$-depletions are believed to represent large meltwater fluxes occurring during Greenland stadials associated with H-events (hereafter indicating the temporal association, not the character, of a H-event). It is further assumed that the changes in surface water-mass properties are influenced by the same surface currents, in particular the EGC and the Irminger Current.

Finally, seven visually tuned tie-points were used for the synchronization between 22CC and PS2644 (Table 2 and Figure 2). The $\delta^{13}C$ tie-point constrains the sharp MIS4/3 transition whereas the $\delta^{18}O$ tie-points were added to tune the depleted $\delta^{18}O$ peaks to the H-events recorded in PS2644. Sedimentation rates vary between ~2.5 and 12 cm/ky with the highest values occurring prior to H6 and during the middle of MIS3, and the lowest values occurring during H6 and MIS2 (Table 2 and Figure 2).

For this study, the age model of SU90-24 (Elliot et al., 1998) was updated using the IntCal13 calibration curve (Reimer et al., 2013), tuned to the GICC05 age scale (Voelker, 2018) and adjusted to b2k by adding 50 years.

The age-depth relationship of the final age model is shown in Figure 2f. Positive age offsets between the calibrated ages and the ages of the final age model are assumed to reflect the magnitude of contamination (Table 1). Negative age offsets of up to 1.92 ka (+405 years) might indicate a closed sea-ice cover similar to age offsets previously reported for the Younger Dryas and other cold events (e.g. Bard et al., 1994; Sarnthein et al., 2015; Waelbroeck et al., 2001). The measured ^{14}C ages are not in a stratigraphic order from 410 cm downwards.

5. Results

5.1. Lithic Grain and Foraminifer Abundances

On average, the sediment samples contain 689 lithic grains (45 to 6133 grains/g), 1385 planktic (0 to 6048 specimens/g) and 14 benthic foraminifers per gram (0 to 58 specimen/g) in the >150 μm size fraction (Figure 3). The concentrations of benthic and planktic foraminifers follow a similar trend. The lithic/(lithic+foraminifer) ratio shows that planktic foraminifers dominate the sediment between 530 cm and 400 cm (Figure 3). From 400 cm upwards, lithic grains dominate Greenland stadials whereas planktic foraminifers are dominant during Greenland interstadials, albeit with a generally increasing contribution of lithic grains from 315 cm to 240 cm and during H3. Before and after H3, planktic foraminifers are more abundant than lithic grains. Volcanic grains were counted separately in order to detect tephra horizons. We observe one pronounced tephra peak independent of the lithic grain concentration at 474 cm depth. This horizon contained mostly transparent rhyolitic tephra shards corresponding to NAAZ II. The calculated fluxes (Figures 4 and 5) generally follow the above trends; only during H6 (514-524 cm) and H3 (218-220 cm) the foraminifer and IRD signals are smeared out due to the low sedimentation rates.

The planktic foraminifer assemblages are dominated by *N. pachyderma* with minor occurrences of *Neogloboquadrina incompta*, *Turborotalita quinqueloba, Globigerina bulloides, Globigerinita glutinata* and *Globigerinita uvula*. The lowest %Np values (95.1%, 92.7% and 93%) were observed corresponding to Greenland interstadials at ~52.5 ka b2k, ~45.7 ka b2k and ~37.7 ka b2k, respectively (Figures 4 and 5).

5.2. Stable Isotope Data

The stable oxygen isotope record shows three distinct $\delta^{18}O$ depletions at Greenland stadials coinciding with H6, H5 and H4. These depletions have values of ~3.47 ‰, ~3.38 ‰ and ~3.41 ‰, respectively (Figures 2 and 3). The $\delta^{18}O$ signals with values lower than the recorded average (4.15 ‰) indicate additional minima from ca. 480-400 cm, 365-340 cm, 314 cm, 302 cm, 262 cm and 222 cm (H3). Each of these minima is followed by a rapid switch to heavier $\delta^{18}O$ values by up to 1 ‰. Maximum values of 4.71 ‰ are recorded from 316-324 cm resulting in an overall amplitude of up to 1.33 ‰.

The stable carbon isotope record shows an average $\delta^{13}C$ value of 0.22 ‰ (Figure 3). The lowest $\delta^{13}C$ values are observed during the three depth intervals corresponding to low $\delta^{18}O$ values, from ca. 530-430 cm (including H6), 290-262 cm (including H4) and 225-200 cm (MIS2), with the most pronounced minimum coinciding with H6 (-0.26 ‰). Maximum values of 0.51 to 0.60 ‰ occur during MIS3. In general, the $\delta^{13}C$ record seems to show lower values during Greenland stadials.

6. Discussion

The relationship between the abundance of lithic grains (hereafter IRD) and planktic foraminifers (Figure 3) leads to a subdivision of the 22CC records into two different regimes. Regime 1 spans from approximately 65 to 49 ka b2k and is characterized by an overall dominance of planktic foraminifers in the coarse fraction (>150 μm) compared to the IRD content. During regime 2 (~49-25 ka b2k), a generally higher flux of IRD is observed with specific IRD events marked by an IRD content nearly one order of magnitude higher than the rest of this period. The abundance of planktic foraminifers during regime 2 is highly variable, from almost barren in some intervals to relatively high amounts in others. This “on and off” signal in foraminifer abundance seems to oscillate on millennial timescales related to abrupt climate oscillations recorded in Greenland ice cores. After the proxy records of 22CC are discussed, the 22CC records will be set into a regional context by comparing them with proxy records from the Greenland Sea (PS2644, Voelker et al., 1998) and from the Irminger basin (SU90-24, Elliot et al., 1998) on the basis of the Greenland stadial/interstadial (GS/GI) changes.

In the following discussion we use some general characteristics for subdividing the studied period and interpreting the environmental conditions:

- As foraminifer production and flux in the polar region is highly influenced by food availability, an extensive sea-ice cover in the polar region and its associated limited light penetration, is the primary influence leading to reduced fluxes (Carstens et al., 1997; Kohfeld et al., 1996; Ramseier et al., 2001). Hence, as light

and nutrients are limited below sea-ice, the foraminifer flux can be used as a proxy for sea-ice cover changes (Greco et al., 2019). Oceanic frontal processes provide an increased nutrient supply and enhanced productivity although they are also linked to the extent of the summer (polar front) or winter (arctic front) sea-ice cover (Johannessen et al., 1994). The salinity changes induced by meltwater derived from a melting sea-ice cover also affect planktic foraminifer production and their habitat depth.

- The flux of IRD is primarily influenced by iceberg supply and iceberg melting rates. A dense sea-ice cover inhibits iceberg transport and reduces IRD flux, whereas the associated cold surface waters cause lower melt rates. Warmer waters enhance melting and IRD flux (e.g. Straneo & Heimbach, 2013), if the melting icebergs still contain sediment that can be dropped.
- Sedimentation rates over the Eirik Drift are highly variable. During interglacials the Deep Western Boundary Current was active at the depth of the core, leading to enhanced sedimentation of fine material and dilution of coarse-grained particles (Hillaire-Marcel et al., 1994; Hillaire-Marcel et al., 2011; Stoner et al., 1998). During glacial times, on the other hand, the boundary current was less active and shallower, leading to reduced dilution. Hence, the primary control of IRD concentration and calculated fluxes are taken to be a combination of iceberg supply and melt rates.

6.1. GS/GI Oscillations During Regime 1: Stable Climates During a Sea-Ice Covered vs. Open Northeastern Labrador Sea

Regime 1 is defined by overall very low IRD fluxes and can be divided into two sub-intervals; A) the older sub-interval spanning late MIS4 across the MIS4/3 transition to GI-17.2 to GI-16; and B) the younger sub-interval encompassing the interval from GI-16 to GI-13 (Figure 4). The older sub-interval is characterized by relatively low foraminifer fluxes, a shift from depleted (GS-18) to high $\delta^{18}O$ values (MIS4/3 transition) and %Np values around 98 %. Values between 98 and 94 % of *N. pachyderma* in the planktic assemblage are associated with the location of the oceanic polar front nearby which likely represents the extent of the summer sea-ice, as known from the Nordic Seas (Johannessen et al., 1994; Pflaumann et al., 1996). Today, the polar waters along the East-Greenland margin are dominated by the EGC which exports icebergs and sea-ice from the Arctic Ocean and Nordic Seas. South of the Denmark Strait, the polar waters are seasonally sea-ice free allowing for plankton productivity. Combining the %Np data and the foraminifer flux we interpret that our core location was covered by near-perennial sea-ice during the older part of regime 1 although a few icebergs were transported by the EGC which discharged some IRD. Although the foraminifer and IRD concentrations are high (Figure 4) the very low sedimentation rates smear those signals out in terms of their flux. Low sedimentation rates probably reflect a closed sea-ice cover, which limited vertical particle flux and iceberg transport (Dowdeswell et al., 1998). It might also be indicative for times with a weak boundary current at the depth of the site. The enhanced Arctic freshwater export by the EGC associated with H6, indicated by the depleted $\delta^{18}O$ values, could be another reason for the lower surface productivity and hence relatively low foraminifer flux. Just before and after the H6 meltwater peak (GI-18 and GI-17), the 22CC foraminifer flux increases to moderate levels when the $\delta^{18}O$ values increase, apparently as a result of diminished freshwater input. *N. pachyderma* is thought to adjust its depth habitat following the pycnocline and hence inhabits greater depths during conditions of increased freshwater supply or sea-ice (Greco et al., 2019;Pflaumann et al., 2003 ; Simstich et al., 2003). We exclude the possibility of lower fluxes due to sediment export or erosion since we expect bottom currents to be weaker during this glacial period as the thermohaline circulation was also reduced during H6 (Böhm et al., 2015; Hunter, Wilkinson, Louarn, et al., 2007; Rahmstorf, 2002). Thus, the variability of foraminifer fluxes during MIS4 and at the MIS4/3 transition can primarily be attributed to the variable influence of sea-ice and freshwater (e.g. Dokken et al., 2013; Hillaire-Marcel et al., 2011) related to the GI/GS shifts during the older sub-interval of regime 1.

The H6 freshwater signal is also recorded in cores PS2644 and SU90-24, confirming our interpretation of enhanced Arctic freshwater export (e.g. Elliot et al., 1998; Voelker et al., 1998). While the %Np values are similar in 22CC and PS2644, the foraminifer fluxes are lower and the IRD flux is higher in the Greenland Sea throughout the older part of regime 1. The lower foraminifer flux might suggest an extensive sea-ice cover for most of the year in the Greenland Sea in line with independent sea-ice reconstructions by De Schepper et al. (2019). The generally higher IRD flux in core PS2644 is most likely caused by material transported by icebergs with a possible admixture of material transported by sea-ice from coastal areas. Icebergs would contain eroded material from the East-Greenland fjords, Iceland (Andrews et al., 2017) or possibly the

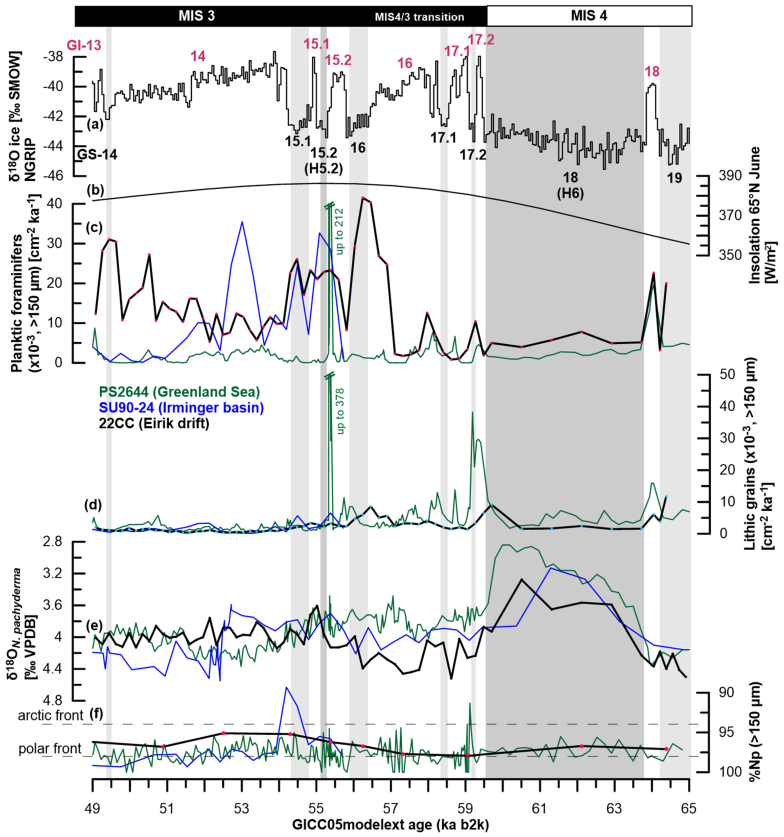

Figure 4. Surface proxy data for sediment regime 1 of core GS16-204-22CC-A (this study, black lines), PS2644 (Greenland Sea, green (Voelker & Haflidason, 2015a; Voelker & Haflidason, 2015b)) and SU90-24 (Irminger basin, blue (Elliot, 2017; Elliot et al., 1998; on modified age model)) versus GICC05 age. All data were adjusted to the b2k scale by adding 50 years. All Greenland stadials are highlighted in grey with a darker grey emphasis on H-associated Greenland stadials (GS) H6 and H5.2. (a) $\delta^{18}O$ of the NGRIP ice core (Seierstad et al., 2014) with indicated Greenland interstadials (GI, red) and Greenland stadials (black). (b) Solar insolation 65°N for June (Laskar et al., 2004). (c) Flux of planktic foraminifers >150 µm. (d) Flux of lithic grains >150 µm. (e) $\delta^{18}O$ of planktic species *N. pachyderma*. (f) %Np indicating the influence of warmer Atlantic water, dashed lines highlight values indicating the oceanic polar front (~98%) and arctic front (<94%) according to Pflaumann et al. (1996).

Eurasian shelf (Stein et al., 1996) as the Fennoscandian ice sheet was well established during MIS4 (Svendsen et al., 2004 and references therein). The IRD event immediately at the onset of MIS3 in PS2644 may have been caused by retreat of the extensive Arctic sea-ice cover which allowed for higher iceberg supply/melt rates, potentially in combination with influx of warmer subsurface waters as observed at the Faeroe Shetland ridge at this time (Ezat et al., 2014). A decrease of %Np (at ~59 ka b2k), following the IRD event, indicates the advection of warmer Atlantic water influenced the site in the Greenland Sea (Figure 4). However, neither the sharp IRD peak nor the higher influence of Atlantic water in PS2644 is recorded by 22CC, indicating a more limited invasion of these waters south of Greenland.

The second part of regime 1 commenced with a sharp increase in foraminifer flux during GI-16 while the IRD fluxes remained minimal and the $\delta^{18}O$ values were quite stable. The foraminifer fluxes reach the highest

values of the entire 22CC record between GI-16 and GI-13 indicating highly productive surface waters. Most likely, the northeastern Labrador Sea was characterized by open-water conditions for most of the year during this time interval. This might have been caused by the solar insolation maximum and consequent warmer atmospheric temperatures during GI-14. The %Np values also reflect slightly warmer sea surface temperatures within the limits of the polar front. When the %Np values are closest to 94% (GI-14), representing the location of the arctic front and hence the winter sea-ice edge, the 22CC foraminifer flux decreased to moderate levels. This might indicate that the EGC shifted closer towards the Greenland continental margin causing an increased influence of the Irminger Current in the northeastern Labrador Sea. In line with this interpretation, several published studies from the North Atlantic note a subsurface warming due to a stronger advection of the North Atlantic Current for GI-14 (e.g. Barker et al., 2015; Hillaire-Marcel et al., 2011; Lackschewitz et al., 1998; Naafs et al., 2013; van Kreveld et al., 2000). Hence, the diminished influence of sea-ice along with decreased nutrient supply and frontal mixing might have reduced food availability from phytoplankton sources (e.g. Belt et al., 2007; Ramseier et al., 2001). Today, *N. pachyderma* represents ca. 95% of the planktic foraminifer assemblage at the Eirik drift and lives in water depths between 70 and 130 m below the EGC (Pflaumann et al., 2003; Simstich et al., 2003) while the polar front is located north of our core site (Yashayaev et al., 2015). Present day conditions correspond well with our interpretations for GI-14. It has been shown that icebergs from fjords in West and East Greenland reached the Eirik drift during the Holocene (White et al., 2016), supporting our hypothesis that environmental conditions during GI-14 might have been similar to Holocene interglacial conditions in the northeastern Labrador Sea.

The %Np values recorded by PS2644 and SU90-24 remain above those of 22CC, except for one peak at ~54.2 ka b2k in SU90-24, representing the higher influence of the EGC at those locations. But, while PS2644 records low foraminifer fluxes and hence an extensive near-perennial sea-ice cover in the Greenland Sea, the foraminifer fluxes recorded in the Irminger basin reach the same levels as in 22CC or even exceed them, for example during GS-15.2 and in parts of GI-14. Core PS2644 also records a peak in foraminifer flux during GS-15.2, accompanied by a sharp peak in IRD flux, which might be related to conditions following the volcanic eruptions of NAAZ II (e.g. Frogner et al., 2001). The peak in foraminifer flux during GI-14 in SU90-24 might indicate the higher food availability due to the higher influence of sea-ice, either at the summer sea-ice edge or exported by the EGC, compared to our core site. Additionally, the very low IRD input during GI-14 seems to be a phenomenon in wide parts of the North Atlantic basin (e.g. Barker et al., 2015; Elliot et al., 1998; Hagen & Hald, 2002; Hillaire-Marcel et al., 2011; Lackschewitz et al., 1998; van Kreveld et al., 2000; Voelker et al., 1998).

In summary, our proxy records show similar trends with those recorded by the Greenland ice cores for regime 1, specifically the colder climate conditions during MIS4 shifting towards a warmer climate without DO-like temperature oscillations on millennial-scale (GI-14 to GI-13) (Huber et al., 2006; Seierstad et al., 2014). Until GI-16, the summer sea-ice edge (and polar front) was close to the study site. Thereafter, it retreated northwards while the high plankton productivity was maintained by melt of the sea-ice after the winter months. The slightly warmer sea surface temperatures, very low iceberg activity and high productivity in the northeastern Labrador Sea during GI-14, suggests environmental conditions similar to Holocene conditions. These may have been caused by the solar insolation maximum at that time. In contrast, an extensive, near-perennial sea-ice cover was maintained in the Greenland Sea.

6.2. GS/GI Oscillations During Regime 2: High Variability of Environmental Conditions

Regime 2, which covers the younger half of MIS3 and the beginning of MIS2 (GS-13 to GS-3, Figure 5), shows large variability in all analyzed proxies that in part appear to be related to the GI/GS oscillations recorded by the Greenland ice cores. The $\delta^{18}O$ record exhibits notably pronounced excursions to strongly depleted values during GS-13 and GS-9, corresponding to the North Atlantic H-events H5 and H4, respectively. Additional time periods with pronounced low values are the younger part of GI-12, GS-12, GS-8 and GS-5.1 (H3). In association with the strongly depleted $\delta^{18}O$ values, %Np are lower than 94% in GI-12 and GI-8 which follow H5 and H4. The planktic assemblages in GI-12 and GI-8 of 22CC reveal an increased number of subpolar species *T. quinqueloba* and *G. bulloides* indicating the presence of warm Atlantic water. The lower %Np might indicate a temperature increase in the subsurface as suggested for the Greenland Sea, Fram Strait, central North Atlantic and Nordic Seas (e.g. Dokken et al., 2013; Knutz et al., 2011; Rasmussen & Thomsen, 2004; Voelker et al., 1998). It seems likely that the advection of warm Atlantic water was enhanced facilitating

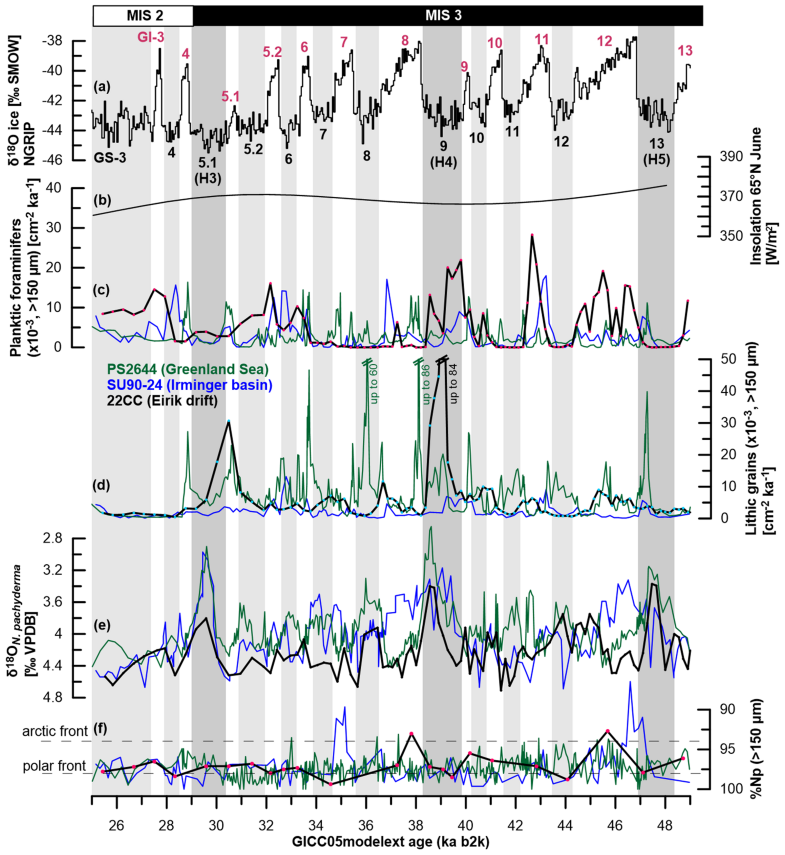

Figure 5. Surface proxy data for sediment regime 2 of core GS16-204-22CC-A (this study, black lines), PS2644 (Greenland Sea, green (Voelker & Haflidason, 2015a; Voelker & Haflidason, 2015b)) and SU90-24 (Irminger basin, blue (Elliot, 2017; Elliot et al., 1998; on modified age model)) versus GICC05 age. All data were adjusted to the b2k scale by adding 50 years. All Greenland stadials are highlighted in grey with a darker grey emphasis on H-associated Greenland stadials (GS) H5 to H3. (a) $\delta^{18}O$ of the NGRIP ice core (Seierstad et al., 2014) with indicated Greenland interstadials (GI, red) and Greenland stadials (black). (b) Solar insolation 65°N for June (Laskar et al., 2004). (c) Flux of planktic foraminifers >150 µm. (d) Flux of lithic grains >150 µm. (e) $\delta^{18}O$ of planktic species *N. pachyderma*. (f) %Np indicating the influence of warmer Atlantic water, dashed lines highlight values indicating the oceanic polar front (~98%) and arctic front (<94%) according to Pflaumann et al. (1996).

the reestablishment of the thermohaline circulation patterns (Mignot et al., 2007) after the reduced mode that might have occurred due to the large freshwater input during H-events (Böhm et al., 2015; Rahmstorf, 2002). Apart from those two excursions the %Np values, where this proxy could be applied, stay within or above the values defining the location of the polar front indicating seasonally open waters with the EGC as the dominant surface current.

During most GSs of regime 2, the %Np proxy could not be applied because foraminifer abundance is too low. This is also reflected in the foraminifer fluxes which show large variability in regime 2. All time periods where foraminifers are nearly absent in the coarse fraction, tend to fall within GSs, although some of those periods extend into GIs (GI-8, GI-7). We argue that during those time periods our core location was covered by near-perennial sea-ice. During periods of minimum foraminifer flux, IRD flux is also reduced, which might indicate that a thick sea-ice cover prevented icebergs from entering the area or cold surface temperatures inhibited melt-out from icebergs. The higher $\delta^{18}O$ values observed during many GSs in core 22CC are

Table 2
Age Control Points in Sediment Core GS16-204-22CC-A Used for the Established Chronology

Pointer based on:	Depth (cm)	Age of tie point (ka b2k)	Sedimentation rate (cm/ky)
AMS ^{14}C	150.5	15.09	4.8
$\delta^{18}O$	221.5	29.79	4.3
AMS ^{14}C	230.25	31.89	7.4
$\delta^{18}O$	265.00	36.56	10.5
$\delta^{18}O$	282.25	38.2	11.2
$\delta^{18}O$	384.00	47.26	11.1
Ash layer (NAAZ II[a])	474.25	55.38	9.3
$\delta^{13}C$	514.25	59.7	2.5
$\delta^{18}O$	524.75	63.92	11.9
$\delta^{13}C$	604.5	70.64	11.9

[a]55.38 ± 1.184 (NGRIP; Svensson et al. (2008))

consistent with a reduced meltwater influence in the northeastern Labrador Sea (Figure 5). Extensive sea-ice cover throughout most of the year would prevent light penetrating the water column and reduce primary production, leading to limited food availability for the planktic as well as benthic foraminifers. Thus, the sea-ice edge was probably located south of our site accompanied by a southward expansion of the EGC. The short increase in foraminifer flux occurring simultaneously with the low %Np value during the sea-ice covered GI-8 might indicate the opening of a polynya caused by the northward advected Atlantic water which could have triggered an increase in plankton production (e.g. Duprat et al., 2016; Smith et al., 2007; Stern et al., 2015; Vettoretti & Peltier, 2016). Vettoretti and Peltier (2016) found that a North Atlantic polynya could have appeared at the onset of each DO-warming event during wintertime. Low light conditions during winter could explain why the foraminifer flux during GI-8 increased, albeit to low levels. Although dissolution due to more corrosive bottom waters cannot be completely excluded, the foraminifers that we find in these low flux time periods appear pristine. Additionally, the sediment deposited at this time at site 22CC is dominated by the fine fraction, which strongly implies an extensive, near perennial sea-ice cover and a weak bottom current. At the end of GI-8, following the increased foraminifer flux peak and the low %Np, the IRD flux increases, confirming that conditions changed above our core site. In particular, the break-up of the sea-ice cover is likely, and allowed for the passing (and melting) of icebergs and potentially the (subsurface) influx of the Atlantic waters. Observations at core sites CH69-K09 (southeast of Newfoundland, Labeyrie et al., 1999) and SO82-05 (Reykjanes ridge, van Kreveld et al., 2000) suggest an influx of warm waters at the end of GI-8; these observations support our interpretation, assuming the warmer waters reached the northeastern Labrador Sea. Similar conditions probably occurred during GS-10 when foraminifer fluxes also increase accompanied by moderate IRD fluxes and lower %Np values.

Moderate to high foraminifer fluxes are mainly recorded during GIs of regime 2 as well as during GS-9 (H4), GS5.2 and GS-3. While the GSs of the older part of regime 2 are characterized by a near-perennial sea-ice cover, the seasonally open water conditions during the GIs allow for iceberg transport as well as higher productivity and food availability for the foraminifers. Different mechanisms must have driven the environmental conditions in the younger part of regime 2 (GS-9, GI-7 to GS-3) because foraminifer and IRD fluxes are no longer in phase. Instead, the foraminifer fluxes are higher when the IRD fluxes are lower and vice versa.

In time periods with high $\delta^{18}O$ values, low foraminifer fluxes and increased IRD fluxes (middle of GS-9, end of GI-8, GS-7, GI-5.1 into GS-5.1) during regime 2, iceberg activity could have had a negative impact on foraminifer productivity (similar to that observed in the Southern Ocean; Schwarz & Schodlok, 2009). A high number of melting icebergs may cause water column stratification with a meltwater lid forming at the surface. The planktic foraminifers would be expected to follow the pycnocline to greater water depths were the food availability (or quality) might have been limited. We suggest that this explanation is sufficient for the high numbers of icebergs reaching our site associated with the H4 and H3 calving events, but this does not necessarily explain the increase of IRD fluxes between H4 and H3 (end of GI-8, GS-7). Here we suggest that sea surface conditions were not favorable for plankton blooms. The IRD flux likely represents iceberg transport via the EGC, and not any particular calving events.

The $\delta^{18}O$ values are high while the foraminifer fluxes are increased, and the IRD fluxes are low at the beginning of GS-9, from GI-6 to GS-5.2 and GI-3 to GS-3. One possible explanation could be that although the sea-ice retreated during the summer months and iceberg transport routes were free, melting was hampered by very cold surface waters. A cold and seasonally ice-covered northeastern Labrador Sea from 31 ka was also reported from a dinocyst and coccolithophore study (Rahman & de Vernal, 1994). On the other hand, melting starts with water temperatures around 0°C and our %Np values do not indicate especially cold temperatures compared to intervals where iceberg melting occurred. Other explanations could be that either polynyas developed in the area that allowed plankton productivity (e.g. Duprat et al., 2016; Ramseier et al., 2001; Schwarz & Schodlok, 2009; Smith et al., 2007; Stern et al., 2015) or that icebergs passing the site during the given time periods transported less sedimentary material. Additionally, the increasingly high $\delta^{18}O$ values recorded in core 22CC during regime 2 incorporate the signal of the increasing global continental ice volume towards the last glacial maximum. Global benthic isotope records as well as models show that sea level was dropping from ~32 ka until it reached its minimum around 21 ka while ice sheets reached their maximum volumes at ~30 ka and remained constant until ~19 ka (Clark & Mix, 2002; Lambeck et al., 2002; Waelbroeck et al., 2002). Hence, fewer icebergs might have been discharged between 30 to 19 ka due to a stable mass balance and a near-perennial sea-ice cover in the Greenland Sea and the Arctic Ocean (De Schepper et al., 2019; Patton et al., 2016).

To evaluate the transport of icebergs and freshwater by the EGC during regime 2, we again compare the records from our core site (22CC) to the proxy records from the Greenland Sea (PS2644, Voelker et al., 1998) and the Irminger Basin (SU90-24, Elliot et al., 1998). We observe that the SU90-24 records are more similar to our data than those of PS2644 (Figure 5), particularly the trends in the foraminifer fluxes. Apparent temporal offsets between core SU90-24 and 22CC are most likely caused by the uncertainty of the age models rather than climatic conditions. IRD fluxes at site SU90-24 stay low during regime 2, but are synchronously coupled to the increase in the foraminifer fluxes during GIs. Elliot et al. (1998) explain this by invoking rapid fluctuations in sea-ice extent, leading to seasonal sea-ice edge conditions resulting in increased IRD flux and sea surface productivity. This explanation has been promoted by several other studies (e.g. Bond, 1997; Johannessen et al., 1994; Ramseier et al., 2001) and corresponds well with our interpretation for most GIs of regime 2.

The %Np data of SU90-24 are also similar to that recorded in 22CC (Figure 5) and indicate a proximal location of the polar front and hence the summer sea-ice edge. Exceptions to this overall trend occur during GI-12 (as in 22CC) and GI-7, indicating subsurface warming and possibly a longer sea-ice free season throughout the year. During GI-12 the low %Np values are accompanied by low $\delta^{18}O$ values in core SU90-24 which contradicts the high $\delta^{18}O$ values observed in 22CC. Those differences could be explained by different calcification depths of *N. pachyderma* related to local sea-ice cover, meltwater lenses or isotopically light brines (Hillaire-Marcel et al., 2011; Simstich et al., 2003). Unexpectedly, neither the inferred warm water nor the freshwater flux changes seem to affect the IRD and foraminifer fluxes which stay low at site SU90-24. Similar to SU90-24, core SO82-05 (Figure 1) also records low $\delta^{18}O$ values during GI-12 and GI-7 associated with increasing sea surface temperatures and salinities, clearly indicating the higher influence of Atlantic water during those GIs (van Kreveld et al., 2000). This hypothesis is further supported by benthic isotope records and chemical water tracers indicating the return to well-ventilated deep waters and thus an active thermohaline circulation during the GIs following H-events (Böhm et al., 2015; Elliot et al., 2002; Henry et al., 2016; Labeyrie et al., 1999; van Kreveld et al., 2000). The activated deep and surface water circulation could also have influenced the hydrography of the Labrador Sea. Hence, the high $\delta^{18}O$ values recorded by 22CC could reflect a salinity signal as the result of an active subpolar gyre circulation while site SU90-24 was mainly influenced by the EGC, similar to conditions today.

According to the %Np data, PS2644 is not influenced by Atlantic water advection but records shifts of the polar front. Foraminifer fluxes are lower in PS2644 compared to site 22CC, but they also increase during most GIs and drop during most GSs (Figure 5). Interestingly, foraminifer fluxes also increase between GI-8 and GS-7, whereas foraminifers are nearly absent in SU90-24 and 22CC. In the same time period, besides the peak at the end of GS-13, PS2644 records three very pronounced peaks in IRD fluxes right after H4, during GS-8 and GI-6 indicating significant calving events north of the Denmark Strait, contrary to conditions south of the Denmark Strait.

Table 3
Summary of Characteristics of Heinrich Events 3-6 in Core GS16-204-22CC

Heinrich event	Approximate age (ka b2k)	Planktic $\delta^{18}O$ (meltwater)	IRD flux	Foraminifer flux	Subsurface warming
3	30.3-29.0	Low	High	Low	No
4	39.9-38.2	Depleted	High	Moderate	Yes (GI-8)
5	48.3-46.9	Depleted	Very low	Very low	Yes (GI-12)
6	63.8-59.5	depleted	Very low	Low	No

Apart from the differences caused by local hydrography, all three sites show evidence of a shifting winter sea-ice edge influencing plankton productivity and iceberg transport on GS/GI timescales. Changes on a millennial timescale seem to be quite common in the marine records from the North Atlantic after H5 and north of 55°N, possibly related to their proximity to continental ice sheets (Andrews et al., 1998; Barker et al., 2015; Elliot et al., 2002; Lackschewitz et al., 1998; van Kreveld et al., 2000).

6.3. The H-Associated GSs

The most pronounced IRD layers caused by the collapses of the Laurentide (H5 and H4) and Eurasian (H6 and H3) ice sheets were discovered in the Ruddiman belt (Bond et al., 1993; Grousset et al., 1993; Grousset et al., 2001; Hemming, 2004; Ruddiman, 1977). It is often assumed that the sea-ice cover extended to the northern edge of that belt at 55°N (Dokken et al., 2013; Vettoretti & Peltier, 2016) because the sea-ice edge would have blocked potential northward iceberg movement as well as northward oceanic heat transport making the Ruddiman belt the most suitable region for melting. During H-events the overturning circulation was reduced (e.g. Böhm et al., 2015; Henry et al., 2016; Rahmstorf, 2002) and the restart of the overturning circulation is observed in North Atlantic proxy records as a temperature overshoot indicating the increased advection of warm water (e.g. Dokken et al., 2013; Knutz et al., 2011; Rasmussen & Thomsen, 2004; Sadatzki et al., 2019; Sessford et al., 2018; van Kreveld et al., 2000; Voelker et al., 1998). The glacial surface hydrography of the northeastern Labrador Sea was influenced by Arctic freshwater and Atlantic water and probably iceberg transport and melt from the Laurentide, Eurasian and Greenland ice sheets (Death et al., 2006; Hemming, 2004; Stoner et al., 1998). Consequently, we would expect to observe H-related meltwater peaks associated with increased IRD fluxes and low foraminifer fluxes, followed by a signal of subsurface warming indicating an active surface and deep water circulation. Instead, the only proxy in the analyzed core sections of 22CC that shows clear evidence of all H-events is $\delta^{18}O$, indicating each H-related meltwater event. Only H6, H5 and H3 are associated with low foraminifer fluxes, H4 and H3 with pronounced IRD peaks and H5 and H4 are followed by subsurface warming (Table 3). Following the interpretations of the proxy records from this site, these differences can largely be explained by the specific environmental conditions in which the H-associated GSs of regime 2 and 1 are placed. Accordingly, the core site appears to have been sea-ice covered for most of the year during H6 and H5 while sea-ice conditions during H5.2, H4 and H3 must have been more open based on the moderate foraminifer flux (H5.2 and parts of H4) and/or high IRD flux (H4 and H3). Hence, the source of the meltwater and transport routes to the northeastern Labrador Sea must have been variable. Possible transport mechanisms are 1) via the EGC, which transported meltwater from the Arctic Ocean, the eastern Greenland ice sheet and the Nordic Seas; 2) via the subpolar gyre, which redistributed meltwater from the Eurasian and Laurentide ice sheets and the associated iceberg melt in the Ruddiman belt; and/or 3) via nepheloid layer transport from the Northwest Atlantic Mid Ocean Channel (NAMOC), triggered by the collapse of the Hudson Strait ice stream (Hesse et al., 2004; Hesse & Khodabakhsh, 2017; Rashid et al., 2003a). However, the latter mechanism can most likely be excluded for our core site because it is located outside of the direct Laurentide ice sheet meltwater plume and the influence of the NAMOC (Stoner et al., 1996). In order to discuss the other two scenarios, we again must compare our $\delta^{18}O$ signal to other core sites within the pathways of the EGC or the North Atlantic/Irminger Current (Figure 1). A north to south gradient is clearly apparent from the core sites along the East and South Greenland margins (Figures 4 and 5). Thus, the most depleted $\delta^{18}O$ signal during H-related GSs is always recorded by northernmost core PS2644, suggesting meltwater transport by the EGC and potential local sources from Iceland. However, the $\delta^{18}O$ values of cores PS2644 and SU90-24 show the biggest difference to 22CC during H6 and H3. At the same time, H6 and H3 are the two

events in core 22CC not followed by a subsurface warming signal. This might suggest that within H6 and H3 iceberg transport and any associated melting occurred within the EGC while current transport into the northeastern Labrador Sea might have been limited. Core SO82-05 also records a meltwater signal for H3 but with a smaller amplitude than PS2644 and SU90-24, which might reflect active subpolar gyre transport with a large component of meltwater from the Eurasian ice sheet, as also suggested by IRD provenance studies from the Ruddiman belt (Hemming, 2004 and references therein). Labeyrie et al. (1999) state that polar waters invaded the North Atlantic at the surface down towards the southern limit of the Ruddiman belt. This freshwater lid is thought to have disrupted the North Atlantic surface circulation, decreasing deep-water formation and subsequently ventilation during H-associated GSs as well as regular GSs. Such a scenario is in agreement with the absence of the Deep Western Boundary Current at the Eirik Drift (Hillaire-Marcel et al., 1994). The resumption of good ventilation at core site CH69-K09 did not follow directly after the H-events but was delayed by several hundred years. Labeyrie et al. (1999) explained this delay by the temporal lead of the meltwater signal at high latitudes and the great depth of their core site (>4000 m) compared to e.g. SU90-24 (Vidal et al., 1997).

7. Conclusions

In this study we present high-resolution stable isotope data, IRD and foraminifer abundances and low-resolution planktic assemblage counts from marine core 22CC (Eirik drift, northeastern Labrador Sea), covering the period between ~65 ka b2k and ~25 ka b2k. Our proxy data provide new evidence about the variability of the sea-ice cover at this location as well as surface productivity and iceberg transport during the abrupt climate shifts of MIS3. Core 22CC records both ice sheet and/or sea-ice responses on millennial timescales (>55°N, Cortijo et al., 1995) as well as various characteristics of H-events 6 to 3.

Our interpretation of the proxy data from this site suggests that: (1) from ~67 ka b2k to ~56 ka b2k site 22CC was covered by near perennial sea-ice, limiting surface productivity and iceberg transport, while from ~56 to 49 ka b2k the sea-ice cover retreated northwards due to the solar insolation maximum. (2) From ~49 ka b2k to ~25 ka b2k, this site was covered by near-perennial sea-ice during most GSs which decreased to seasonal sea-ice cover during most GIs. (3) After H3, the Greenland ice sheet´s ice shelf most likely triggered higher productivity. (4) The surface conditions and convection in the northeastern Labrador Sea are driven by regional mechanisms because all recorded H-events are characterized by different environmental conditions. (5) The southern extent and the lateral expansion of the EGC is not restricted to H-associated GSs at the Eirik drift but seems to be characteristic for the investigated time period.

The comparison of three core sites combined (22CC, SU90-24, PS2644) provides insight into mechanisms potentially involved in creating the environmental conditions seen during the studied period of the last glacial period, especially sea-ice cover extent, plankton productivity and iceberg discharge:

- Orbital forcing enhanced early MIS3 warming and a subsequent cooling trend characterized by more sea-ice and iceberg presence towards the last glacial maximum;
- Increased surface productivity and retreat of winter sea-ice during the solar insolation maximum (GI-14);
- Regime 1 was characterized by a more pronounced general presence of subpolar water masses compared to regime 2. In regime 2, subpolar water masses appeared only during short events in the GIs;
- The similarity between the Eirik Drift and Irminger Sea core indicate both a linkage of signals along the EGC and a more active subpolar gyre during warmer periods;
- Enhanced meltwater flux, in particular during GS-18, GS-13, GS-9 and GS-5.1 by the EGC leading to water column stratification, reduced food availability and furthermore weakened deep-water convection and subpolar gyre;
- Subsurface warming and concomitant heat advection to the sea-ice covered areas (GI-12, GI-8) could have resulted in the opening of polynyas, allowing for the restart of thermohaline convection;
- Iceberg calving episodes associated with H-events are recorded, but differ between the different H-events. Outside of the H-events there was a continued flux of icebergs along the EGC;
- Iceberg calving events (H4 and H3) which occurred during the greatest ice sheet extent led to reduced plankton productivity. The calving events as documented by IRD occurred prior to the main meltwater advection ($\delta^{18}O$ signal) to the area.

Acknowledgments

We thank Eivind W. N. Støren for the facilities of EARTHLAB, Dag Inge Blindheim and Ulysses S. Ninnemann for helping with the stable isotope analyses as well as the use of FARLAB. A thankyou goes to the R/V *G.O. Sars* crew for the successful cruise in 2016 where the analyzed core was retrieved. We also thank Mary Elliot for providing the data necessary to calculate the fluxes of SU90-24 and Sevasti E. Modestou for language editing. We appreciate the positive and constructive suggestions from the reviewers which helped to greatly improve this manuscript. The funding for this research was granted by the European Research Council under European Community's Seventh Framework Programme (FP7/2007-2013) ERC grant agreement 610055 as part of the ice2ice project. A. Voelker acknowledges financial support from the Fundação de a Ciencia e a Tecnologia through grants IF/01500/2014 and UID/Multi/04326/2019. The data shown in this publication is available at the Pangaea data base https://doi.pangaea.de/10.1594/PANGAEA.904065. The supporting information provides figures showing foraminifer and IRD concentrations of core sites 22CC, PS2644 and SU90-24 for regime 1 (S1) and regime 2 (S2).

References

Alley, R. B., Andrews, J. T., Brigham-Grette, J., Clarke, G. K. C., Cuffey, K. M., Fitzpatrick, J. J., et al. (2010). History of the Greenland Ice Sheet: paleoclimatic insights. *Quaternary Science Reviews*, *29*(15-16), 1728–1756. https://doi.org/10.1016/j.quascirev.2010.02.007

Andrews, J., Dunhill, G., Vogt, C., & Voelker, A. (2017). Denmark Strait during the Late Glacial Maximum and Marine Isotope Stage 3: Sediment sources and transport processes. *Marine Geology*, *390*, 181–198.

Andrews, J., Kirby, M., Aksu, A., Barber, D., & Meese, D. (1998). Late Quaternary detrital carbonate (DC-) layers in Baffin Bay marine sediments (67°–74° N): correlation with Heinrich events in the North Atlantic? *Quaternary Science Reviews*, *17*(12), 1125–1137.

Andrews, J. T. (2000). Icebergs and iceberg rafted detritus (IRD) in the North Atlantic: facts and assumptions. *Oceanography*, *13*, 100–108.

Austin, W. E., Wilson, L. J., & Hunt, J. B. (2004). The age and chronostratigraphical significance of North Atlantic Ash Zone II. *Journal of Quaternary Science*, *19*(2), 137–146.

Bagniewski, W., Meissner, K. J., & Menviel, L. (2017). Exploring the oxygen isotope fingerprint of Dansgaard-Oeschger variability and Heinrich events. *Quaternary Science Reviews*, *159*, 1–14.

Bard, E., Arnold, M., Mangerud, J., Paterne, M., Labeyrie, L., Duprat, J., et al. (1994). The North Atlantic atmosphere-sea surface 14C gradient during the Younger Dryas climatic event. *Earth and Planetary Science Letters*, *126*(4), 275–287. https://doi.org/10.1016/0012-821X(94)90112-0

Barker, S., Chen, J., Gong, X., Jonkers, L., Knorr, G., & Thornalley, D. (2015). Icebergs not the trigger for North Atlantic cold events. *Nature*, *520*(7547), 333–336. https://doi.org/10.1038/nature14330

Belt, S. T., Massé, G., Rowland, S. J., Poulin, M., Michel, C., & LeBlanc, B. (2007). A novel chemical fossil of palaeo sea ice: IP25. *Organic Geochemistry*, *38*(1), 16–27.

Böhm, E., Lippold, J., Gutjahr, M., Frank, M., Blaser, P., Antz, B., et al. (2015). Strong and deep Atlantic meridional overturning circulation during the last glacial cycle. *Nature*, *517*(7532), 73–76. https://doi.org/10.1038/nature14059

Bond, G. (1997). A pervasive millennial-scale cycle in North Atlantic Holocene and glacial climates. *Science*, *278*(5341), 1257–1266. https://doi.org/10.1126/science.278.5341.1257

Bond, G., Broecker, W., Johnsen, S., McManus, J., Labeyrie, L., Jouzel, J., & Bonani, G. (1993). Correlations between climate records from North Atlantic sediments and Greenland ice. *Nature*, *365*(6442), 143–147.

Bond, G., Heinrich, H., Broecker, W., Labeyrie, L., McManus, J., Andrews, J., et al. (1992). Evidence for massive discharges of icebergs into the North Atlantic ocean during the last glacial period. *Nature*, *360*(6401), 245–249. https://doi.org/10.1038/360245a0

Born, A., & Mignot, J. (2012). Dynamics of decadal variability in the Atlantic subpolar gyre: a stochastically forced oscillator. *Climate Dynamics*, *39*(1), 461–474.

Born, A., Nisancioglu, K. H., & Risebrobakken, B. (2011). Late Eemian warming in the Nordic Seas as seen in proxy data and climate models. *Paleoceanography*, *26*, PA2207. https://doi.org/10.1029/2010PA002027

Carstens, J., Hebbeln, D., & Wefer, G. (1997). Distribution of planktic foraminifera at the ice margin in the Arctic (Fram Strait). *Marine Micropaleontology*, *29*(3-4), 257–269.

Channell, J. E. T., Hodell, D. A., Romero, O., Hillaire-Marcel, C., de Vernal, A., Stoner, J. S., et al. (2012). A 750-kyr detrital-layer stratigraphy for the North Atlantic (IODP Sites U1302–U1303, Orphan Knoll, Labrador Sea). *Earth and Planetary Science Letters*, *317-318*, 218–230. https://doi.org/10.1016/j.epsl.2011.11.029

Clark, P. U., & Mix, A. C. (2002). Ice sheets and sea level of the Last Glacial Maximum. *Quaternary Science Reviews*, *21*(1-3), 1–7.

Cortijo, E., Labeyrie, L., Vidal, L., Vautravers, M., Chapman, M., Duplessy, J.-C., et al. (1997). Changes in sea surface hydrology associated with Heinrich event 4 in the North Atlantic Ocean between 40 and 60 N. *Earth and Planetary Science Letters*, *146*(1-2), 29–45. https://doi.org/10.1016/S0012-821X(96)00217-8

Cortijo, E., Yiou, P., Labeyrie, L., & Cremer, M. (1995). Sedimentary record of rapid climatic variability in the North Atlantic Ocean during the last glacial cycle. *Paleoceanography*, *10*(5), 911–926.

Daniault, N., Mercier, H., Lherminier, P., Sarafanov, A., Falina, A., Zunino, P., et al. (2016). The northern North Atlantic Ocean mean circulation in the early 21st century. *Progress in Oceanography*, *146*, 142–158. https://doi.org/10.1016/j.pocean.2016.06.007

Dansgaard, W., Johnsen, S. J., Clausen, H. B., Dahl-Jensen, D., Gundestrup, N. S., Hammer, C. U., et al. (1993). Evidence for general instability of past climate from a 250-kyr ice-core record. *Nature*, *364*(6434), 218–220. https://doi.org/10.1038/364218a0

De Schepper, S., Ray, J. L., Skaar, K. S., Sadatzki, H., Ijaz, U. Z., Stein, R., & Larsen, A. (2019). The potential of sedimentary ancient DNA for reconstructing past sea ice evolution. *The ISME Journal*, *13*(10), 2566–2577. https://doi.org/10.1038/s41396-019-0457-1

de Vernal, A., & Hillaire-Marcel, C. (2000). Sea-ice cover, sea-surface salinity and halo-/thermocline structure of the northwest North Atlantic: modern versus full glacial conditions. *Quaternary Science Reviews*, *19*(1-5), 65–85.

Death, R., Siegert, M. J., Bigg, G. R., & Wadley, M. R. (2006). Modelling iceberg trajectories, sedimentation rates and meltwater input to the ocean from the Eurasian Ice Sheet at the Last Glacial Maximum. *Palaeogeography, Palaeoclimatology, Palaeoecology*, *236*(1-2), 135–150. https://doi.org/10.1016/j.palaeo.2005.11.040

Dickson, B., Yashayaev, I., Meincke, J., Turrell, B., Dye, S., & Holfort, J. (2002). Rapid freshening of the deep North Atlantic Ocean over the past four decades. *Nature*, *416*(6883), 832–837. https://doi.org/10.1038/416832a

Dokken, T. M., Nisancioglu, K. H., Li, C., Battisti, D. S., & Kissel, C. (2013). Dansgaard-Oeschger cycles: Interactions between ocean and sea ice intrinsic to the Nordic seas. *Paleoceanography*, *28*, 491–502. https://doi.org/10.1002/palo.20042

Dowdeswell, J., Elverhøi, A., & Spielhagen, R. (1998). Glacimarine sedimentary processes and facies on the Polar North Atlantic margins. *Quaternary Science Reviews*, *17*(1-3), 243–272.

Drijfhout, S., Gleeson, E., Dijkstra, H., & Livina, V. (2013). Spontaneous abrupt climate change due to an atmospheric blocking–sea-ice–ocean feedback in an unforced climate model simulation. *Proceedings of the National Academy of Sciences of the United States of America*, *110*(49), 19,713–19,718. https://doi.org/10.1073/pnas.1304912110

Duprat, L. P. A. M., Bigg, G. R., & Wilton, D. J. (2016). Enhanced Southern Ocean marine productivity due to fertilization by giant icebergs. *Nature Geoscience*, *9*(3), 219–221. https://doi.org/10.1038/ngeo2633

Elliot, M. (2017). Paleoclimate data from core SU90-24, Irminger basin. https://doi.org/10.1594/PANGAEA.881875

Elliot, M., Labeyrie, L., Bond, G., Cortijo, E., Turon, J. L., Tisnerat, N., & Duplessy, J. C. (1998). Millennial-scale iceberg discharges in the Irminger Basin during the last glacial period: Relationship with the Heinrich events and environmental settings. *Paleoceanography*, *13*(5), 433–446.

Elliot, M., Labeyrie, L., Dokken, T., & Manthé, S. (2001). Coherent patterns of ice-rafted debris deposits in the Nordic regions during the last glacial (10–60 ka). *Earth and Planetary Science Letters*, *194*(1-2), 151–163.

Elliot, M., Labeyrie, L., & Duplessy, J.-C. (2002). Changes in North Atlantic deep-water formation associated with the Dansgaard–Oeschger temperature oscillations (60–10ka). *Quaternary Science Reviews*, *21*(10), 1153–1165.

Evans, H. F., Channell, J. E., Stoner, J. S., Hillaire-Marcel, C., Wright, J. D., Neitzke, L. C., & Mountain, G. S. (2007). Paleointensity-assisted chronostratigraphy of detrital layers on the Eirik Drift (North Atlantic) since marine isotope stage 11. *Geochemistry, Geophysics, Geosystems*, *8*, Q11007. https://doi.org/10.1029/2007GC001720

Ezat, M. M., Rasmussen, T. L., & Groeneveld, J. (2014). Persistent intermediate water warming during cold stadials in the southeastern Nordic seas during the past 65 ky. *Geology*, *42*(8), 663–666.

Frogner, P., Gíslason, S. R., & Óskarsson, N. (2001). Fertilizing potential of volcanic ash in ocean surface water. *Geology*, *29*(6), 487–490.

Funder, S., Jennings, A., & Kelly, M. (2004). Middle and late Quaternary glacial limits in Greenland. In *Developments in Quaternary Sciences* (Vol. 2, pp. 425–430). Elsevier.

Funder, S., Kjeldsen, K. K., Kjær, K. H., & Cofaigh, C. Ó. (2011). The Greenland Ice Sheet during the past 300,000 years: A review. In *Developments in Quaternary Sciences* (Vol. 15, pp. 699–713). Elsevier.

Galaasen, E. V., Ninnemann, U. S., Irvalı, N., Kleiven, H. K. F., Rosenthal, Y., Kissel, C., & Hodell, D. A. (2014). Rapid reductions in North Atlantic Deep Water during the peak of the last interglacial period. *Science*, *343*(6175), 1129–1132. https://doi.org/10.1126/science.1248667

Ganopolski, A., Calov, R., & Claussen, M. (2010). Simulation of the last glacial cycle with a coupled climate ice-sheet model of intermediate complexity. *Climate of the Past*, *6*(2), 229–244.

Garcia-Ibanez, M. I., Pérez, F. F., Lherminier, P., Zunino, P., Mercier, H., & Tréguer, P. (2018). Water mass distributions and transports for the 2014 GEOVIDE cruise in the North Atlantic. *Biogeosciences*, *15*(7), 2075–2090.

Greco, M., Jonkers, L., Kretschmer, K., Bijma, J., & Kucera, M. (2019). Variable habitat depth of the planktonic foraminifera Neogloboquadrina pachyderma in the northern high latitudes explained by sea-ice and chlorophyll concentration. *Biogeosciences Discuss*, *2019*, 1–30. https://doi.org/10.5194/bg-2019-79

Grousset, F. E., Cortijo, E., Huon, S., Hervé, L., Richter, T., Burdloff, D., et al. (2001). Zooming in on Heinrich layers. *Paleoceanography*, *16*(3), 240–259. https://doi.org/10.1029/2000PA000559

Grousset, F. E., Labeyrie, L., Sinko, J. A., Cremer, M., Bond, G., Duprat, J., et al. (1993). Patterns of ice-rafted detritus in the glacial North Atlantic (40–55° N). *Paleoceanography*, *8*(2), 175–192. https://doi.org/10.1029/92PA02923

Hagen, S., & Hald, M. (2002). Variation in surface and deep water circulation in the Denmark Strait, North Atlantic, during marine isotope stages 3 and 2. *Paleoceanography and Paleoclimatology*, *17*(4), 1061. https://doi.org/10.1029/2001PA000632

Hátún, H., Sandø, A. B., Drange, H., Hansen, B., & Valdimarsson, H. (2005). Influence of the Atlantic subpolar gyre on the thermohaline circulation. *Science*, *309*(5742), 1841–1844. https://doi.org/10.1126/science.1114777

Heinrich, H. (1988). Origin and consequences of cyclic ice rafting in the northeast Atlantic Ocean during the past 130,000 years. *Quaternary Research*, *29*(2), 142–152.

Hemming, S. R. (2004). Heinrich events: Massive late Pleistocene detritus layers of the North Atlantic and their global climate imprint. *Reviews of Geophysics*, *42*, RG1005. https://doi.org/10.1029/2003RG000128

Henry, L., McManus, J. F., Curry, W. B., Roberts, N. L., Piotrowski, A. M., & Keigwin, L. (2016). North Atlantic ocean circulation and abrupt climate change during the last glaciation. *Science*, *353*(6298), 470–474. https://doi.org/10.1126/science.aaf5529

Hesse, R., & Khodabakhsh, S. (2017). Reprint of Anatomy of Labrador Sea Heinrich layers. *Marine Geology*, *393*, 67–92.

Hesse, R., Rashid, H., & Khodabakhsh, S. (2004). Fine-grained sediment lofting from meltwater-generated turbidity currents during Heinrich events. *Geology*, *32*(5), 449–452.

Hillaire-Marcel, C., de Vernal, A., & McKay, J. (2011). Foraminifer isotope study of the Pleistocene Labrador Sea, northwest North Atlantic (IODP Sites 1302/03 and 1305), with emphasis on paleoceanographical differences between its "inner" and "outer" basins. *Marine Geology*, *279*(1), 188–198.

Hillaire-Marcel, C., Vernal, A. d., Bilodeau, G., & Wu, G. (1994). Isotope stratigraphy, sedimentation rates, deep circulation, and carbonate events in the Labrador Sea during the last~ 200 ka. *Canadian Journal of Earth Sciences*, *31*(1), 63–89.

Hiscott, R. N., Aksu, A. E., Mudie, P. J., & Parsons, D. F. (2001). A 340,000 year record of ice rafting, palaeoclimatic fluctuations, and shelf-crossing glacial advances in the southwestern Labrador Sea. *Global and Planetary Change*, *28*(1-4), 227–240.

Hoff, U., Rasmussen, T. L., Stein, R., Ezat, M. M., & Fahl, K. (2016). Sea ice and millennial-scale climate variability in the Nordic seas 90[thinsp]kyr ago to present. *Nat Commun*, *7*(1), 1–10. https://doi.org/10.1038/ncomms12247

Holliday, N. P., Meyer, A., Bacon, S., Alderson, S. G., & de Cuevas, B. (2007). Retroflection of part of the east Greenland current at Cape Farewell. *Geophysical Research Letters*, *34*, L07609. https://doi.org/10.1029/2006GL029085

Hopkins, T. S. (1991). The GIN Sea—A synthesis of its physical oceanography and literature review 1972–1985. *Earth-Science Reviews*, *30*(3-4), 175–318.

Huber, C., Leuenberger, M., Spahni, R., Flückiger, J., Schwander, J., Stocker, T. F., et al. (2006). Isotope calibrated Greenland temperature record over Marine Isotope Stage 3 and its relation to CH4. *Earth and Planetary Science Letters*, *243*(3-4), 504–519.

Huck, T. (2010). Recent changes in the North Atlantic circulation. Paper presented at the Iceland in the Central Northern Atlantic: hotspot, sea currents and climate change.

Hunter, S., Wilkinson, D., Louarn, E., McCave, I. N., Rohling, E., Stow, D. A., & Bacon, S. (2007). Deep western boundary current dynamics and associated sedimentation on the Eirik Drift, Southern Greenland Margin. *Deep Sea Research Part I: Oceanographic Research Papers*, *54*(12), 2036–2066.

Hunter, S., Wilkinson, D., Stanford, J., Stow, D., Bacon, S., Akhmetzhanov, A., & Kenyon, N. (2007). The Eirik Drift: a long-term barometer of North Atlantic deepwater flux south of Cape Farewell, Greenland. *Geological Society, London, Special Publications*, *276*(1), 245–263.

ice2ice (2016). Ice2Ice Cruise GS16-204, 16. Aug - 5. Sept 2016. Retrieved from https://www.bcdc.no/files/bcdc-theme/documents/GS16-204_cruise%20report.pdf

Irvalı, N., Ninnemann, U. S., Kleiven, H. K. F., Galaasen, E. V., Morley, A., & Rosenthal, Y. (2016). Evidence for regional cooling, frontal advances, and East Greenland Ice Sheet changes during the demise of the last interglacial. *Quaternary Science Reviews*, *150*, 184–199.

Jansen, E. (1989). The use of stable oxygen and carbon isotope stratigraphy as a dating tool. *Quaternary international*, *1*, 151–166.

Johannessen, T., Jansen, E., Flatøy, A., & Ravelo, A. C. (1994). The relationship between surface water masses, oceanographic fronts and paleoclimatic proxies in surface sediments of the Greenland, Iceland, Norwegian Seas. In *Carbon cycling in the glacial ocean: constraints on the ocean's role in global change* (pp. 61–85). Springer.

Kleppin, H., Jochum, M., Otto-Bliesner, B., Shields, C. A., & Yeager, S. (2015). Stochastic Atmospheric Forcing as a Cause of Greenland Climate Transitions. *Journal of Climate*, *28*(19).

Knutz, P. C., Sicre, M. A., Ebbesen, H., Christiansen, S., & Kuijpers, A. (2011). Multiple-stage deglacial retreat of the southern Greenland Ice Sheet linked with Irminger Current warm water transport. *Paleoceanography*, *26*, PA3204. https://doi.org/10.1029/2010PA002053

Kohfeld, K. E., Fairbanks, R. G., Smith, S. L., & Walsh, I. D. (1996). Neogloboquadrina pachyderma (sinistral coiling) as paleoceanographic tracers in polar oceans: Evidence from Northeast Water Polynya plankton tows, sediment traps, and surface sediments. *Paleoceanography*, *11*(6), 679–699.

Kozdon, R., Eisenhauer, A., Weinelt, M., Meland, M. Y., & Nürnberg, D. (2009). Reassessing Mg/Ca temperature calibrations of Neogloboquadrina pachyderma (sinistral) using paired δ44/40Ca and Mg/Ca measurements. *Geochemistry, Geophysics, Geosystems*, *10*, Q03005. https://doi.org/10.1029/2008GC002169

Labeyrie, L., Leclaire, H., Waelbroeck, C., Cortijo, E., Jean-Claude, D., Vidal, L., et al. (1999). Temporal variability of the surface and deep waters of the North West Atlantic Ocean at orbital and millennial scales. *Geophysical Monograph-American Geophysical Union*, *112*, 77–98.

Lackschewitz, K. S., Baumann, K.-H., Gehrke, B., Wallrabe-Adams, H.-J., Thiede, J., Bonani, G., et al. (1998). North Atlantic ice sheet fluctuations 10,000–70,000 yr ago as inferred from deposits on the Reykjanes Ridge, southeast of Greenland. *Quaternary research*, *49*(2), 171–182. https://doi.org/10.1006/qres.1997.1948

Lambeck, K., Yokoyama, Y., & Purcell, T. (2002). Into and out of the Last Glacial Maximum: sea-level change during Oxygen Isotope Stages 3 and 2. *Quaternary Science Reviews*, *21*(1-3), 343–360.

Laskar, J., Robutel, P., Joutel, F., Gastineau, M., Correia, A., & Levrard, B. (2004). A long-term numerical solution for the insolation quantities of the Earth. *Astronomy & Astrophysics*, *428*(1), 261–285.

Li, C., Battisti, D. S., & Bitz, C. M. (2010). Can North Atlantic sea ice anomalies account for Dansgaard–Oeschger climate signals? *Journal of Climate*, *23*(20), 5457–5475.

Li, C., & Born, A. (2019). Coupled atmosphere-ice-ocean dynamics in Dansgaard-Oeschger events. *Quaternary Science Reviews*, *203*, 1–20.

McCave, I., & Tucholke, B. (1986). Deep current-controlled sedimentation in the western North Atlantic. *The Geology of North America*, *1000*, 451–468.

Mignot, J., Ganopolski, A., & Levermann, A. (2007). Atlantic subsurface temperatures: Response to a shutdown of the overturning circulation and consequences for its recovery. *Journal of Climate*, *20*(19), 4884–4898.

Moffa-Sánchez, P., Hall, I. R., Barker, S., Thornalley, D. J., & Yashayaev, I. (2014). Surface changes in the eastern Labrador Sea around the onset of the Little Ice Age. *Paleoceanography*, *29*, 160–175. https://doi.org/10.1002/2013PA002523

Müller-Michaelis, A., & Uenzelmann-Neben, G. (2014). Development of the Western Boundary Undercurrent at Eirik Drift related to changing climate since the early Miocene. *Deep Sea Research Part I: Oceanographic Research Papers*, *93*, 21–34.

Naafs, B. D. A., Hefter, J., Gruetzner, J., & Stein, R. (2013). Warming of surface waters in the mid-latitude North Atlantic during Heinrich events. *Paleoceanography*, *28*, 153–163. https://doi.org/10.1029/2012PA002354

Nicholl, J. A., Hodell, D. A., Naafs, B. D. A., Hillaire-Marcel, C., Channell, J. E., & Romero, O. E. (2012). A Laurentide outburst flooding event during the last interglacial period. *Nature Geoscience*, *5*(12), 901.

Paillard, D., Labeyrie, L., & Yiou, P. (1996). Macintosh program performs time-series analysis. *Eos, Transactions American Geophysical Union*, *77*(39), 379–379.

Patton, H., Hubbard, A., Andreassen, K., Winsborrow, M., & Stroeven, A. P. (2016). The build-up, configuration, and dynamical sensitivity of the Eurasian ice-sheet complex to Late Weichselian climatic and oceanic forcing. *Quaternary Science Reviews*, *153*, 97–121.

Peck, V. L., Hall, I. R., Zahn, R., Grousset, F., Hemming, S., & Scourse, J. (2007). The relationship of Heinrich events and their European precursors over the past 60ka BP: a multi-proxy ice-rafted debris provenance study in the North East Atlantic. *Quaternary Science Reviews*, *26*(7), 862–875.

Pflaumann, U., Duprat, J., Pujol, C., & Labeyrie, L. D. (1996). SIMMAX: A modern analog technique to deduce Atlantic sea surface temperatures from planktonic foraminifera in deep-sea sediments. *Paleoceanography*, *11*(1), 15–35.

Pflaumann, U., Sarnthein, M., Chapman, M., d'Abreu, L., Funnell, B., Huels, M., et al. (2003). Glacial North Atlantic: Sea-surface conditions reconstructed by GLAMAP 2000. *Paleoceanography*, *18*(3), 1065. https://doi.org/10.1029/2002PA000774

Rahman, A., & de Vernal, A. (1994). Surface oceanographic changes in the eastern Labrador Sea: Nannofossil record of the last 31,000 years. *Marine Geology*, *121*(3-4), 247–263.

Rahmstorf, S. (2002). Ocean circulation and climate during the past 120,000 years. *Nature*, *419*(6903), 207–214. https://doi.org/10.1038/nature01090

Ramseier, R. O., Garrity, C., & Martin, T. (2001). An overview of sea-ice conditions in the Greenland Sea and the relationship of oceanic sedimentation to the ice regime. In *The Northern North Atlantic* (pp. 19–38). Springer.

Rashid, H., Hesse, R., & Piper, D. J. (2003a). Distribution, thickness and origin of Heinrich layer 3 in the Labrador Sea. *Earth and Planetary Science Letters*, *205*(3-4), 281–293.

Rashid, H., Hesse, R., & Piper, D. J. (2003b). Evidence for an additional Heinrich event between H5 and H6 in the Labrador Sea. *Paleoceanography*, *18*(4), 1077. https://doi.org/10.1029/2003PA000913

Rasmussen, T. L., & Thomsen, E. (2004). The role of the North Atlantic Drift in the millennial timescale glacial climate fluctuations. *Palaeogeography, Palaeoclimatology, Palaeoecology*, *210*(1), 101–116.

Reimer, P. J., Bard, E., Bayliss, A., Beck, J. W., Blackwell, P. G., Ramsey, C. B., et al. (2013). IntCal13 and Marine13 radiocarbon age calibration curves 0–50,000 years cal BP. *Radiocarbon*, *55*(4), 1869–1887. https://doi.org/10.2458/azu_js_rc.55.16947

Rhein, M., Kieke, D., Hüttl-Kabus, S., Roessler, A., Mertens, C., Meissner, R., et al. (2011). Deep water formation, the subpolar gyre, and the meridional overturning circulation in the subpolar North Atlantic. *Deep Sea Research Part II: Topical Studies in Oceanography*, *58*(17-18), 1819–1832. https://doi.org/10.1016/j.dsr2.2010.10.061

Ruddiman, W. F. (1977). Late Quaternary deposition of ice-rafted sand in the subpolar North Atlantic (lat 40 to 65 N). *Geological Society of America Bulletin*, *88*(12), 1813–1827.

Sadatzki, H., Dokken, T. M., Berben, S. M. P., Muschitiello, F., Stein, R., Fahl, K., et al. (2019). Sea ice variability in the southern Norwegian Sea during glacial Dansgaard-Oeschger climate cycles. *Science Advances*, *5*(3). https://doi.org/10.1126/sciadv.aau6174

Sarnthein, M., Balmer, S., Grootes, P. M., & Mudelsee, M. (2015). Planktic and benthic 14 C reservoir ages for three ocean basins, calibrated by a suite of 14 C plateaus in the glacial-to-deglacial Suigetsu atmospheric 14 C record. *Radiocarbon*, *57*(1), 129–151.

Sarnthein, M., Stattegger, K., Dreger, D., Erlenkeuser, H., Grootes, P., Haupt, B., et al. (2001). Fundamental Modes and Abrupt Changes in North Atlantic Circulation and Climate over the last 60 ky–Concepts, Reconstruction and Numerical Modeling. The Northern North Atlantic: A changing environment., 365-410.

Schlitzer, R. (2015). Ocean Data View. Retrieved from odv.awi.de

Schwarz, J., & Schodlok, M. (2009). Impact of drifting icebergs on surface phytoplankton biomass in the Southern Ocean: Ocean colour remote sensing and in situ iceberg tracking. *Deep Sea Research Part I: Oceanographic Research Papers*, *56*(10), 1727–1741.
Seierstad, I. K., Abbott, P. M., Bigler, M., Blunier, T., Bourne, A. J., Brook, E., et al. (2014). Consistently dated records from the Greenland GRIP, GISP2 and NGRIP ice cores for the past 104 ka reveal regional millennial-scale δ18O gradients with possible Heinrich event imprint. *Quaternary Science Reviews*, *106*, 29–46.
Sessford, E., Tisserand, A., Risebrobakken, B., Andersson, C., Dokken, T., & Jansen, E. (2018). High-Resolution Benthic Mg/Ca Temperature Record of the Intermediate Water in the Denmark Strait Across D-O Stadial-Interstadial Cycles. *Paleoceanography and Paleoclimatology*, *33*, 1169–1185. https://doi.org/10.1029/2018PA003370
Simstich, J., Sarnthein, M., & Erlenkeuser, H. (2003). Paired δ 18 O signals of Neogloboquadrina pachyderma (s) and Turborotalita quinqueloba show thermal stratification structure in Nordic Seas. *Marine Micropaleontology*, *48*(1), 107–125.
Smith, K. L., Robison, B. H., Helly, J. J., Kaufmann, R. S., Ruhl, H. A., Shaw, T. J., et al. (2007). Free-drifting icebergs: hot spots of chemical and biological enrichment in the Weddell Sea. *Science*, *317*(5837), 478–482. https://doi.org/10.1126/science.1142834
Stein, R., Nam, S.-I., Grobe, H., & Hubberten, H. (1996). Late Quaternary glacial history and short-term ice-rafted debris fluctuations along the East Greenland continental margin. *Geological Society, London, Special Publications*, *111*(1), 135–151.
Stern, A. A., Johnson, E., Holland, D. M., Wagner, T. J. W., Wadhams, P., Bates, R., et al. (2015). Wind-driven upwelling around grounded tabular icebergs. *Journal of Geophysical Research: Oceans*, *120*, 5820–5835. https://doi.org/10.1002/2015JC010805
Stoner, J., Channell, J., & Hillaire-Marcel, C. (1998). A 200 ka geomagnetic chronostratigraphy for the Labrador Sea: Indirect correlation of the sediment record to SPECMAP. *Earth and Planetary Science Letters*, *159*(3), 165–181.
Stoner, J. S., Channell, J. E., & Hillaire-Marcel, C. (1996). The magnetic signature of rapidly deposited detrital layers from the Deep Labrador Sea: Relationship to North Atlantic Heinrich layers. *Paleoceanography*, *11*, 309–325.
Straneo, F., & Heimbach, P. (2013). North Atlantic warming and the retreat of Greenland's outlet glaciers. *Nature*, *504*(7478), 36–43. https://doi.org/10.1038/nature12854
Straneo, F., Sutherland, D. A., Holland, D., Gladish, C., Hamilton, G. S., Johnson, H. L., et al. (2012). Characteristics of ocean waters reaching Greenland's glaciers. *Annals of Glaciology*, *53*, 60.
Svendsen, J. I., Alexanderson, H., Astakhov, V. I., Demidov, I., Dowdeswell, J. A., Funder, S., et al. (2004). Late Quaternary ice sheet history of northern Eurasia. *Quaternary Science Reviews*, *23*(11-13), 1229–1271. https://doi.org/10.1016/j.quascirev.2003.12.008
Svensson, A., Andersen, K. K., Bigler, M., Clausen, H. B., Dahl-Jensen, D., Davies, S. M., et al. (2008). A 60 000 year Greenland stratigraphic ice core chronology. *Climate of the Past*, *4*(1), 47–57. https://doi.org/10.5194/cp-4-47-2008
Thornalley, D. J. R., Oppo, D. W., Ortega, P., Robson, J. I., Brierley, C. M., Davis, R., et al. (2018). Anomalously weak Labrador Sea convection and Atlantic overturning during the past 150 years. *Nature*, *556*(7700), 227–230. https://doi.org/10.1038/s41586-018-0007-4
van Kreveld, S., Sarnthein, M., Erlenkeuser, H., Grootes, P., Jung, S., Nadeau, M. J., et al. (2000). Potential links between surging ice sheets, circulation changes, and the Dansgaard-Oeschger cycles in the Irminger Sea, 60–18 kyr. *Paleoceanography*, *15*(4), 425–442. https://doi.org/10.1029/1999PA000464
Vasskog, K., Langebroek, P. M., Andrews, J. T., Nilsen, J. E. Ø., & Nesje, A. (2015). The Greenland Ice Sheet during the last glacial cycle: Current ice loss and contribution to sea-level rise from a palaeoclimatic perspective. *Earth-Science Reviews*, *150*, 45–67.
Vettoretti, G., & Peltier, W. R. (2016). Thermohaline instability and the formation of glacial North Atlantic super polynyas at the onset of Dansgaard-Oeschger warming events. *Geophysical Research Letters*, *43*, 5336–5344. https://doi.org/10.1002/2016GL068891
Vidal, L., Labeyrie, L., Cortijo, E., Arnold, M., Duplessy, J. C., Michel, E., et al. (1997). Evidence for changes in the North Atlantic Deep Water linked to meltwater surges during the Heinrich events. *Earth and Planetary Science Letters*, *146*(1-2), 13–27. https://doi.org/10.1016/S0012-821X(96)00192-6
Voelker, A. H., Grootes, P. M., Nadeau, M.-J., & Sarnthein, M. (2000). Radiocarbon levels in the Iceland Sea from 25–53 kyr and their link to the Earth's magnetic field intensity. *Radiocarbon*, *42*(3), 437–452.
Voelker, A. H., & Haflidason, H. (2015a). Refining the Icelandic tephrachronology of the last glacial period–the deep-sea core PS2644 record from the southern Greenland Sea. *Global and Planetary Change*, *131*, 35–62.
Voelker, A. H., Sarnthein, M., Grootes, P. M., & Schleicher, M. (1998). Correlation of marine 14C ages from the Nordic Seas with the GISP2 isotope record: Implications for 14C calibration beyond 25 ka BP. Paper presented at the Radiocarbon.
Voelker, A. H. L. (2018). Calendar Age based age model for core SU90-24. https://doi.org/10.1594/PANGAEA.886728
Voelker, A. H. L., & Haflidason, H. (2015b). Deep-sea sediment core PS2644 record from the southern Greenland Sea. *Global and Planetary Change* Retrieved from, *131*, 35–62. https://doi.org/10.1594/PANGAEA.831474
Waelbroeck, C., Duplessy, J.-C., Michel, E., Labeyrie, L., Paillard, D., & Duprat, J. (2001). The timing of the last deglaciation in North Atlantic climate records. *Nature*, *412*(6848), 724–727. https://doi.org/10.1038/35089060
Waelbroeck, C., Labeyrie, L., Michel, E., Duplessy, J. C., McManus, J. F., Lambeck, K., et al. (2002). Sea-level and deep water temperature changes derived from benthic foraminifera isotopic records. *Quaternary Science Reviews*, *21*(1-3), 295–305. https://doi.org/10.1016/S0277-3791(01)00101-9
White, L. F., Bailey, I., Foster, G. L., Allen, G., Kelley, S. P., Andrews, J. T., et al. (2016). Tracking the provenance of Greenland-sourced, Holocene aged, individual sand-sized ice-rafted debris using the Pb-isotope compositions of feldspars and 40Ar/39Ar ages of hornblendes. *Earth and Planetary Science Letters*, *433*, 192–203. https://doi.org/10.1016/j.epsl.2015.10.054
Yashayaev, I., Seidov, D., & Demirov, E. (2015). *A new collective view of oceanography of the Arctic and North Atlantic basins*. Elsevier.

Graphic design: Communication Division, UiB / Print: Skipnes Kommunikasjon AS

uib.no

ISBN: 9788230862698 (print)
9788230867013 (PDF)